Design, Synthesis and Pharmacological Screening of Novel Substituted Thiazolo[3,2-a]pyrimidine and Thiazolo[2,3-b]quinazoline Derivatives

A

THESIS

SUBMITTED IN FULFILLMENT FOR THE AWARD OF THE DEGREE OF

Doctor of Philosophy

IN

PHARMACEUTICAL SCIENCES

Submitted By

AMIT KUMAR KESHARI

Enrollment No. 250/13

Supervisor

Dr. SUDIPTA SAHA

DEPARTMENT OF PHARMACEUTICAL SCIENCES

SCHOOL FOR BIOSCIENCES AND BIOTECHNOLOGY

BABASAHEB BHIMRAO AMBEDKAR UNIVERSITY

(A CENTRAL UNIVERSITY)

VIDYA VIHAR, RAIBARELI ROAD, LUCKNOW-226025 (U.P.), INDIA

(2017)

Dedicated

To

My Lovely

Parents and Family

DECLARATION

I hereby declare that the thesis titled **"Design, Synthesis and Pharmacological Screening of Novel Substituted Thiazolo[3,2-a]pyrimidine and Thiazolo[2,3-b]quinazoline Derivatives"** has been prepared by me under the supervision of **Dr. Sudipta Saha** at Department of Pharmaceutical Sciences, School for Biosciences and Biotechnology, Babasaheb Bhimrao Ambedkar University, Lucknow (U.P.).

No part of this thesis has formed the basis for the award of any degree, diploma or fellowship previously. I further declare that the material embodied in the present work is based on original research work and indebtedness to others has been duly acknowledged at relevant places. This thesis is essentially free from all kinds of plagiarism.

Amit Kumar Keshari
14-12-17

Amit Kumar Keshari
Candidate

14/12/17

Dr. Sudipta Saha
Supervisor

CERTIFICATE

This is to certify that the thesis titled **"Design, Synthesis and Pharmacological Screening of Novel Substituted Thiazolo[3,2-a]pyrimidine and Thiazolo[2,3-b]quinazoline Derivatives"** submitted by Mr. **Amit Kumar Keshari** is an original research work and has not been previously submitted in part or full, for the award of any other degree or diploma to this or any other university.

The thesis submitted to Babasaheb Bhimrao Ambedkar University Lucknow, satisfies all the requirements as stipulated in the Doctor of Philosophy (Ph.D.) regulations - 1999 as amended in 2010 and it is fit for submission and evaluation for the award of the degree of Doctor of Philosophy of the University.

Date: 14/12/17

Supervisor 14/12/17

Head of the Department
18/12/17

ACKNOWLEDGEMENT

*All are meaningless without paying gratitude to **Almighty GOD**. At the end of my thesis, it is a pleasant task to express my thanks to all those who contributed in many ways to the success of this research work and made it an unforgettable experience for me and without them it is impossible to complete my work.*

*At this moment of accomplishment, first of all, I wish to express my deepest sense of gratitude and special thanks to my research advisor, mentor **Dr. Sudipta Saha,** Assistant Professor Department of Pharmaceutical Sciences, **Babasaheb Bhimrao Ambedkar University (A Central University), Lucknow,** Uttar Pradesh, India, under whose guidance, I have carried out my Ph.D. research work. It was his keen interest, **constant encouragement, valuable suggestions and guidelines,** which enable me to complete this work. His suggestions will remain with me as an in exhaustic source of scientific learning throughout my life. He has always given me a lot of encouragement, constant motivation, valuable ideas and timely support when ever needed.*

*With sincerity and immense pleasure, I express my deep sense of gratitude to **Prof R. C. Sobti, Honorable Vice Chancellor** of Babasaheb Bhimrao Ambedkar University, Lucknow, for providing infrastructure facilities for carrying the project advices throughout my academic career.*

*I warmly thank **Prof. (Dr.) Shubhini A. Saraf,** Professor and Head, Department of Pharmaceutical sciences, Babasaheb Bhimrao Ambedkar University, Lucknow for her valuable advice, constructive criticism and her extensive discussions around my research work.*

*It gives me great pleasure to acknowledge the support and cooperation rendered by **Departmental Research Committee (DRC) members** of B.B.A.U, Lucknow.*

*I accord my thanks to the **Dr. V. Elangovan and Dr. Sangeeta Saxena, Dr. Mukesh** BBAU, Lucknow for providing me **University Science Instrumentation Centre (USIC) facilities** to carry out my project.*

I am deeply grateful to **Dr. Anand Prakash,** *Department of Biotechnology, Babasaheb Bhimrao Ambedkar University, Lucknow for providing qRT-PCR facilities.*

I express my sincere gratitude to **Dr. Dinesh Kumar,** *Centre of Biomedical Research (CBMR), Lucknow for providing the NMR facilities.*

I also express my sincere gratitude to **Dr. Jyoti Kode,** *the Advanced Centre for Treatment, Research and Education in Cancer (ACTREC), Tata Memorial Centre, Navi Mumbai, India for providing the in vitro SRB assay for anti-cancer screening of drugs.*

I also acknowledge the **University Grant Commission,** *Government of India for providing me with the necessary funding and fellowship to pursue my Doctoral research at B.B.A.U., Lucknow.*

I would like to express sincere thanks to **Dr. Sunil Goria** *(Librarian),* **Mr. O.P. Saini** *and* **Mr. Nitesh Verma** *(Asst. Librarian), B.B.A.U for their kind support.*

It gives me pleasure to acknowledge the support and co-operation rendered by office staff and non-teaching staff **Mr. Bhandari,** **Mr. Amarjit** *and* **Mr. Anand** *during the research work.*

I would like to thank my fellow labmates **Vinit Raj, Amit Rai** *and* **Ashok K Singh** *for friendly and open-hearted support throughout my research period in this university.*

All my colleagues **Chandra Bhushan, Poonam Parashar, Malti Arya** *and* **Umesh Kumar (CBMR)** *are always there for me who directly or indirectly have a big hand in success of our work.*

I express my special gratitude to my junior **Pranesh Kumar** *and to my senior's* **Jovita Kanoujia, Mahendra Singh and Pooja Singh** *for their help and moral support during the work.*

My acknowledgement will be incomplete if I do not mention ***my parents*** *with whom blessings I was able to achieve my goal successfully.*

I wish to express my deepest sense of gratitude to my brothers, sisters and family members ***Mr. Sundeep Keshari, Mr. Pradeep Keshari, Mr. Sujeet Keshari*** *and my lovely nieces* ***Suraksha, Sanya, Pihu and Jessica*** *and nephew* ***utkarsh and shiv.***

Amit Kumar Keshari

Date: 14-12-17 ***Amit Kumar Keshari***

TABLE OF CONTENTS

List OF TABLES

LIST OF FIGURES

List of abbreviations

4A	(2-methoxy-4-(2-methoxy-6,7-dihydro-5H-benzo[h]thiazolo[2,3-b]quinazolin-7-yl)phenol)
6A	(3-methoxy-7-(3,4,5-trimethoxyphenyl)-6,7-dihydro-5H-benzo[h]thiazolo[2,3-b]quinazoline)
5-FU	5-Fluorouracil
ADMET	Absorption, distribution, metabolism, excretion, and toxicity
ALT	Alanine aminotransferase
AST	Aspartate aminotransferase
ATP	Adenosine triphosphate
BSA	Bovine serum albumin
CAT	Catalase
CC	Carcinogen control
CK	Creatine phosphokinase
CMC	Carboxymethyl cellulose
DNPH	2,4-dinitrophenylhydrazine
EDTA	Ethylene diamine tetra acetic acid
ELISA	Enzyme-linked immunosorbent assay
ESI	Electrospray ionization
FTIR	Fourier-transform infrared spectroscopy
GI_{50}	Growth inhibition of 50%
GSH	Glutathione
H^1 NMR	Proton nuclear magnetic resonance
C^{13}NMR	carbon nuclear magnetic resonance
H_2O_2	Hydrogen peroxide

HCC	Human hepatocellular carcinoma
HDL	High-density lipoprotein
HepG-2	Human hepatoma cells
IL-1β	Interleukin-1β
IL-2	Interleukin-2
IL-6	Interleukin-6
IL-10	Interleukin-10
ILs	Interleukins
IR	Infrared Spectroscopy
LC_{50}	Lethal concentration 50
LDH	Lactate dehydrogenase
MD	Molecular dynamics
MDA	malonaldehyde
MS	Mass spectrometry
NAA	N-acetyl aspartate
NAG	N-acetyl glutamate
NC	Normal control
NCBI	National centre for biotechnology information
NMR	Nuclear magnetic resonance
OPLS-DA	orthogonal partial least squares discriminant analysis
PC	Protein carbonyl
PCA	Principal component analysis
PDB	Protein data bank
PGs	Prostaglandins
ppm	Parts per million

QC	Quality control
qRT-PCR	Quantitative real-time reverse transcription-polymerase chain reaction
SEM	Scanning electron microscope
SOD	Superoxide dismutase
SRB	Sulforhodamine B
TBARS	Thiobarbituric acid reactive substances
TCA	Tricarboxylic acid
TGI	Total growth inhibition
TV	Tumor volume
VIP	Variable importance in projection

ABSTRACT

In our efforts to address the rising incidence of hepatocellular carcinoma (HCC), we have made a commitment to the synthesis of novel molecules to combat HCC. Thiazolo[2,3-b] quinazoline and thiazolo[3,2-a]pyrimidine scaffolds are known to have an anti-tumor effects on certain types of human malignancies; however, their effect on HCC remains unclear. A facile and highly efficient one-pot, multicomponent reaction has been successfully devised utilizing a *p*-toluenesulfonic acid (*p*-TSA)-catalyzed domino Knoevenagel/Michael/ intramolecular cyclization approach for the synthesis of novel 5H-benzo[h]thiazolo[2,3-b]quinazoline and indeno[1,2-d]thiazolo[3,2-a]pyrimidine analogs bearing a bridgehead nitrogen atom. This domino protocol constructed one new ring by the concomitant formation of multiple bonds (C–C, C–N, and C=N) involving multiple steps without the use of any metal catalysts in one-pot, with all reactants efficiently exploited.

All the newly synthesized compounds were authenticated by means of Fourier transform infrared spectroscopy, liquid chromatography–mass spectrometry, proton nuclear magnetic resonance spectroscopy, and carbon-13 nuclear magnetic resonance spectroscopy, together with elemental analysis, and their antitumor activity was evaluated in vitro on a Hep-G2 human cancer cell line by sulforhodamine B assay. Computational molecular modeling studies were carried out on cancer-related targets, including interleukin-2, interleukin-6, Caspase-3, and Caspase-8. Two compounds (4A and 6A) showed growth inhibitory activity comparable to the positive control Adriamycin, with growth inhibition of 50%, 10μg/mL. The results of the comprehensive structure–activity relationship study confirmed the assumption that two or more electronegative groups on the phenyl ring attached to the thiazolo[2,3-b]quinazoline system showed the optimum effect. The in silico simulations suggested crucial hydrogen bond and π–π stacking interactions, with a good ADMET (absorption, distribution, metabolism, excretion and toxicity) profile and molecular dynamics, in order to explore the molecular targets of HCC which were in complete agreement with the in vitro findings. Considering their significant anticancer activity, 4A and 6A are potent inhibitors among the series. Therefore, it is logical to speculate that these compounds might be alternatives to treat HCC in vivo.

Further, we investigated the in vivo antitumor activity and the mechanism underlying the effects of 4A and 6A in N-nitrosodiethylamine (NDEA)-induced HCC using male Wistar rats. NDEA was administered weekly intraperitoneal injections of 100 mg/kg for 6 weeks.

Various physiological and morphological changes, oxidative parameters, liver marker enzymes and cytokines, were assessed to evaluate the antitumor effect of 4A and 6A.

In addition, Proton nuclear magnetic resonance (^{1}H-NMR)-based serum metabolomics were performed to analyse the effects of 4A and 6A against HCC-induced metabolic alterations. Significant tumour incidences with an imbalance in carcinogen metabolizing enzymes and cellular redox status were observed in carcinogenic rats. Tumour inhibitory effects of 4A and 6A were noted by histopathology and biochemical profiles in NDEA-induced hepatic cancer. Compounds 4A and 6A had potential role to normalize the elevated levels of inflammatory mediators such as interleukin-1β (IL-1β), IL-2, IL-6, and IL-10. In molecular level, the real-time quantitative reverse-transcribed polymerase chain reaction (qRT-PCR) analysis revealed that 4A and 6A attenuated the IL-6 gene over-expression in hepatic cancer. Further, orthogonal partial least squares discriminant analysis (OPLS-DA) scores plot demonstrated a significant separation of 4A and 6A treated groups from carcinogen control group. Both the compounds have potential to restore the imbalanced metabolites due to HCC, signifying promising hepatoprotective activities.

Collectively, all these findings suggested that 4A and 6A could be potential drug candidates to treat HCC. In addition, the protocols that we have outlined should open up new avenues of investigation, with enormous implications for achieving diversity in green synthesis.

Keywords:

Thiazolo[2,3-b]quinazoline and thiazolo[3,2-a]pyrimidine, Hepatocellular carcinoma (HCC), domino reactions, multi-component reactions, interleukins, caspases, molecular docking, ADMET, dynamics, N-nitrosodiethylamine (NDEA), ^{1}H-NMR based metabolomics.

1. INTRODUCTION

One in six human deaths globally is due to multifaceted disease, such as cancer. Liver cancer accounted for 788,000 deaths in 2015 and is the second most common cause of cancer-related deaths, worldwide. The most prevalent primary liver cancer with poor prognosis is hepatocellular carcinoma (HCC), which has potentially lethal human malignacy worldwide, particularly in Asia and Africa [1, 2].

In men, HCC is the fifth most commonly diagnosed cancer and the second leading cause of cancer deaths; in women, it is the seventh most frequently diagnosed cancer, and worldwide, overall, it is the sixth commonest cause of cancer-related deaths [3].

In spite of continuous efforts to develop novel therapeutic strategies to treat HCC, it remains a challenge. As a consequence, therefore, increased attention has been paid, especially in the field of liver cancer therapy, to the discovery and development of safe and novel anticancer agents, together with improved cytotoxicity toward cancerous cells [4].

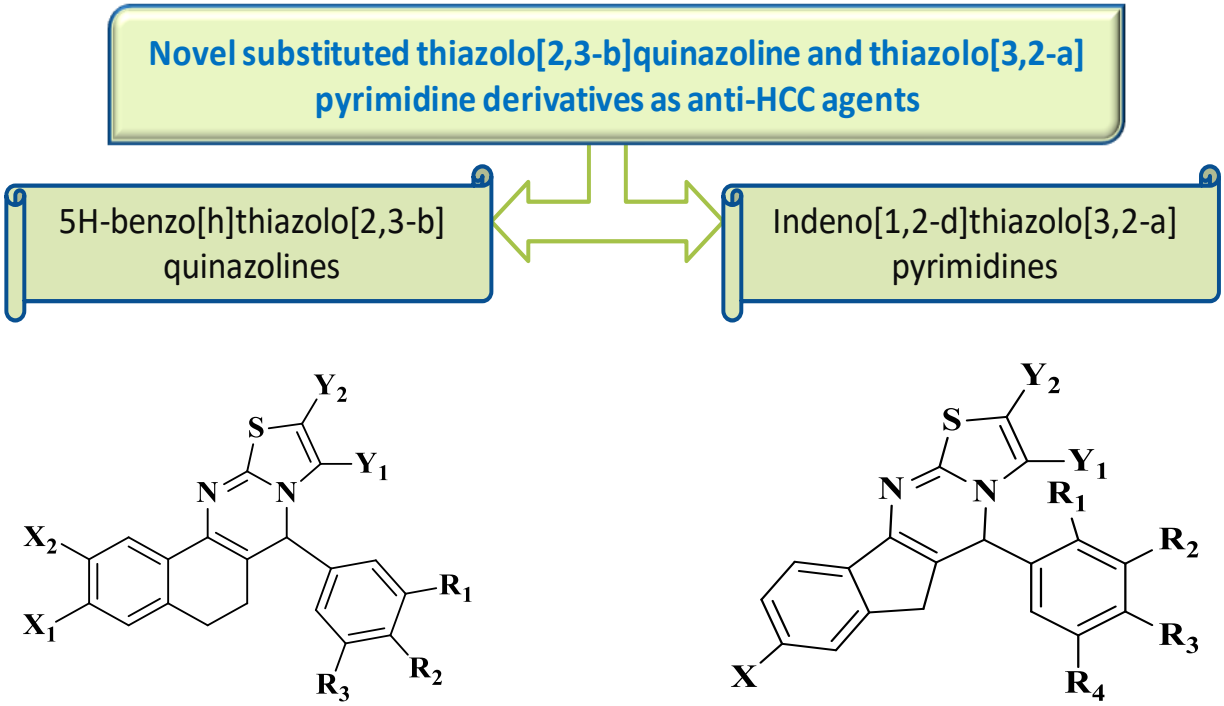

Figure 1.1 Novel substituted thiazolo[2,3-b]quinazoline and thiazolo[3,2-a]pyrimidine derivatives as anti-HCC agents.

1.1 Hepatocellular Carcinoma

Various types of cancer can form in the liver. The most common type of liver cancer is HCC. It is a malignant tumor arising from hepatocytes, the liver's parenchymal cells. The cell(s) of origin are believed to be the hepatic stem cells, although this remains the subject of investigation. Other types of liver cancer, for instance hepatoblastoma and intrahepatic cholangiocarcinoma, are much less common.

It occurs predominantly in patients with chronic liver inflammation and it is closely related to chronic viral hepatitis infection (hepatitis B or C) or exposure to toxins for instance alcohol, fungal toxins (aflatoxins), toxic industrial chemicals and air, and water pollutants. Certain diseases, such as hemochromatosis and alpha 1-antitrypsin deficiency, markedly increase the risk of developing HCC [5-7].

Human liver metabolizes ingested material and is the major site in the body. Moreover, HCC is seldom detected at an early stage due to high tolerance of liver and in most cases, once detected treatment faces a poor prognosis [8]. HCC is one of the most common malignancies with high prevalence and poor prognosis and the second leading cause of cancer-associated deaths worldwide [1, 5]. Its rate of incidence is dramatically increasing in the United States and other developing countries due to increased underlying hepatic conditions, for instance, alcoholic liver disease, non-alcoholic fatty liver disease and hepatitis B and C infection.

The worldwide mortality rate of all other leading cancers (such as lung, breast and prostate cancers) is declining, whereas the death rate of liver cancer is increased by 2.8% in men and 3.4% in women each year [9, 10]. Approximately 748,000 new cases (9.2% of all new global cancer cases) of HCC are being diagnosed every year worldwide [11].

It is responsible for over 12,000 deaths every year in the United States where the incidence of the disease is approximately 2.5 per 100,000 populations. Globally, over a million deaths every year (approx 10% of all deaths in the adult age range) can be attributed to HCC [7].

1.1.1 Signs and symptoms

HCC occurs in most people who already have signs and symptoms of chronic liver disease. It may appear either with or without worsening of signs and symptoms at the time of cancer detection. It may directly present with yellow discoloration of skin, unintentional weight loss, easy bruising from blood clotting abnormalities, loss of appetite, abdominal swelling, abdominal pain, nausea, vomiting, general weakness and fatigue [12].

1.1.2 Risk factors

The vast majority of HCC mainly occurs in people with cirrhosis of the liver. It includes most forms of chronic liver disease that may lead to cirrhosis. Certain risk factors are commonly associated with HCC than others. For instance, while consumption of heavy alcohol is estimated to cause 60-70% of cirrhosis cases, and the HCC mostly occurs in cirrhosis of the liver attributed to viral hepatitis [13].

Various recognized risk factors include:

1. Chronic viral hepatitis with HBV or HCV: Globally, estimated cause of 80% cases

- Chronic hepatitis B, HBV (approx. 50%)
- Chronic hepatitis C, HCV (approx. 25%) [14]

2. Toxins:

- Heavy alcohol use: the leading cause of cirrhosis [13]
- Intake of aflatoxins

3. Metabolic disorders:

- Non-alcoholic fatty liver disease (NAFLD) [15]
- Type 2 diabetes [16]

4. Congenital disorders:

- α-1 antitrypsin deficiency
- Various amino acid, bile acid, carbohydrate, and lipid disorders
- Wilson's disease (controversial; while some theorized the risk increases) [17-19]
- Hemophilia, although statistically related to higher risk of HCC, [20] this is due to coincident chronic viral hepatitis infection associated with repeated blood transfusions over lifetime [21].

The significance of all of these risk factors varies worldwide. In regions where HBV is endemic, such as southeast China, this is the major cause. In populations largely protected by hepatitis B vaccination, such as the United States, HCC is most often related to causes of cirrhosis such as chronic hepatitis C, obesity, and alcohol abuse [22].

1.1.3 Pathobiology

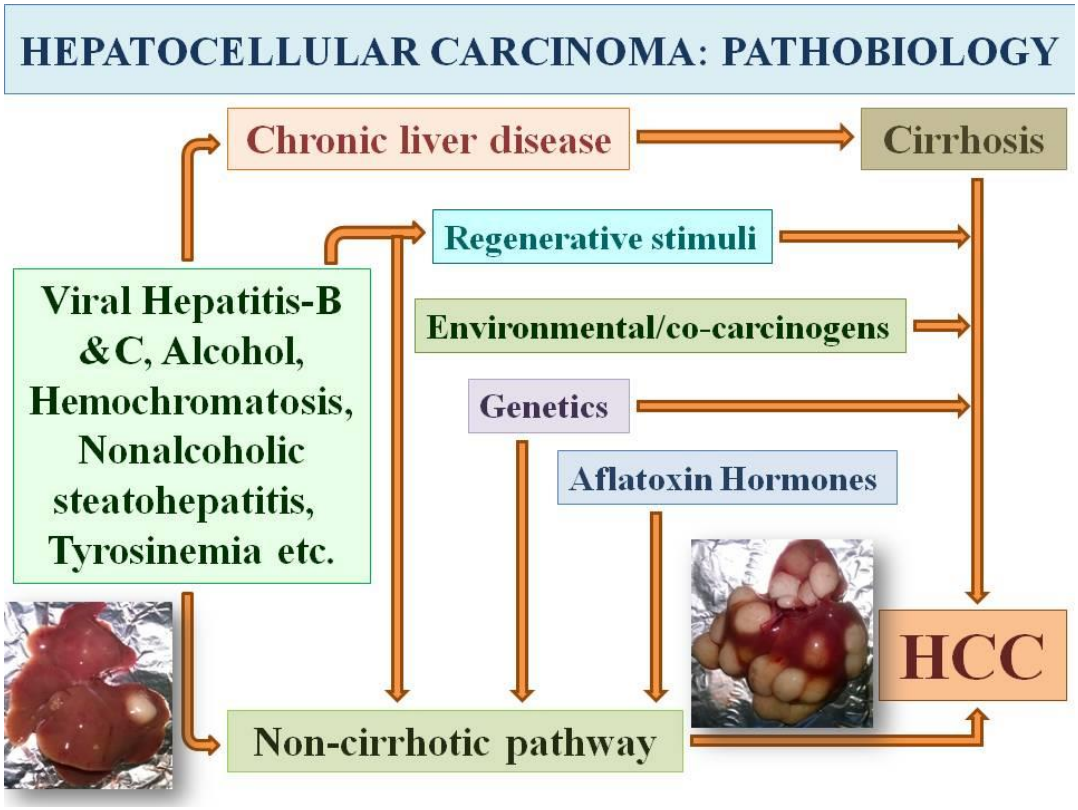

Figure 1.2 Pathobiology of Hepatocellular carcinoma

1.1.4 Diagnosis

The hepatic nodules can be identified by Ultrasounds (US), consisting of contrast-enhanced ultrasound (CEUS), or by other noninvasive techniques, for instance multi-detector computed tomography (MDCT), magnetic resonance imaging (MRI) and positron emission tomography (PET). The typical vascular profile/hallmarks of HCC on dynamic imaging is characterized by hypervascularity in the arterial phase with washout in the portal and/or late phases as compared to surrounding liver parenchyma [23].

In addition, molecular biomarkers could potentially be used for prognosis, as well as diagnostic evaluation and may help defining the individualized therapeutic approach to HCC.

Imaging techniques

Ultrasounds

Early identification of HCC is important because, as anticipated, treatment is more effective when the tumor is small [24-26]. The dysplastic nodules (DNs) may develop into carcinoma and the early detection of DNs with small areas of HCC is basic for safe and effective treatment [27].

Abdominal US evaluation is generally recommended for HCC surveillance in cirrhotic patients at six-monthly intervals and it is relatively inexpensive, simple to perform, widely available, and is radiation-free. It is still, however, the diagnosis of nodules from a small HCC may be challenging, as it is often difficult to differentiate malignant lesions from benign in the context of nodular cirrhosis.

Computed tomography

CT is mostly used in the radiological diagnosis of HCC after nodules are detected on US. Most centers use a four phase MDCT scan, which consists of a non-enhanced phase, an arterial phase (30 to 35 seconds after beginning the injection), a portal phase (75 to 90 seconds) and a late phase (3 minutes).

Magnetic resonance imaging

MRI is an appealing imaging technique to detect and characterize the different nodules, which may develop in cirrhosis and it does not use any ionizing radiation. By using magnetic fields, it allows the differentiation between normal and tumoral liver parenchyma, even without a contrast media [28].

MRI has become the diagnostic imaging modality of choice for HCC at many institutions worldwide. It appears superior to CT for the identification of HCC nodules [29, 30], but its sensitivity is lowest when evaluating tumors less than 2 cm in diameter [31, 32].

Nuclear imaging

Both 11C-acetate and 18F-FDG PET imaging techniques have been used for the detection and staging of HCC. Nevertheless, up to 40-50% cases of HCC are not sensitive to 18F-FDG PET, because of their high expression to glucose-6-phosphatase enzyme, which inhibits intracellular accumulation of 18F-FDG [33-35].

In contrast, 11C-acetate, which is believed to primarily participate in fatty acid synthesis in the liver, has been suggested to have increased sensitivity and specificity as compare to 18F-FDG [33, 35-36]. However, various literatures reported that 11C-acetate PET does not properly differentiate HCC from benign lesions [35, 37-39]. Some recent reports [35, 38-41] have suggested dynamic PET with kinetic modeling to be a promising tool to differentiate HCC from benign hepatic tumors.

Biomarkers

AFP, A-fetoprotein is well known and the most widely used biomarker for HCC. However, utility of AFP as an independent tool for the screening of HCC is not recommended by current guidelines due to its low sensitivity and specificity. In the past, a significant concentration of AFP in the serum of a cirrhotic patients and liver tumors > 2 cm was enough to diagnose HCC [42].

On the other hand, the current diagnostic algorithms endorsed by AASLD, the American Association for the Study of Liver Diseases and EASL, the European Association for the Study of the Liver strongly rely on typical radiological hallmarks in dynamic contrast-enhanced imaging techniques apart from biomarkers [42, 43].

1.1.5 Treatment

Numerous therapeutic options are available for HCC, depending on HCC stage, liver function, comorbidities, and local clinical expertise. A multidisciplinary team, comprising of hepatologists, oncologists, pathologists, radiologists, and surgeons, is fundamental for the proper management.

Surgery

The estimation of liver functional reserve before surgical resection is fundamental the maximum amount of liver mass that can be safely removed while overestimation of liver functional may lead to hepatic failure. Conversely, poor resection may notably increase the risk of early recurrence of HCC. The most important methods to evaluate liver function before hepatectomy are the indocyanine green (ICG) test, ^{99}mTc-galactosyl human serum albumin liver scintigraphy and the galactose tolerance test.

Liver transplantation

Liver transplantation (replacing the diseased liver with a cadaveric or a living donor liver) has become a feasible alternative for several patients with HCC, given the advances in immunosuppression and surgical techniques.

Non-surgical management

Among non-surgical alternatives, percutaneous ethanol injection (PEI), percutaneous radiofrequency ablation (RFA) and microwave ablation (MWA) represent the most commonly employed techniques for the curative treatments of HCC less than 5 cm in diameter and/or with less than 3 tumoral lesions [44].

New Therapies

The management of advanced HCC patients has been characterized for decades by limited therapeutic options since both the hormonal and chemotherapeutic agents have failed to show a substantial benefit for HCC patients [45-47].

An extensive knowledge of molecular hepato-carcinogenesis and the following introduction of targeted agents that particularly act on the neo-plastic pathways, have created a novel therapeutic interventions of hepatic cancer [48].

1.2. REVIEW OF LITERATURE

It is interesting to note from chemical literature that several organic compounds containing a fused six membered heterocyclic ring, i.e. thiazolo[2,3-b]quinazolines and thiazolo[3,2-a] pyrimidine analogs make up a broad class that attracted attention in the past few years owing to its wide range of biological activities, especially anti-cancer.

A large number of novel thiazolo[2,3-b]quinazoline and thiazolo[3,2-a]pyrimidine derivatives have been synthesised and evaluated as potential biological activities which are following as:

Al-Omary *et al.* (2012) designed and synthesized a novel series of thiazolo[2,3-b]quinazoline and pyrido[4,3-d]thiazolo[3,2-a]pyrimidine analogues. The obtained compounds were evaluated for their in-vitro antitumor activity and showed remarkable broad-spectrum antitumor activity. Compound **(I)** was found to be almost nine fold more active than 5-FU [49].

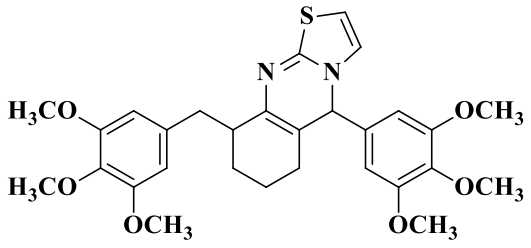

(I)

Nagarapu *et al.* (2013) synthesized and evaluated a novel series of building blocks consisting of benzo[4,5]thiazolo[1,2-a]pyrimidine-3-carboxylate have been synthesized as potential anticancer compounds. These compounds were prepared from 2-amino benzothiazole, benzaldehyde and ethyl acetoacetate in ethylene glycol by catalysing with TBAHS to give benzo[4,5]thiazo[1,2-a]pyrimidine derivatives followed by the formation of amide by reaction with several secondary amines in good yields. The cytotoxicity of these compounds was evaluated against human cancer cell lines in vitro (A549, HeLa, MDA-MB-231 and MCF-7) while compound **(II)** showed promising cytotoxicity against MDA-MB-231 (IC50 value of 5.01 mM) [50].

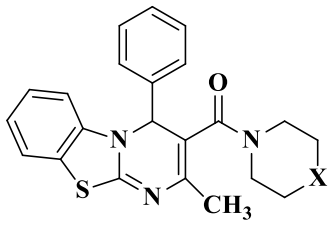

(II)

El-Messery *et al.* (2012) synthesized and evaluated a novel series of 2-acetamido and 2 or 3-propanamido derivatives of 4- or 5-substituted-thiazoles. Compounds bearing straight chain substituent or 4-phenyl function proved to be more active than their branched or 4-methyl congeners. Compound **(III)** exhibited broad spectrum antitumor activity [51].

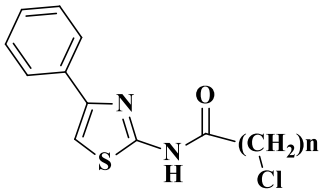

(III)

Synthesis, antiproliferative and apoptosis-inducing activity of thiazolo[5, 4-*d*]pyrimidines by Singh *et al.* (2013). The morpholine substituted analog **(IV)** displayed promising anticancer activity in HL-60 cells [52].

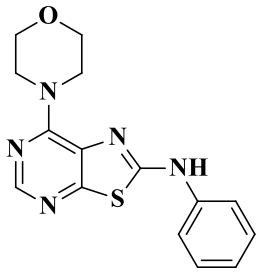

(IV)

A novel series of 2-acetamido- or 2-propanamido-4-(4-substituted phenyl)-1,3-thiazoles were synthesized by Al-Omary *et al.* (2012) and were tested for their antitumor activity. Compound **(V)** proved to be nine and sevenfold more active than the standard antitumor drug 5-FU [53].

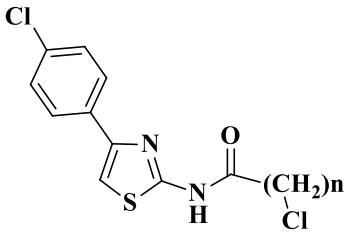

(V)

Agarwal *et al***.** (2004) designed and synthesized 4-(Substituted-benzylidine)-2-substituted-5,6-dihydrobenzo quinazoline and 4-(substituted benzylidine)-2-substituted-3,4,5,6-tetrahydro benzo quinazoline have been synthesized from 2-(substituted benzylidine) tetralone-1 and several substituted guanidine sulphates. These compounds were tested for their in vitro antileishmanial activity. Compound **(VI)** show promising antileishmanial activity against Leishmania donovani [54].

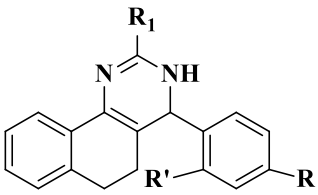

(VI)

Rajanarendar *et al.* demonstrated a mild and efficient PTSA catalyzed synthesis of novel isoxazolo[2,3-c][1,3,5]thiadiazepin-2-ones (VII) in excellent yields by one-pot three-component Domino reaction without the production of toxic waste products using *p*-toluene sulfonic acid (PTSA) as a Lewis acid catalyst [55].

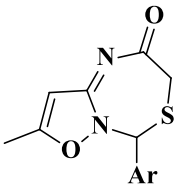

(VII)

Sakram *et al.* demonstrated Benzo[h]thiazolo[2,3-b]quinazolines (VIII) by an efficient *p*-toluenesulfonic acid-catalyzed one-pot two-step tandem reaction [56].

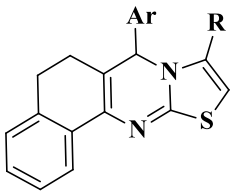

(VIII)

Warekar *et al.* has been developed a simple, clean and convenient one pot method for the synthesis of 4-phenyl-3,4-dihydro-1H-indeno[1,2-d]pyrimidine-2,5-dione and 4-phenyl-2-thioxo-1,2,3,4-tetrahydro-5H-indeno[1,2-d]pyrimidine-5-one by multi-component condensation of 1,3 indanedione, aromatic aldehydes and urea/thiourea using phosphorus pentoxide [57].

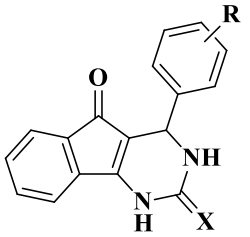

(IX)

Synthesis, spectroscopic characterization and DFT studies on the novel indeno-thiazolo pyrimidine heterocyclic system were reported by Gupta *et al.* [58].

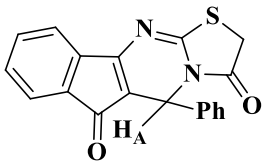

(X)

1.3. RESEARCH ENVISAGED

In our efforts to address the rising incidence of hepatocellular carcinoma, we have made a commitment to the synthesis of novel molecules for HCC treatment. Thiazolo[2,3-b] quinazoline and thiazolo[3,2-a]pyrimidine analogs are known to have an antitumor effect on certain types of malignancies, however its effect on HCC remains unclear.

Indanone, tetralone and related compounds have been studied for various biological activities including cancer. These are also used as drug intermediates and thiazole containing heterocyclic compounds attracted the interest of medicinal chemists due to their synthetic feasibility and their incorporation into variety of therapeutically active agents.

In addition, computational molecular modeling studies of these analogs with various cancer-related targets, including interleukin (IL)-2, IL-6, Caspase-3, and Caspase-8 receptor sites, revealed that the interaction energy were found to be $\geq$ 5.0 Kcal/mole which strengthened the hypothesis.

Thus, in the proposed study, we designed novel 5H-benzo[h]thiazolo[2,3-b]quinazoline and indeno[1,2-d]thiazolo[3,2-a]pyrimidine analogs by incorporation of these moieties, i.e. substituted 2-benzylidene-3,4-dihydronaphthalen-1(2H)-one and 2-benzylidene-2,3-dihydro-1H-inden-1-one with the different type of 2-amino thiazoles with an anticipation of enhanced antitumor activity against N-nitrosodiethylamine (NDEA)-induced HCC using male albino Wistar rats.

We rationally designed and prepared a template for synthetic scheme from various literatures and commercially available anticancer agents which are illustrated as follows:

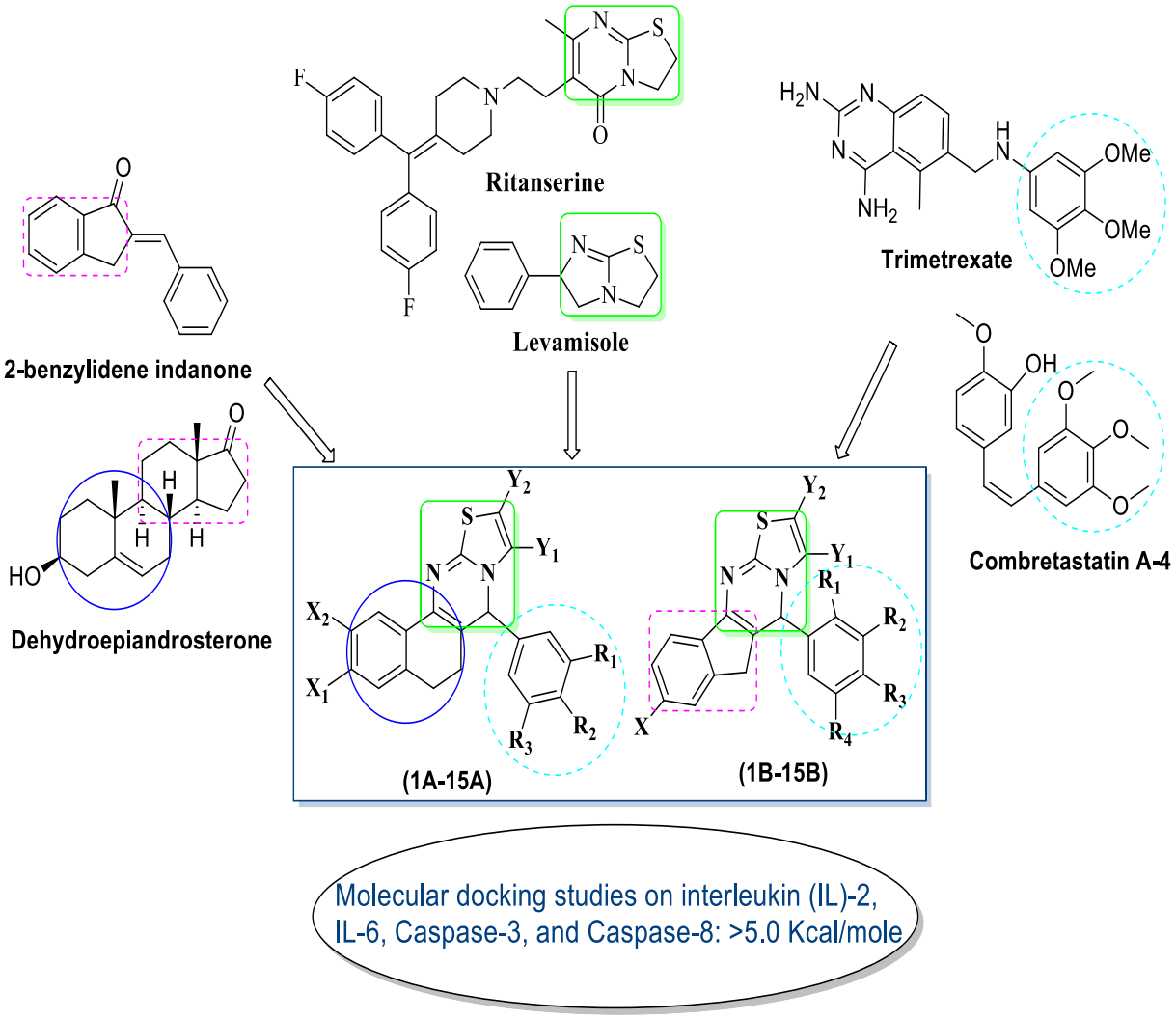

Targeted Rational Template

Figure 1.3 Rationally designed and prepared a template for synthetic scheme from anticancer agents

1.4. PLAN OF WORK

Part 1 Literature Survey & Procurement of Materials

Part 2 Design and syntheses of novel 5H-benzo[h]thiazolo[2,3-b]quinazoline and indeno[1,2-d]thiazolo[3,2-a]pyrimidine analogs.

Part 2 (I) Purification: Re-crystallization

(II) Characterization

A) Physical analysis	**B) Spectral analysis**
(a) Color	**(a)** UV Spectroscopy
(b) State	**(b)** IR Spectroscopy
(c) Solubility	**(c)** Mass Spectrometry
(d) Melting range	**(d)** NMR spectroscopy
(e) Determination of Rf value	**(e)** Elemental analyses

Part 3 Computational molecular modeling studies

(a) Molecular docking

(b) ADME (absorption, distribution, metabolism, excretion, and toxicity) Profile

(c) Molecular dynamics (MD) simulation

Part 4 *In-vitro* anti-tumor activity against Human hepatoma (Hep-G2) cells using sulforhod-amine B assay.

Part 5 *In-vivo* antitumor activity using Wistar albino rats

(a) Acute oral toxicity study

(b) N-nitrosodiethylamine (NDEA)-induced HCC using Wistar albino rats model

Evaluation parameters

- **Biochemical studies on serum**
  - Aspartate aminotransferase (AST)
  - Alanine aminotransferase (ALT)
  - Lactate dehydrogenase (LDH)

- Creatine phosphokinase (CK)

- **Catabolic byproducts**
  - Bilirubin
  - Biliverdin
- **Inflammatory biomarkers related to HCC**
  - Interleukin-1β (IL-1β)
  - Interleukin-2 (IL-2)
  - Interleukin-6 (IL-6)
  - Interleukin-10 (IL-10)
- **Antioxidant estimation**
  - Glutathione (GSH)
  - Thiobarbituric acid reactive substances (TBARS)
  - Superoxide dismutase (SOD)
  - Catalase (CAT)
  - Protein carbonyl (PC)
- Histopathology and scanning electron microscopy (SEM)
- Real-time quantitative reverse-transcribed polymerase chain reaction (qRT-PCR) analysis

Part 6 Proton nuclear magnetic resonance (1H-NMR) based serum metabolomics

- Multivariate analysis via MetaboAnalyst 3.0 tool
- Principal component analysis (PCA)
- Partial least squares discriminant analysis (PLS-DA)
- Orthogonal partial least squares discriminant analysis (OPLS-DA)
- The scores of variable importance in projection (VIP)
- Student's t-test

Part 7 Statistical analysis & compilation of data

1.5. REFERENCES

[1] World Health Organization. Cancer fact sheet, February 2017. Available from: http://www.who.int/mediacentre/factsheets/fs297/en/. Accessed on May 19, 2017.

[2] Zhang B, Wang N, Zhang C, et al. Novel multi-substituted benzyl acridone derivatives as survivin inhibitors for hepatocellular carcinoma treatment. Eur J Med Chem. 2017;129:337–348.

[3] Eldehna WM, Fares M, Ibrahim HS et al. Indoline ureae as potential anti-hepatocellular carcinoma agents targeting VEGFR-2: Synthesis, in vitro biological evaluation and molecular docking. Eur J Med Chem. 2015;100:89–97.

[4] Gregoric T, Sedic M, Grbcic P et al. Novel pyrimidine-2,4-dione 1,2,3-triazole and furo[2,3-d]pyrimidine-2-one 1,2,3-triazole hybrids as potential anti-cancer agents: Synthesis, computational and X-ray analysis and biological evaluation. Eur J Med Chem. 2017;125:1247–1267.

[5] Gupta P, Bansal MP, Koul A. Evaluating the effect of lycopene from Lycopersicum esculentum on apoptosis during NDEA induced hepatocarcinogenesis. Biochem Biophys Res Commun. 2013;434:479–485.

[6] Kumar V, Fausto N, Abbas A. Robbins & Cotran Pathologic Basis of Disease. Saunders. Edition-9, 2015;ISBN 978-1455726134:870–873.

[7] https://www.hopkinsmedicine.org/gastroenterology_hepatology/_pdfs/liver/hepatocellular_carcinoma_liver_cancer.pdf

[8] Singh BN, Singh BR, Sarma BK, Singh HB. Potential chemoprevention of N-nitrosodiethylamine-inducedhepatocarcinogenesis by polyphenolics from Acacia nilotica bark. Chem Biol Interact. 2009;181:20–28.

[9] Hashim D, Boffetta P, La Vecchia C et al. The global decrease in cancer mortality: trends and disparities. Ann Oncol. 2016;27(5):926–933.

[10] Chacko S, Samanta S. A novel approach towards design, synthesis and evaluation of some Schiff base analogues of 2-aminopyridine and 2-aminobezothiazole against hepatocellular carcinoma. Biomed Pharmacother. 2017;89:162–176.

[11] Kew MC. Hepatocellular carcinoma: epidemiology and risk factors. J Hepatocell Carcinoma. 2014;1:115–125.

[12] "Liver cancer overview". Mayo Clinic. Accessed May 19, 2017.

[13] Heidelbaugh Joel J, Bruderly M. Cirrhosis and chronic liver failure: part I. Diagnosis and evaluation. American Family Physician. 2006;74(5):756–762.

[14] Alter MJ. Epidemiology of hepatitis C virus infection. World J Gastroenterol. 2007;13(17):2436–41.

[15] White DL, Kanwal F, El-Serag HB. Association between nonalcoholic fatty liver disease and risk for hepatocellular cancer, based on systematic review. Clin Gastroenterol Hepatol. 2012;10(12):1342–59.

[16] El–Serag HB, Hampel H, Javadi F. The association between diabetes and hepatocellular carcinoma: a systematic review of epidemiological evidence. Clin Gastroenterol Hepatol. 2006;4(3):369–380.

[17] Wang XW, Hussain SP, Huo TI, Wu CG, Forgues M, Hofseth LJ, Brechot C, Harris CC. Molecular pathogenesis of human hepatocellular carcinoma. Toxicology. 2002;181–182:43–47.

[18] Heidelbaugh JJ, Bruderly M. Cirrhosis and chronic liver failure: Part I. Diagnosis and evaluation. Am Fam Physician 2006;74:756-762.

[19] Arun JS, Seung KY, Riccardo L. The Etiology of Hepatocellular Carcinoma and Consequences for Treatment. The Oncologist 2010;15:14 –22.

[20] Huang YC, Tsan YT, Chan WC et al. Incidence and survival of cancers among 1,054 hemophilia patients: A nationwide and 14-year cohort study. Am J Hematol. 2015;90(4):E55–E59.

[21] Shetty S, Sharma N, Ghosh K. Epidemiology of hepatocellular carcinoma (HCC) in hemophilia. Crit Rev Oncol Hematol. 2016;99:129–133.

[22] Tanaka M, Katayama F, Kato H et al. Hepatitis B and C virus infection and hepatocellular carcinoma in China: A review of epidemiology and control measures. J Epidemiol. 2011;21(6):01–416.

[23] Marrero JA, Hussain HK, Nghiem HV, Umar R, Fontana RJ, Lok AS. Improving the prediction of hepatocellular carcinoma in cirrhotic patients with an arterially-enhancing liver mass. Liver Transpl. 2005;11:281–289.

[24] Choi BI. Hepatocarcinogenesis in liver cirrhosis: imaging diagnosis. J Korean Med Sci. 1998;13:103–116.

[25] Eskesen AN, Bjøro K, Aandahl EM, Line PD, Melum E. Low use of surveillance and early diagnosis of hepatocellular carcinoma in Norway--a population-based cohort study. Cancer Epidemiol. 2014;38:741–747.

[26] Chen MH, Yan K, Yang W et al. Long term (5 years) outcome of radiofrequency ablation for hepatocellular carcinoma in 256 cases. Beijing Daxue Xuebao. 2005;37:671–672.

[27] Matsui O, Kobayashi S, Sanada J et al. Hepatocelluar nodules in liver cirrhosis: hemodynamic evaluation (angiography-assisted CT) with special reference to multi-step hepatocarcinogenesis. Abdom Imaging. 2011;36:264–272.

[28] Ariff B, Lloyd CR, Khan S et al. Imaging of liver cancer. World J Gastroenterol. 2009;15:1289–1300.

[29] Burrel M, Llovet JM, Ayuso C et al. Barcelona Clínic Liver Cancer Group. MRI angiography is superior to helical CT for detection of HCC prior to liver transplantation: an explant correlation. Hepatology. 2003;38:1034–1042.

[30] Kim YK, Kim CS, Chung GH et al. Comparison of gadobenate dimeglumine-enhanced dynamic MRI and 16-MDCT for the detection of hepatocellular carcinoma. AJR Am J Roentgenol. 2006;186:149–157.

[31] Ebara M, Ohto M, Watanabe Y et al. Diagnosis of small hepatocellular carcinoma: correlation of MR imaging and tumor histologic studies. Radiology. 1986;159:371–377.

[32] Krinsky GA, Lee VS, Theise ND et al. Transplantation for hepatocellular carcinoma and cirrhosis: sensitivity of magnetic resonance imaging. Liver Transpl. 2002;8:1156–1164.

[33] Ho CL, Yu SC, Yeung DW. 11C-acetate PET imaging in hepatocellular carcinoma and other liver masses. J Nucl Med. 2003;44:213–221.

[34] Delbeke D, Pinson CW. 11C-acetate: a new tracer for the evaluation of hepatocellular carcinoma. J Nucl Med. 2003;44:222–223.

[35] Park JW, Kim JH, Kim SK et al. A prospective evaluation of 18F-FDG and 11C-acetate PET/CT for detection of primary and metastatic hepatocellular carcinoma. J Nucl Med. 2008;49:1912–1921.

[36] Sacks A, Peller PJ, Surasi DS, Chatburn L, Mercier G, Subramaniam RM. Value of PET/CT in the management of primary hepatobiliary tumors, part 2. AJR Am J Roentgenol. 2011;197:260–265.

[37] Karhunen PJ. Benign hepatic tumours and tumour like conditions in men. J Clin Pathol. 1986;39:183–188.

[38] Delbeke D, Martin WH, Sandler MP, Chapman WC, Wright JK, Pinson CW. Evaluation of benign vs. malignant hepatic lesions with positron emission tomography. Arch Surg. 1998;133:510-516.

[39] Gibbs JF, Litwin AM, Kahlenberg MS. Contemporary management of benign liver tumors. Surg Clin North Am. 2004;84:463–480.

[40] Chen S, Ho C, Feng D, Chi Z. Tracer kinetic modeling of 11C-acetate applied in the liver with positron emission tomography. IEEE Trans Med Imaging. 2004;23:426–432.

[41] Huo L, Guo J, Dang Y et al. Kinetic analysis of dynamic (11) C-acetate PET/CT imaging as a potential method for differentiation of hepatocellular carcinoma and benign liver lesions. Theranostics. 2015;5:371–377.

[42] Bruix J, Sherman M. Management of hepatocellular carcinoma. Hepatology. 2005;42:1208–1236.

[43] European Association For The Study Of The Liver, European Organisation For Research And Treatment Of Cancer. EASL-EORTC clinical practice guidelines: management of hepatocellular carcinoma. J Hepatol. 2012;56:908–943.

[44] Bellissimo F, Pinzone MR, Cacopardo B, Nunnari G1. Diagnostic and therapeutic management of hepatocellular carcinoma. World J Gastroenterol. 2015;21(42):12003-21.

[45] Nowak A, Findlay M, Culjak G, Stockler M. Tamoxifen for hepatocellular carcinoma. Cochrane Database Syst Rev. 2004;3:1-27.

[46] Yeo W, Mok TS, Zee B et al. A randomized phase III study of doxorubicin versus cisplatin/interferon alpha-2b/doxorubicin/fluorouracil (PIAF) combination chemotherapy for unresectable hepatocellular carcinoma. J Natl Cancer Inst. 2005;97:1532-8.

[47] Zhu AX. Systemic therapy of advanced hepatocellular carcinoma: how hopeful should we be? Oncologist. 2006;11:790–800.

[48] Llovet JM, Bruix J. Molecular targeted therapies in hepatocellular carcinoma. Hepatology. 2008;48:1312–27.

[49] El-Messery SM, Hassan GS, Al-Omary FAM, El-Subbagh HI. Substituted thiazoles V. Synthesis and antitumor activity of novel thiazolo [2,3-b] quinazoline and pyrido [4,3-d] thiazolo [3,2-a] pyrimidine analogues. Eur. J. Med. Chem. 2012;47:65-72.

[50] Nagarapu L, Vanaparthi S. Synthesis of novel benzo [4,5] thiazolo [1,2-a] pyrimidine-3-carboxylate derivatives and biological evaluation as potential anticancer agents. Eur. J. Med. Chem. 2012;69:817-822.

[51] El-Messery, SM, Hassan, GS, Al-Omary, FAM, El-Subbagh HI. Substituted thiazoles VI. Synthesis and antitumor activity of new 2 acetamido- and 2 or 3-propanamido-thiazole analogs. Eur. J. Med. Chem. 2012;54:615-625.

[52] Singh B, Guru SK, Kour S, Jain, S et al. Synthesis, antiproliferative and apoptosis-inducing activity of thiazolo [5,4-*d*] pyrimidines. Eur. J. Med. Chem. 2013;10.039.

[53] El-Messery SM, Hassan GS, Al-Omary FAM, El-Subbagh HI. Substituted thiazoles VII. Synthesis and antitumor activity of certain 2-(substituted amino)-4-phenyl-1,3-thiazole analogs. Bioorg. & Med. Chem. Lett. 2012;22:6318–6323.

[54] Agarwal KC, Sharma V, Shakya N, Gupta S. Design and synthesis of novel substituted quinazoline derivatives as antileishmanial agents. Bioorg. & Med. Chem. Lett. 2009;19:5474–5477.

[55] Rajanarendar E, Venkateshwarlu P, Krishna SR, Reddy KG, Thirupathaiah K. One-Pot Three Component Domino Reaction for the Synthesis of Novel Isoxazolo[2,3-c] [1,3,5]Thiadiazepin-2-Ones Catalyzed by PTSA—A Green Chemistry Approach. Green Sustain Chem. 2015;5:107-114.

[56] Sakram B, Sonyanaik B, Ashok K, Rambabu S, Johnmiya SK. Benzo[h]thiazolo[2,3-b] quinazolines by an efficient p-toluenesulfonic acid-catalyzed one-pot two-step tandem reaction. Res Chem Intermed. 2016;42(3):1699–1705.

[57] Warekar PP, Kolekar GB, Deshmukh MB, Anbhule PV. An Efficient and Modified Biginelli type Synthesis of 3,4-dihydro-1H-indeno[1, 2-d]pyrimidine-2,5-dione Using Phosphorous Pentoxide. Synth Commun. 2014; DOI:10.1080/00397911.2014.947652.

[58] Gupta R, Chaudhary RP. Synthesis, spectroscopic characterization and DFT studies on the novel indeno-thiazolopyrimidine heterocyclic system. J Sulfur Chem. 2014;35(1):86–97

2. INTRODUCTION

During our ongoing searches aimed at the discovery of unique structure endowed with diverse pharmacological activities, we found that thiazolo[2,3-b]quinazoline and thiazolo[3,2-a]pyrimidine bearing bridge-head (ring junction) nitrogen atom as a ubiquitous structural fragments in medicinal chemistry showed an interesting anti-tumour activity often associated with high or moderate specificity for certain human tumour cell lines [1, 2].

These biologically important scaffolds are now-a-days attracting the attention of many medicinal chemists throughout the world to explore this framework for its potential and these are formed by the fusion of two aromatic rings i.e. thiazole and pyrimidine, in such a way that one carbon atom at the ring junction is replaced by a nitrogen atom and is, therefore, being common for both the heterocyclic rings [3].

Heterocyclic compounds bearing nitrogen and sulphur have long been the prime focus of synthetic chemistry research due to their broad spectrum of applications in biological, pharmaceutical, and material areas [4].

Domino reactions involving simultaneous formation of C–C and C–heteroatom multiple bonds in a single flask are a means to achieving economical methods for the manufacture of especially unusual, fused heterocyclic, medicinally privileged scaffolds without any separation of intermediates throughout the process. Moreover, domino reactions, being attractively appealing, are frequently connected with savings in terms of energy and reaction periods, are highly convergent, have fewer environmental impacts, and show atom economy in a single-step process starting from multiple reactants [5, 6].

Conventional multistep chemical reactions suffer from various limitations compared with the one-pot domino technique, as they require a large number of synthetic operations, including isolation and purification of the products of each individual step. The multistep synthetic approach, therefore, has led to synthetic inefficiency, is time-consuming, or contains side reactions generating large amounts of waste [7]. A key challenge in recent drug development processes is to design a rapid, versatile, and efficient synthesis that provides target molecules containing structural complexity and diversity with a choice of fascinating biologic activities [8].

Thiazole-based heterocycles are central to modern chemical synthesis due to their synthetic feasibility and their incorporation into various types of therapeutically useful agents and are of paramount interest in the development of important pharmacophores in the drug discovery endeavour [9, 10].

Functionalized quinazoline and fused quinazolines have long been of increasing interest in the field of synthetic organic and medicinal chemistry on account of the wide range of biologic activities [11–14] including anticancer [15], anti-inflammatory [16], antituberculosis [17], anticonvulsant [18], antimalarial [19], antihypertensive [20], antidiabetic [21] and so on. Furthermore, suitably substituted thiazolo[2,3-b]quinazolines also serve as versatile building blocks in synthetic chemistry.

Nowadays, bridgehead (ring junction) nitrogen atom-containing thiazolo[3,2-a] pyrimidines command much attention as privileged scaffolds comprising a vital class of heterocyclic structures possessing exciting and varied pharmacologic activities [3, 22-23] such as: being potential inhibitors of cyclin-dependent kinase [24], CDC25B phosphatase enzymes [25], IspF proteins [26], and YycG histidine kinase [27], antibacterial [28], analgesic, and anti-inflammatory activities [29] acting as a corticotropin-releasing factor receptor antagonist [30], hypolipidemic activity [31], antiviral including anti-HIV effects, anticancer [32, 33], cardiotonic and inotropic effects [34] acting as potent A2A adenosine receptor inverse agonists with antinociceptive activity [35] and so on.

To the best of our knowledge, among the earlier reported methods devoted to the synthesis of especially 5H-benzo[h]thiazolo[2,3-b]quinazolines [36, 37] only a few are described, and metal-free multicomponent domino reactions (MDRs) [38, 39] are still rare. In this regard, most of the reported methods have suffered from various drawbacks, for example, harsh reaction conditions, multistep synthetic routes, costly reagents/catalysts, prolonged reaction periods, tedious workups after each step, and poor availability of starting materials.

There is no route for the direct construction of the indeno[1,2-d]thiazolo[3,2-a]pyrimidine moiety through domino reactions, and a literature survey revealed only one report to be available, which includes the synthesis of 5-phenylindeno[1,2-d]thiazolo[3,2-a]pyrimidine-3,6(2H,5H)-dione and 5-phenyl-2,3-dihydro indeno[1,2-d]thiazolo[3,2-a]pyrimidin-6(5H)-one in two steps [40].

In order to arrive at a highly proficient and convergent synthetic strategy for the construction of these two vital structural elements, while at the same time avoiding several limitations of earlier reports, and in our venture toward the development of a modern synthetic approach, we first report herein an operationally simple and straightforward metal-free, one-pot MDR for obtaining a panel of novel 5H-benzo[h]thiazolo[2,3-b]quinazoline (1A–15A) and indeno[1,2-d]thiazolo[3,2-a]pyrimidine (1B–15B) analogs using the reactions of highly substituted α-tetralone or α-indanone with some aromatic aldehydes and distinctive 2-aminothiazoles in ethanol (EtOH) in the presence of catalytic amounts of *p*-toluenesulfonic acid (*p*-TSA; 20 mol%) [7, 41-42].

Readily available and cheap starting materials, together with an environmentally benign and mild acidic catalyst, were employed to achieve these diversely decorated skeletons in impressive yields. They have also been synthesized by conventional two-step reactions and compared with the preferred MDRs described above [23, 43–45].

Additionally, all of the newly synthesized compounds were evaluated for their antitumor activity in vitro on a Hep-G2 human cancer cell line by sulforhodamine B (SRB) assay and structure–activity relationship prediction on the basis of in vitro findings. Furthermore, computational molecular modeling studies with ADMET (absorption, distribution, metabolism, excretion, and toxicity) profiling and molecular dynamic (MD) simulation were carried out on cancer-related targets, including interleukin (IL)-2, IL-6, Caspase-3, and Caspase-8 receptor sites, to identify the potential modes of action of the named compounds.

2.1 MATERIALS AND METHODS

2.1.1 General information

All of the reactions described below were carried out with commercially available chemicals of reagent grade that were used as received without further purification unless otherwise noted. Reagents were purchased from Merck and Sigma-Aldrich chemical companies. Melting points (m.p.) were determined on an m.p. apparatus and are uncorrected. Compounds were named following the International Union of Pure and Applied Chemistry rules as applied by Advanced Chemistry Development/ChemSketch. Elemental analyses were performed with a Euro EA 3000 Elemental Analyzer for C, H, N, and the results were within ±0.4% of the theoretical values. Infrared (IR) spectra were recorded on a Thermo Scientific Nicolet 6700 Fourier transform IR spectroscopy spectrometer. Nuclear magnetic resonance (NMR) spectra were obtained on a Bruker 800 MHz NMR spectrometer (1H 800 MHz, 13C 200 MHz) (Bruker, Rheinstetten, Germany) and processed in TopSpin 2.1. Chemical shifts are expressed in parts per million (ppm) downfield from tetramethylsilane as the internal standard. Coupling constants are expressed in Hz. All of the compounds were analyzed for mass data using a liquid chromatography–mass spectrometry (LCMS)-2020 mass spectrometer (Schimadzu, Tokyo, Japan). All the compounds were dissolved in 1:1 (v/v) mixtures of acetonitrile:methanol, and 10 µL of the resulting solution was injected to acquire the data. The analysis was performed in electrospray ionization mode using a capillary column at a flow rate of 0.2 mL/min with a 50% water/methanol (1:1) mixture for 120 s. Data analysis was performed using lab solution LCMS data processing software. Reaction progress as well as the purity of the compounds were evaluated with thin layer chromatography (TLC) plates by using ethylacetate:n-hexane (3:7) as the eluent, and the developed chromatogram was visualized under ultraviolet light and iodine vapors.

2.1.2 General experimental procedures for characterization of the synthesized compounds

One-pot efficient synthesis of substituted 5H-benzo[h]thiazolo[2,3-b]quinazolines(1A–15A)

A mixture of substituted tetralone (1 mmol), appropriate aromatic aldehydes (1 mmol), and distinctive 2-aminothiazoles (1 mmol) in EtOH (5.0 mL) in the presence of 20 mol% *p*-TSA was heated under reflux for 3–4 h. The reaction mixture was poured into ice-cold water. A solid product was obtained, which was filtered, washed thoroughly with distilled water, and recrystallized from EtOH. Pure crystals were obtained (Scheme 1). The progress of the

reaction was monitored by TLC on pre-coated silica gel-G plates using 30% ethylacetate:n-hexane as the solvent system. TLC revealed just a single spot, which proved the presence of a single product.

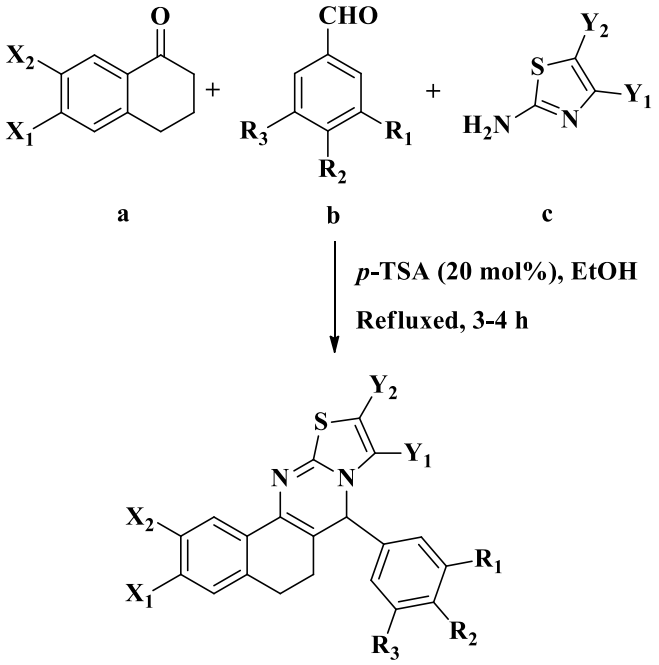

5H-benzo[h]thiazolo[2,3-b]quinazolines (1A-15A)

Scheme 1 One-pot efficient synthetic route to the titled compound (1A–15A)

Note: substituted α-tetralone (a), substituted aromatic aldehydes (b) and distinctive 2-aminothiazoles (c)

Abbreviations: EtOH, ethanol; *p*-TSA, *p*-toluenesulfonic acid.

Two-step synthesis of substituted 5H-benzo[h]thiazolo[2,3-b]quinazolines(1A–15A)

These compounds were synthesized as follows.

Step I

A mixture of substituted tetralones (1 mmol), appropriate aldehydes (1 mmol), piperidine (0.1 mmol), and glacial acetic acid (0.1 mmol) in EtOH (5.0 mL) was heated under reflux for 10–12 h. The reaction mixture was cooled to room temperature for a few minutes and then poured into ice-cold water. A solid product, substituted benzylidene-tetralones, was obtained, which was filtered, washed thoroughly with distilled water, and dried. The dry residue was recrystallized from EtOH. The progress of the reaction was monitored by TLC on precoated silica gel-G plates using 40% ethylacetate:n-hexane as the solvent system.

Step II

A solution of distinctive 2-aminothiazoles (1 mmol) and appropriate benzylidene-tetralones in glacial acetic acid (2.0 mL) was heated under reflux for 18–20 h. The solvent was evaporated under vacuum and then the residue obtained was dissolved in chloroform, washed with water, and the organic layer separated, dried, and evaporated. The resulting solid obtained was recrystallized from EtOH to yield the target compounds (1A–15A; Scheme 2).

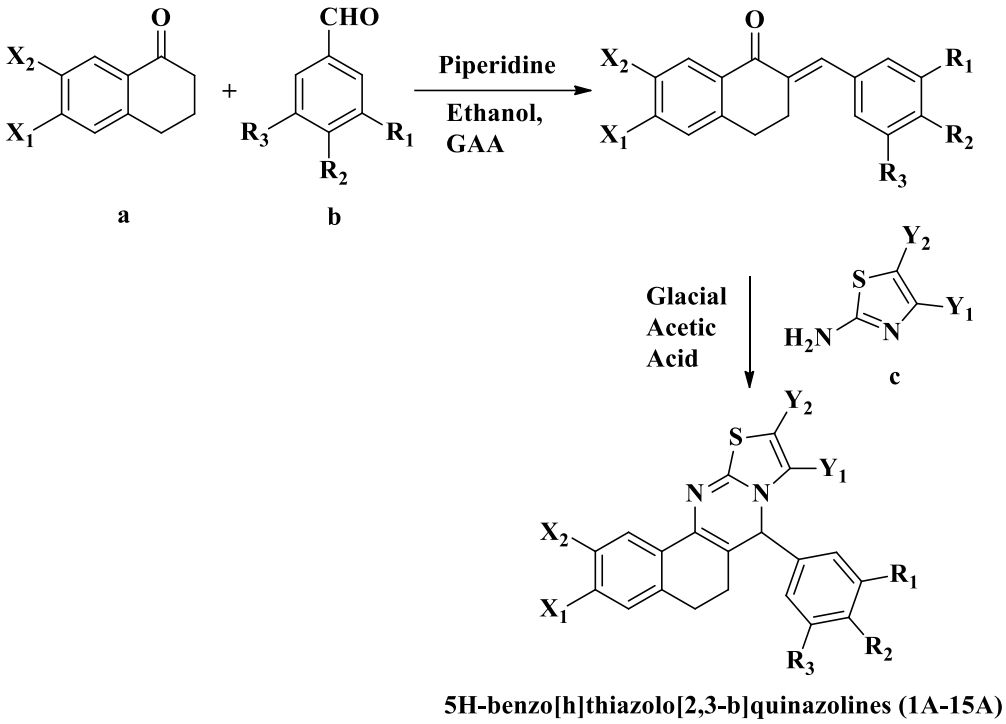

Scheme 2 Two-step synthetic route to the titled compound (1A–15A)

Note: substituted α-tetralone (a), substituted aromatic aldehydes (b) and distinctive 2-aminothiazoles (c)

Abbreviations: GAA, glacial acetic acid.

2.1.2.1 Physical and spectral characterizations

***7-(4-bromophenyl)-6,7-dihydro-5H-benzo[h]thiazolo[2,3-b]quinazoline* (1A)**

Yellow crystals; Yield: 77%; m.p. 190-192ºC; Rf = 0.55 (SiO_2, ethylacetate:*n*-hexane, 3:7, v/v). IR (KBr, cm^{-1}): 3067.7 (C–H, aromatic), 2944.7 (C–H), 1665.8 (C=N), 1595.0 (C=C), 1295.8 (C–N), 1068.4 (C–Br), 740.7 (C–S). ^{1}H NMR (dimethyl sulfoxide [DMSO]-d6, 800 MHz) δppm: 2.95 (t, 2H, J = 8Hz), 3.07 (t, 3H, J = 8Hz), 7.40-7.44 (m, 2H), 7.50 (d, 2H, J = 8Hz), 7.59 (t, 1H, J = 8Hz), 7.67 (d, 4H, J = 8Hz), 7.97 (d, 1H, J = 8Hz). ^{13}C NMR (DMSO-d_6, 200 MHz) δ ppm: 27.12, 28.27, 39.76, 39.87, 39.97, 40.07, 40.18, 122.61, 127.54, 127.90, 129.07, 132.03, 132.43, 133.21, 134.13, 134.83, 134.91, 136.66, 143.93, 187.08. LCMS

(m/z): 393.25 [M - H]$^-$. Anal. calcd. for $C_{20}H_{15}BrN_2S$: C, 60.77; H, 3.82; N, 7.09; Anal. found: C, 60.87; H, 3.83; N, 7.07.

7-(4-bromophenyl)-3-methoxy-10-methyl-6,7-dihydro-5H-benzo[h]thiazolo[2,3-b] quinazoline **(2A)** Yellow crystals; Yield: 82%; m.p. 200-202ºC; Rf = 0.58. (SiO_2, ethylacetate:*n*-hexane, 3:7, v/v). IR (KBr, cm^{-1}): 3013.1 (C–H, aromatic), 2945.5 (C–H), 1663.7 (C=N), 1596.9 (C=C), 1332.5 (C–N), 1263.9 (C–O), 1070.0 (C–Br), 761.9 (C–S). ^{1}H NMR (DMSO-d6, 800 MHz) δppm: 2.92 (t, 2H, J = 8Hz), 3.03 (t, 2H, J = 8Hz), 3.55 (s, 4H), 3.86 (s, 3H), 6.93 (t, 2H, J = 8Hz), 7.48 (d, 2H, J = 8Hz), 7.62 (t, 3H, J = 8Hz), 7.94 (d, 1H, J = 8Hz). ^{13}C NMR (DMSO-d_6, 200 MHz) δ ppm: 27.16, 28.67, 39.76, 39.86, 39.97, 40.07, 40.18, 56.06, 112.81, 114.31, 122.39, 126.65, 130.44, 131.99, 132.35, 134.08, 135.08, 136.84, 146.54, 163.84, 185.75. LCMS (m/z): 437.20 [M - H]$^-$. Anal. calcd. for $C_{22}H_{19}BrN_2OS$: C, 60.14; H, 4.36; N, 6.38. Anal. found: C, 60.25; H, 4.35; N, 6.40.

2-methoxy-7-(3,4,5-trimethoxyphenyl)-6,7-dihydro-5H-benzo[h]thiazolo[2,3-b]quinazoline **(3A)** Yellow crystals; Yield: 83%; m.p. 214-216ºC; Rf = 0.67. (SiO_2, ethylacetate:*n*-hexane, 3:7, v/v). IR (KBr, cm^{-1}): 3002.4 (C–H, aromatic), 2935.5 (C–H), 1661 (C=N), 1578.2 (C=C), 1324.1 (C–N), 1283.9, 1248.4 (C–O), 760.5 (C–S). ^{1}H NMR (DMSO-d6, 800 MHz) δppm: 2.88 (t, 2H, J = 8Hz), 3.13 (t, 2H, J = 8Hz), 3.72 (s, 3H), 3.83 (s, 10H), 6.86 (s, 3H), 7.18 (dd, 1H, J = 8Hz and J = 8Hz), 7.32 (d, 1H, J = 8Hz), 7.44 (d, 1H, J = 8Hz), 7.69 (s, 1H). ^{13}C NMR (DMSO-d_6, 200 MHz) δ ppm: 27.44, 27.54, 39.76, 39.86, 39.97, 40.07, 40.18, 55.77, 56.46, 60.59, 108.04, 110.59, 121.34, 130.34, 131.18, 134.21, 135.25, 136.32, 136.70, 138.58, 153.24, 158.65, 187. LCMS (m/z): 437.20 [M + H]$^+$. Anal. calcd. for $C_{24}H_{24}N_2O_4S$: C, 66.03; H, 5.54; N, 6.42. Anal. found: C, 66.20; H, 5.52; N, 6.45.

2-methoxy-4-(2-methoxy-6,7-dihydro-5H-benzo[h]thiazolo[2,3-b]quinazolin-7-yl)phenol **(4A)** Yellow crystals; Yield: 82%; m.p. 218-220ºC; Rf = 0.50 (SiO_2, ethylacetate:*n*-hexane, 3:7, v/v). IR (KBr, cm^{-1}): 3451 (–OH), 3020.2 (C–H, aromatic), 2937.2 (C–H), 1659.8 (C=N), 1572.5 (C=C), 1326.4 (C–N), 1248.9 (C–O), 744 (C–S). ^{1}H NMR (DMSO-d6, 800 MHz) δppm: 2.86 (t, 2H, J = 8Hz), 3.10 (t, 2H, J = 8Hz), 3.82 (s, 7H), 6.87 (d, 1H, J = 8Hz), 7.05 (d, 1H, J = 8Hz), 7.14-7.18 (m, 3H), 7.31 (d, 1H, J = 8Hz), 7.43 (s, 1H), 7.68 (s, 1H), 9.57 (s, 1H). ^{13}C NMR (DMSO-d_6, 200 MHz) δ ppm: 27.41, 39.76, 39.86, 39.97, 40.07, 55.75, 56.12, 110.61, 115.01, 115.97, 121.03, 124.23, 127, 130.22, 132.93, 134.43, 136.07, 137.28, 147.94, 148.35, 158.62, 186.89. LCMS (m/z): 391.10 [M - H]$^-$. Anal. calcd. for $C_{22}H_{20}N_2O_3S$: C, 67.33; H, 5.14; N, 7.14. Anal. found: C, 67.44; H, 5.16; N, 7.13.

7-(4-bromophenyl)-3-methoxy-6,7-dihydro-5H-benzo[h]thiazolo[2,3-b]quinazoline **(5A)** Yellow crystals; Yield: 78%; m.p. 194-196ºC; Rf = 0.52 (SiO_2, ethylacetate:*n*-hexane, 3:7, v/v). IR (KBr, cm^{-1}): 3012.8 (C–H, aromatic), 2945.7 (C–H), 1663.2 (C=N), 1597 (C=C), 1332.6 (C–N), 1263.4 (C–O), 1070 (C–Br), 762.5 (C–S). ^{1}H NMR (DMSO-d6, 800 MHz) δppm: 2.92 (t, 2H, J = 8Hz), 3.03 (t, 2H, J = 8Hz), 3.86 (s, 4H), 6.93-6.98 (m, 2H), 7.48 (d, 2H, J = 8Hz), 7.62 (s, 1H), 7.66 (d, 3H, J = 8Hz), 7.94 (d, 1H, J = 8Hz). ^{13}C NMR (DMSO-d_6, 200 MHz) δ ppm: 27.15, 28.67, 39.74, 39.84, 39.95, 40.05, 40.15, 56.06, 112.81, 114.31, 122.39, 126.64, 130.44, 131.99, 132.35, 134.08, 135.07, 136.84, 146.55, 163.84, 185.76. LCMS (m/z): 425.15 [M^+]. Anal. calcd. for $C_{21}H_{17}BrN_2OS$: C, 59.30; H, 4.03; N, 6.59. Anal. found: C, 59.19; H, 4.04; N, 6.61.

3-methoxy-7-(3,4,5-trimethoxyphenyl)-6,7-dihydro-5H-benzo[h]thiazolo[2,3-b]quinazoline **(6A)** Light brown; Yield: 86%; m.p. 214-216ºC; Rf = 0.66 (SiO_2, ethylacetate:*n*-hexane, 3:7, v/v). IR (KBr, cm^{-1}): 3050.6 (C–H, aromatic), 2944.8 (C–H), 1659 (C=N), 1598.4 (C=C), 1336.1 (C–N), 1258.6 (C–O), 769.2 (C–S). ^{1}H NMR (DMSO-d6, 800 MHz) δppm: 2.92 (t, 2H, J = 8Hz), 3.12 (t, 2H, J = 8Hz), 3.71 (s, 3H), 3.82 (s, 7H), 3.86 (s, 3H), 6.84 (s, 3H), 6.93 (s, 1H), 6.96 (s, 1H), 7.64 (s, 1H), 7.93 (d, 1H, J = 8Hz). ^{13}C NMR (DMSO-d_6, 200 MHz) δ ppm: 27.27, 28.76, 39.73, 39.84, 39.94, 40.05, 40.15, 56.04, 56.45, 60.58, 107.93, 112.79, 114.15, 126.79, 130.38, 131.34, 135.49, 135.86, 138.43, 146.46, 153.23, 163.73, 185.88. LCMS (m/z): 435.15 [M - H]$^-$. Anal. calcd. for $C_{24}H_{24}N_2O_4S$: C, 66.03; H, 5.54; N, 6.42. Anal. found: C, 66.21; H, 5.56; N, 6.41.

4-(6,7-dihydro-5H-benzo[h]thiazolo[2,3-b]quinazolin-7-yl)phenol **(7A)**

Light brown; Yield: 70%; m.p. 190-192ºC; Rf = 0.45 (SiO_2, ethylacetate:*n*-hexane, 3:7, v/v). IR (KBr, cm^{-1}): 3204.2 (–OH), 2951.5 (C–H, aromatic), 2895.1 (C–H), 1639.9 (C=N), 1556.1 (C=C), 1370.2 (C–N), 740.3 (C–S). ^{1}H NMR (DMSO-d6, 800 MHz) δppm: 2.93 (t, 2H, J = 8Hz), 3.09 (t, 3H, J = 8Hz), 6.86 (d, 2H, J = 8Hz), 7.37-7.44 (m, 5H), 7.56 (t, 1H, J = 8Hz), 7.67 (s, 1H), 7.94 (d, 1H, J = 8Hz), 9.98 (s, 1H). ^{13}C NMR (DMSO-d_6, 200 MHz) δ ppm: 27.18, 28.29, 39.76, 39.86, 39.97, 40.07, 40.17, 116, 126.54, 127.40, 127.75, 128.88, 132.65, 132.79, 133.58, 133.73, 136.83, 143.63, 158.91, 187.06. LCMS (m/z): 331.05 [M - H]$^-$. Anal. calcd. for $C_{20}H_{16}N_2OS$: C, 72.26; H, 4.85; N, 8.43. Anal. found: C, 72.45; H, 4.87; N, 8.39.

7-(4-chlorophenyl)-2-methoxy-9-methyl-6,7-dihydro-5H-benzo[h]thiazolo[2,3-b] quinazoline **(8A)** Yellow crystals; Yield: 65%; m.p. 196-198ºC; Rf = 0.40 (SiO_2, ethylacetate:*n*-hexane, 3:7, v/v). IR (KBr, cm^{-1}): 3067.6 (C–H, aromatic), 2941.2 (C–H), 1660.7 (C=N), 1589.1 (C=C), 1322.7 (C–N), 1251.5 (C–O), 1031.5 (C–Cl), 743.9 (C–S). ^{1}H

NMR (DMSO-d6, 800 MHz) δppm: 2.88 (t, 4H, J = 8Hz), 3.04 (t, 4H, J = 8Hz), 3.36 (s, 3H), 7.19 (dd, 1H, J = 16Hz and J = 16Hz), 7.32 (d, 1H, J = 16Hz), 7.45 (d, 1H, J = 8Hz), 7.53-7.58 (m, 4H), 7.69 (s, 1H). ^{13}C NMR (DMSO-d_6, 200 MHz) δ ppm:27.30, 27.46, 39.78, 39.88, 39.99, 40.09, 40.19, 55.79, 110.61, 121.49, 129.10, 130.43, 132.19, 133.83, 134.06, 134.59, 134.83, 136.39, 136.56, 158.68, 186.92. LCMS (m/z): 397.20 [M^{+2}]. Anal. calcd. for $C_{22}H_{19}ClN_2OS$: C, 66.91; H, 4.85; N, 7.09. Anal. found: C, 66.79; H, 4.87; N, 7.12.

7-(4-chlorophenyl)-3-methoxy-9-methyl-6,7-dihydro-5H-benzo[h]thiazolo[2,3-b] quinazoline **(9A)** Yellow crystals; Yield: 68%; m.p. 196-198ºC; Rf = 0.42 (SiO_2, ethylacetate:*n*-hexane, 3:7, v/v). IR (KBr, cm^{-1}): 3050.8 (C–H, aromatic), 2943.9 (C–H), 1660.5 (C=N), 1587.9 (C=C), 1336.3 (C–N), 1274.7 (C–O), 1030.8 (C–Cl), 760.5 (C–S). ^{1}H NMR (DMSO-d6, 800 MHz) δppm: 2.92 (t, 4H, J = 8Hz), 3.04 (t, 4H, J = 8Hz), 3.43 (s, 3H), 6.93-6.97 (m, 2H), 7.52 (dd, 4H, J = 24Hz and J = 24Hz), 7.64 (s, 1H), 7.94 (d, 1H, J = 8Hz). ^{13}C NMR (DMSO-d_6, 200 MHz) δ ppm: 27.14, 28.68, 39.78, 39.88, 39.99, 40.09, 40.19, 56.06, 112.81, 114.30, 126.67, 129.06, 130.43, 132.10, 133.65, 134.01, 136.78, 146.53, 163.84, 185.73. LCMS (m/z): 395.25 [M^+]. Anal. calcd. for $C_{22}H_{19}ClN_2OS$: C, 66.91; H, 4.85; N, 7.09. Anal. found: C, 66.75; H, 4.86; N, 7.11.

7-(4-chlorophenyl)-9-methyl-6,7-dihydro-5H-benzo[h]thiazolo[2,3-b]quinazoline **(10A)** Yellow crystals; Yield: 64%; m.p. 188-190ºC; Rf = 0.44 (SiO_2, ethylacetate:*n*-hexane, 3:7, v/v). IR (KBr, cm^{-1}): 3067.7 (C–H, aromatic), 2944.7 (C–H), 1668.1 (C=N), 1596.4 (C=C), 1317.4 (C–N), 1027.7 (C–Cl), 743 (C–S). ^{1}H NMR (DMSO-d6, 800 MHz) δppm: 2.95 (t, 4H, J = 8Hz), 3.07 (t, 4H, J = 8Hz), 7.39-7.44 (m, 2H), 7.54-7.61 (m, 5H), 7.70 (s, 1H), 7.97 (s, 1H). ^{13}C NMR (DMSO-d_6, 200 MHz) δ ppm: 27.11, 28.28, 39.78, 39.88, 39.99, 40.09, 40.20, 127.53, 127.89, 129.11, 132.20, 133.23, 133.85, 134.12, 134.58, 134.76, 136.61, 143.92, 187.07. LCMS (m/z): 365.20 [M^+]. Anal. calcd. for $C_{21}H_{17}ClN_2S$: C, 69.12; H, 4.70; N, 7.68. Anal. found: C, 69.25; H, 4.71; N, 7.67.

7-(4-chlorophenyl)-2-methoxy-6,7-dihydro-5H-benzo[h]thiazolo[2,3-b]quinazoline **(11A)** Yellow crystals; Yield: 70%; m.p. 194-196ºC; Rf = 0.49 (SiO_2, ethylacetate:*n*-hexane, 3:7, v/v). IR (KBr, cm^{-1}): 3067.8 (C–H, aromatic), 2940.6 (C–H), 1660.6 (C=N), 1589.3 (C=C), 1323.0 (C–N), 1252.2 (C–O), 1031.6 (C–Cl), 744.8 (C–S). ^{1}H NMR (DMSO-d6, 800 MHz) δppm: 2.88 (t, 2H, J = 8Hz), 3.04 (t, 2H, J = 8Hz), 3.82 (s, 4H), 7.20 (d, 1H, J = 8Hz), 7.33 (d, 1H, J = 8Hz), 7.45 (s, 1H), 7.53-7.58 (m, 5H), 7.69 (s, 1H). ^{13}C NMR (DMSO-d_6, 200 MHz) δ ppm: 27.30, 27.46, 39.78, 39.88, 39.99, 40.09, 40.19, 55.79, 110.62, 121.50, 129.10, 130.44, 132.19, 133.83, 134.07, 134.83, 136.56, 158.69, 186.98. LCMS (m/z): 381.25 [M^+].

Anal. calcd. for $C_{21}H_{17}ClN_2OS$: C, 66.22; H, 4.50; N, 7.35. Anal. found: C, 66.32; H, 4.52; N, 7.33.

7-(4-chlorophenyl)-6,7-dihydro-5H-benzo[h]thiazolo[2,3-b]quinazoline **(12A)**

Yellow crystals; Yield: 61%; m.p. 184-186ºC; Rf = 0.43 (SiO_2, ethylacetate:*n*-hexane, 3:7, v/v). IR (KBr, cm^{-1}): 3069.4 (C–H, aromatic), 2944.7 (C–H), 1668.1 (C=N), 1596.4 (C=C), 1317.4 (C–N), 1020.1 (C–Cl), 742.7 (C–S). ^{1}H NMR (DMSO-d6, 800 MHz) δppm: 2.97 (t, 2H, J = 8Hz), 3.09 (t, 3H, J = 8Hz), 7.40-7.44 (m, 2H), 7.54-7.61 (m, 6H), 7.70 (s, 1H), 7.98 (d, 1H, J = 8Hz). ^{13}C NMR (DMSO-d_6, 200 MHz) δ ppm: 27.11, 28.28, 39.78, 39.88, 39.99, 40.09, 40.19, 127.53, 127.89, 129.06, 129.10, 132.20, 133.23, 133.85, 134.11, 134.58, 134.76, 136.60, 143.92, 187.07. LCMS (m/z): 353.0 [M^{+2}]. Anal. calcd. for $C_{20}H_{15}ClN_2S$: C, 68.46; H, 4.31; N, 7.98. Anal. found: C, 68.53; H, 4.34; N, 7.95.

7-(4-chlorophenyl)-2-methoxy-10-methyl-6,7-dihydro-5H-benzo[h]thiazolo[2,3-b] quinazoline **(13A)** Yellow crystals; Yield: 74%; m.p. 198-200ºC; Rf = 0.46 (SiO_2, ethylacetate:*n*-hexane, 3:7, v/v). IR (KBr, cm^{-1}): 3067.9 (C–H, aromatic), 2940.4 (C–H), 1660.7 (C=N), 1591 (C=C), 1324.7 (C–N), 1256.8 (C–O), 1033.4 (C–Cl), 748.3 (C–S). ^{1}H NMR (DMSO-d6, 800 MHz) δppm: 2.88 (t, 4H, J = 8Hz), 3.04 (t, 4H, J = 8Hz), 3.47 (s, 3H), 7.19 (d, 1H, J = 8Hz), 7.32 (d, 1H, J = 8Hz), 7.45 (s, 1H), 7.53-7.58 (m, 4H), 7.68 (s, 1H). ^{13}C NMR (DMSO-d_6, 200 MHz) δ ppm: 27.30, 27.46, 39.78, 39.88, 39.99, 40.09, 40.19, 55.78, 110.61, 121.48, 129.09, 130.42, 132.18, 133.83, 134.06, 134.59, 134.82, 136.38, 136.54, 158.67, 186.91. LCMS (m/z): 393.25 [M - H]$^-$. Anal. calcd. for $C_{22}H_{19}ClN_2OS$: C, 66.91; H, 4.85; N, 7.09. Anal. found: C, 66.83; H, 4.87; N, 7.10.

7-(4-chlorophenyl)-3-methoxy-10-methyl-6,7-dihydro-5H-benzo[h]thiazolo[2,3-b] quinazoline **(14A)** Light brown; Yield: 76%; m.p. 198-200ºC; Rf = 0.48 (SiO_2, ethylacetate:*n*-hexane, 3:7, v/v). IR (KBr, cm^{-1}): 3051.0 (C–H, aromatic), 2938.8 (C–H), 1653.8 (C=N), 1602.6 (C=C), 1339 (C–N), 1266.3 (C–O), 1091.8 (C–Cl), 764.1 (C–S). ^{1}H NMR (DMSO-d6, 800 MHz) δppm: 2.94 (t, 3H, J = 8Hz), 3.06 (t, 4H, J = 8Hz), 3.86 (s, 4H), 6.93-6.98 (m, 2H), 7.53-7.56 (m, 4H), 7.64 (s, 1H), 7.95 (d, 1H, J = 8Hz). ^{13}C NMR (DMSO-d_6, 200 MHz) δ ppm: 27.14, 28.68, 39.78, 39.88, 39.99, 40.09, 40.19, 56.06, 112.81, 114.30, 126.67, 129.07, 130.43, 132.11, 133.65, 134.01, 134.74, 136.79, 146.54, 163.84, 185.74. LCMS (m/z): 393.25 [M - H]$^-$. Anal. calcd. for $C_{22}H_{19}ClN_2OS$: C, 66.91; H, 4.85; N, 7.09. Anal. found: C, 66.79; H, 4.86; N, 7.07.

7-(4-chlorophenyl)-10-methyl-6,7-dihydro-5H-benzo[h]thiazolo[2,3-b]quinazoline **(15A)**

Yellow crystals; Yield: 79%; m.p. 186-188ºC; Rf = 0.56 (SiO_2, ethylacetate:*n*-hexane, 3:7, v/v). IR (KBr, cm^{-1}): 3069.7 (C–H, aromatic), 2944.8 (C–H), 1668.1 (C=N), 1596.1 (C=C), 1317.3 (C–N), 1089.4 (C–Cl), 742.3 (C–S). ^{1}H NMR (DMSO-d6, 800 MHz) δppm: 2.97 (t, 4H, J = 8Hz), 3.09 (t, 4H, J = 8Hz), 7.40-7.44 (m, 2H), 7.55-7.61 (m, 5H), 7.70 (s, 1H), 7.98 (d, 1H, J = 8Hz). ^{13}C NMR (DMSO-d_6, 200 MHz) δ ppm: 27.11, 28.29, 39.79, 39.89, 39.99, 40.09, 40.20, 127.54, 127.90, 129.07, 129.11, 132.21, 133.24, 133.85, 134.13, 134.59, 134.76, 136.61, 143.93, 187.08. LCMS (m/z): 367.30 [M^{+2}]. Anal. calcd. for $C_{21}H_{17}ClN_2S$: C, 69.12; H, 4.70; N, 7.68. Anal. found: C, 69.23; H, 4.72; N, 7.66.

One-pot efficient synthesis of substituted indeno[1,2-d]thiazolo[3,2-a]pyrimidines(1B–15B)

A mixture of substituted α-indanone (1 mmol), appropriate aromatic aldehydes (1 mmol), and distinctive 2-aminothiazoles (1 mmol) in EtOH (5.0 mL) in the presence of 20 mol% *p*-TSA was heated under reflux for 3–4 h. The reaction mixture was then poured into ice-cold water. A solid product was obtained, which was filtered, washed thoroughly with distilled water, and recrystallized from EtOH. Pure crystals were obtained (Scheme 3). The progress of the reaction was monitored by TLC on pre-coated silica gel-G plates using 30% ethylacetate:n-hexane as the solvent system. TLC revealed just a single spot, which proved the presence of a single product.

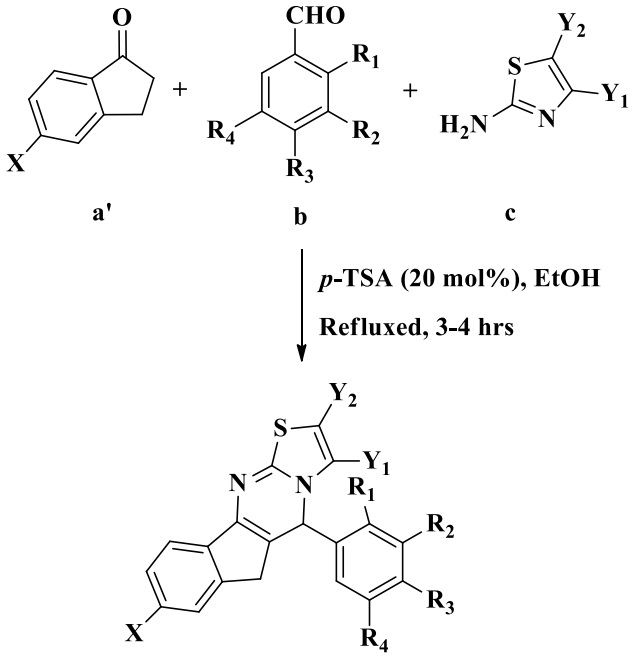

Indeno[1,2-*d*]thiazolo[3,2-*a*]pyrimidines (1B-15B)

Scheme 3 One-pot efficient synthetic route to the titled compound (1B–15B)

Note: substituted α-indanone (a′), substituted aromatic aldehydes (b) and distinctive 2-aminothiazoles (c) **Abbreviations:** EtOH, ethanol; *p*-TSA, *p*-toluenesulfonic acid.

Two-step synthesis of substituted indeno[1,2-d]thiazolo[3,2-a]pyrimidines(1B–15B)

These compounds were synthesized as follows.

Step I

A mixture of substituted indanones (1 mmol), appropriate aldehydes (1 mmol), piperidine (0.1 mmol), and glacial acetic acid (0.1 mmol) in EtOH (5.0 mL) was heated under reflux for 10–12 h. The reaction mixture was cooled to room temperature for a few minutes and then poured into ice-cold water. A solid product, substituted benzylidene-indanones, was obtained, which was filtered, washed thoroughly with distilled water, and dried. The dry residue was recrystallized from EtOH. The progress of the reaction was monitored by TLC on pre-coated silica gel-G plates using 40% ethylacetate:n-hexane as the solvent system.

Step II

A solution of distinctive 2-aminothiazoles (1 mmol) and appropriate benzylidene-indanones in glacial acetic acid (2.0 mL) was heated under reflux for 18–20 h. The solvent was evaporated under vacuum and then the residue obtained was dissolved in chloroform, washed with water, and the organic layer separated, dried, and evaporated. The resulting solid obtained was recrystallized from EtOH to yield the target compounds (1B–15B; Scheme 4).

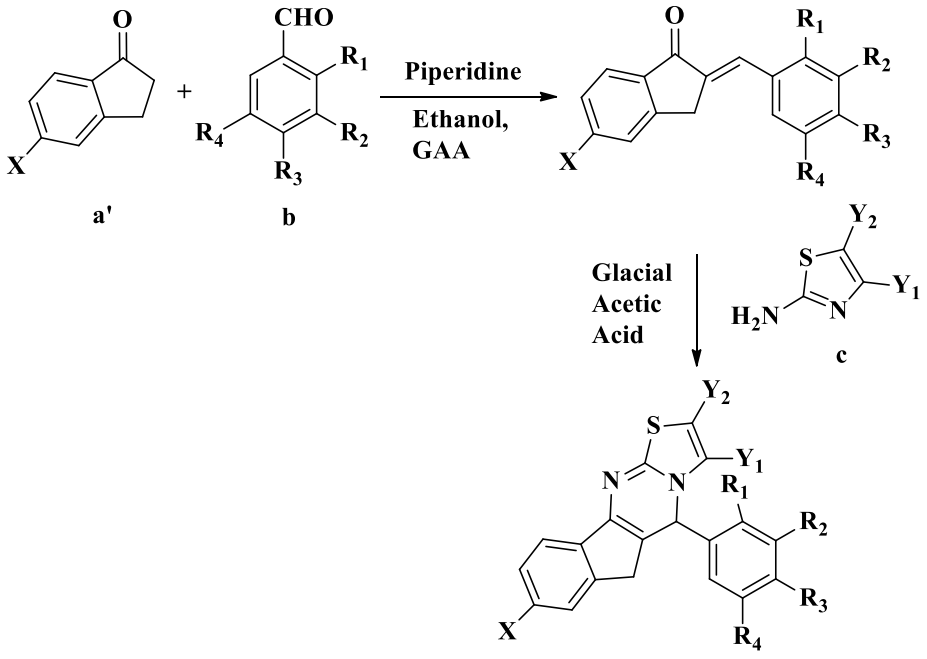

Scheme 4 Two-step synthetic route to the titled compound (1B–15B)

Note: substituted α-indanone (a′), substituted aromatic aldehydes (b) and distinctive 2-aminothiazoles (c).

Abbreviations: GAA, glacial acetic acid.

2.1.2.2 Physical and spectral characterizations

***5-(4-bromophenyl)-5,6-dihydroindeno[1,2-d]thiazolo[3,2-a]pyrimidine* (1B)**

Yellow crystals; Yield: 75%; m.p. 186-188ºC; Rf = 0.54 (SiO_2, ethylacetate:*n*-hexane, 3:7, v/v). IR (KBr, cm^{-1}): 3023.4 (C–H, aromatic), 2928.9 (C–H), 1693.2 (C=N), 1620.8 (C=C), 1325.1 (C–N), 733.9 (C–S), 1070.9 (C–Br). ^{1}H NMR (DMSO-d6, 800 MHz) δppm: 4.14 (s, 3H), 7.50-7.54 (m, 2H), 7.70-7.82 (m, 8H). ^{13}C NMR (DMSO-d_6, 200 MHz) δ ppm: 32.32, 39.76, 39.86, 39.97, 40.07, 40.17, 123.83, 124.19, 127.21, 128.28, 132.01, 132.47, 133.11, 134.61, 135.59, 136.38, 137.56, 150.54, 193.80. LCMS (m/z): 381.25 [M^+]. Anal. calcd. for $C_{19}H_{13}BrN_2S$: C, 59.85; H, 3.44; N, 7.35. Anal. found: C, 59.97; H, 3.42; N, 7.34.

***5-(2-chlorophenyl)-5,6-dihydroindeno[1,2-d]thiazolo[3,2-a]pyrimidine* (2B)**

Yellow crystals; Yield: 66%; m.p. 178-180ºC; Rf = 0.41 (SiO_2, ethylacetate:*n*-hexane, 3:7, v/v). IR (KBr, cm^{-1}): 3064.6 (C–H, aromatic), 2922.5 (C–H), 1697.1 (C=N), 1621.3 (C=C), 1326.1 (C–N), 740.4 (C–S), 1037.4 (C–Cl). ^{1}H NMR (DMSO-d6, 800 MHz) δppm: 4.14 (s, 3H), 7.49-7.53 (m, 4H), 7.63 (d, 1H, 1H, J = 8Hz), 7.68 (d, 1H, J = 8Hz), 7.74 (t, 1H, J = 8Hz), 7.83 (s, 1H), 7.98 (d, 1H, J = 8Hz). ^{13}C NMR (DMSO-d_6, 200 MHz) δ ppm: 31.84, 39.76, 39.86, 39.97, 40.07, 40.17, 124.32, 127.24, 128.33, 130.56, 130.97, 131.70, 132.96, 135.39, 135.76, 137.43, 138.14, 150.80, 193.62. LCMS (m/z): 339.20 [M^{+2}]. Anal. calcd. for $C_{19}H_{13}ClN_2S$: C, 67.75; H, 3.89; N, 8.32. Anal. found: C, 67.65; H, 3.91; N, 8.30.

***5-(4-bromophenyl)-2-methyl-5,6-dihydroindeno[1,2-d]thiazolo[3,2-a]pyrimidine* (3B)**

Yellow crystals; Yield: 80%; m.p. 192-194ºC; Rf = 0.57 (SiO_2, ethylacetate:*n*-hexane, 3:7, v/v). IR (KBr, cm^{-1}): 3024.1 (C–H, aromatic), 2926.7 (C–H), 1693.3 (C=N), 1621.2 (C=C), 1325.3 (C–N), 733.5 (C–S), 1070.4 (C–Br). ^{1}H NMR (DMSO-d6, 800 MHz) δppm: 4.14 (s, 6H), 7.50-7.54 (m, 2H), 7.69-7.78 (m, 6H), 7.81 (d, 1H, J = 8Hz). ^{13}C NMR (DMSO-d_6, 200 MHz) δ ppm: 34.53, 41.97, 42.08, 42.18, 42.29, 42.39, 126.04, 126.40, 129.42, 130.49, 134.23, 134.67, 135.31, 136.82, 137.79, 138.59, 139.77, 152.75, 196. LCMS (m/z): 396.95 [M+ H]$^+$. Anal. calcd. for $C_{20}H_{15}BrN_2S$: C, 60.77; H, 3.82; N, 7.09. Anal. found: C, 60.85; H, 3.81; N, 7.08.

5-(4-bromophenyl)-8-methoxy-3-methyl-5,6-dihydroindeno[1,2-d]thiazolo[3,2-a]pyrimidine **(4B)** Yellow crystals; Yield: 69%; m.p. 198-200ºC; Rf = 0.48 (SiO_2, ethylacetate:*n*-hexane, 3:7, v/v). IR (KBr, cm^{-1}): 3018.7 (C–H, aromatic), 2903.2 (C–H), 1687.0 (C=N), 1622.9 (C=C), 1335.3 (C–N), 1288.7 (C–O), 763.9 (C–S), 1071.3 (C–Br). ^{1}H NMR (DMSO-d6, 800 MHz) δppm: 3.91 (s, 5H), 4.08 (s, 4H), 7.05 (d, 1H, J = 8Hz), 7.20 (s, 1H), 7.44 (s, 1H), 7.71-7.75 (m, 5H). ^{13}C NMR (DMSO-d_6, 200 MHz) δ ppm: 32.39, 39.76, 39.86, 39.97, 40.07, 40.18, 56.32, 110.65, 115.99, 123.49, 126.06, 130.67, 130.88, 132.42, 132.89, 134.77, 136.98, 153.47, 165.53, 191.97. LCMS (m/z): 425.20 [M^+]. Anal. calcd. for $C_{21}H_{17}BrN_2OS$: C, 59.30; H, 4.03; N, 6.59. Anal. found: C, 59.20; H, 4.04; N, 6.61.

5-(4-bromophenyl)-3-methyl-5,6-dihydroindeno[1,2-d]thiazolo[3,2-a]pyrimidine **(5B)** Yellow crystals; Yield: 78%; m.p. 192-194ºC; Rf = 0.54 (SiO_2, ethylacetate:*n*-hexane, 3:7, v/v). IR (KBr, cm^{-1}): 3025.1 (C–H, aromatic), 2928.1 (C–H), 1693.1 (C=N), 1622.1 (C=C), 1324.7 (C–N), 732.9 (C–S), 1070.1 (C–Br). ^{1}H NMR (DMSO-d6, 800 MHz) δppm: 4.14 (s, 6H), 7.51-7.54 (m, 2H), 7.70-7.77 (m, 6H), 7.82 (d, 1H, J = 8Hz). ^{13}C NMR (DMSO-d_6, 200 MHz) δ ppm: 32.32, 39.76, 39.86, 39.97, 40.07, 40.18, 123.83, 124.19, 127.21, 128.28, 132.01, 132.46, 133.10, 134.61, 135.59, 136.38, 137.56, 150.54, 193.79. LCMS (m/z): 395.00 [M^+]. Anal. calcd. for $C_{20}H_{15}BrN_2S$: C, 60.77; H, 3.82; N, 7.09. Anal. found: C, 60.89; H, 3.80; N, 7.11.

5-(4-bromophenyl)-8-methoxy-5,6-dihydroindeno[1,2-d]thiazolo[3,2-a]pyrimidine **(6B)** Yellow crystals; Yield: 75%; m.p. 188-190ºC; Rf = 0.61 (SiO_2, ethylacetate:*n*-hexane, 3:7, v/v). IR (KBr, cm^{-1}): 3018.4 (C–H, aromatic), 2902.6 (C–H), 1686.9 (C=N), 1622.6 (C=C), 1335.0 (C–N), 1288.6 (C–O), 763.9 (C–S), 1071.1 (C–Br). ^{1}H NMR (DMSO-d6, 800 MHz) δppm: 3.91 (s, 3H), 4.08 (s, 3H), 7.06 (d, 1H, J = 8Hz), 7.20 (s, 1H), 7.44 (s, 1H), 7.72-7.75 (m, 6H). ^{13}C NMR (DMSO-d_6, 200 MHz) δ ppm: 32.39, 39.76, 39.86, 39.97, 40.07, 40.18, 56.32, 110.65, 115.99, 123.49, 126.06, 130.67, 130.88, 132.42, 132.89, 134.77, 136.98, 153.47, 165.53, 192.08. LCMS (m/z): 413.25 [M^{+2}]. Anal. calcd. for $C_{20}H_{15}BrN_2OS$: C, 58.40; H, 3.68; N, 6.81. Anal. found: C, 58.31; H, 3.70; N, 6.83.

5-(4-bromophenyl)-8-methoxy-2-methyl-5,6-dihydroindeno[1,2-d]thiazolo[3,2-a]pyrimidine **(7B)** Yellow crystals; Yield: 77%; m.p. 198-200ºC; Rf = 0.47 (SiO_2, ethylacetate:*n*-hexane, 3:7, v/v). IR (KBr, cm^{-1}): 3018.2 (C–H, aromatic), 2902.5 (C–H), 1687.1 (C=N), 1622.7 (C=C), 1335.7 (C–N), 1288.7, 1246.9 (C–O), 763.5 (C–S), 1071.9 (C–Br). ^{1}H NMR (DMSO-d6, 800 MHz) δppm: 3.90 (s, 5H), 4.07 (s, 4H), 7.04 (dd, 1H, J = 8Hz and J = 8Hz), 7.19 (d,

1H, J = 8Hz), 7.44 (s, 1H), 7.70-7.75 (m, 5H). ^{13}C NMR (DMSO-d_6, 200 MHz) δ ppm: 32.39, 39.76, 39.86, 39.97, 40.07, 40.18, 56.31, 110.64, 115.98, 123.49, 126.05, 130.66, 130.88, 132.41, 132.89, 134.77, 136.97, 153.46, 165.52, 191.96. LCMS (m/z): 425.00 [M^+]. Anal. calcd. for $C_{21}H_{17}BrN_2OS$: C, 59.30; H, 4.03; N, 6.59. Anal. found: C, 59.18; H, 4.04; N, 6.60.

5-(3,4,5-trimethoxyphenyl)-5,6-dihydroindeno[1,2-d]thiazolo[3,2-a]pyrimidine **(8B)**

Yellow crystals; Yield: 72%; m.p. 206-208ºC; Rf = 0.52 (SiO_2, ethylacetate:*n*-hexane, 3:7, v/v). IR (KBr, cm^{-1}): 3046.1 (C–H, aromatic), 2942.6 (C–H), 1690.6 (C=N), 1624.7 (C=C), 1328.0 (C–N), 1266.5 (C–O), 736.4 (C–S). ^{1}H NMR (DMSO-d6, 800 MHz) δppm: 3.36 (s, 3H), 3.90 (s, 7H), 4.20 (s, 2H), 7.14 (s, 3H), 7.49-7.54 (m, 2H), 7.71-7.74 (m, 2H), 7.80(s, 1H). ^{13}C NMR (DMSO-d_6, 200 MHz) δ ppm: 32.08, 39.76, 39.86, 39.97, 40.07, 40.18, 56.49, 60.64, 108.84, 124.08, 127.16, 128.18, 130.87, 133.79, 134.58, 135.37, 137.75, 139.59, 150.56, 153.51, 193.82. LCMS (m/z): 393.25 [M+ H]$^+$. Anal. calcd. for $C_{22}H_{20}N_2O_3S$: C, 67.33; H, 5.14; N, 7.14. Anal. found: C, 67.21; H, 5.16; N, 7.16.

8-methoxy-5-(3,4,5-trimethoxyphenyl)-5,6-dihydroindeno[1,2-d]thiazolo[3,2-a]pyrimidine **(9B)** Yellow crystals; Yield: 66%; m.p. 208-210ºC; Rf = 0.68 (SiO_2, ethylacetate:*n*-hexane, 3:7, v/v). IR (KBr, cm^{-1}): 3060.8 (C–H, aromatic), 2939.2 (C–H), 1679.6 (C=N), 1624.6 (C=C), 1330.4 (C–N), 1241.5 (C–O), 760.8 (C–S). ^{1}H NMR (DMSO-d6, 800 MHz) δpp: 3.35 (s, 3H), 3.74 (s, 6H), 3.91 (s, 4H), 4.15 (s, 2H), 7.04 (dd, 1H, J = 8Hz and J = 8Hz), 7.10 (s, 3H), 7.23 (s, 1H), 7.44 (s, 1H), 7.73 (d, 1H, J = 8Hz). ^{13}C NMR (DMSO-d_6, 200 MHz) δ ppm: 32.22, 39.76, 39.86, 39.97, 40.07, 40.18, 56.31, 56.44, 60.63, 108.59, 110.41, 116.15, 125.87, 131.03, 132.40, 135.15, 139.32, 153.49, 165.38, 192.08. LCMS (m/z): 421.15 [M–H]$^-$. Anal. calcd. for $C_{23}H_{22}N_2O_4S$: C, 65.38; H, 5.25; N, 6.63. Anal. found: C, 65.22; H, 5.26; N, 6.64.

5-(4-chlorophenyl)-3-methyl-5,6-dihydroindeno[1,2-d]thiazolo[3,2-a]pyrimidine **(10B)**

Yellow crystals; Yield: 78%; m.p. 182-184ºC; Rf = 0.43 (SiO_2, ethylacetate:*n*-hexane, 3:7, v/v). IR (KBr, cm^{-1}): 3066.8 (C–H, aromatic), 3030.5 (C–H), 1695.5 (C=N), 1623.9 (C=C), 1326.7 (C–N), 729.1 (C–S), 1090.1 (C–Cl). ^{1}H NMR (DMSO-d6, 800 MHz) δppm: 4.13 (s, 6H), 7.49-7.58 (m, 3H), 7.68 (d, 1H, J = 8Hz), 7.72 (d, 1H, J = 8Hz), 7.80-7.83 (m, 4H). ^{13}C NMR (DMSO-d_6, 200 MHz) δ ppm: 32.28, 39.76, 39.86, 39.97, 40.07, 40.18, 124.16, 127.19, 128.25, 129.51, 131.90, 132.88, 134.28, 134.93, 135.55, 136.25, 137.56, 150.52, 193.76.

LCMS (m/z): 351.02 [M^+]. Anal. calcd. for $C_{20}H_{15}ClN_2S$: C, 68.46; H, 4.31; N, 7.98. Anal. found: C, 68.63; H, 4.30; N, 7.96.

***5-(4-chlorophenyl)-8-methoxy-3-methyl-5,6-dihydroindeno[1,2-d]thiazolo[3,2-a]pyrimidine* (11B)** Yellow crystals; Yield: 65%; m.p. 186-188ºC; Rf = 0.48 (SiO_2, ethylacetate:*n*-hexane, 3:7, v/v). IR (KBr, cm^{-1}): 3019.3 (C–H, aromatic), 2967.8 (C–H), 1695.5 (C=N), 1623.9 (C=C), 1326.7 (C–N), 1249.1 (C–O), 729.1 (C–S), 1090.1 (C–Cl). ^{1}H NMR (DMSO-d6, 800 MHz) δppm: 3.90 (s, 5H), 4.07 (s, 4H), 7.03 (d, 1H, J = 8Hz), 7.18 (s, 1H), 7.44 (s, 1H), 7.56 (d, 2H, J = 8Hz), 7.73-7.79 (m, 3H). ^{13}C NMR (DMSO-d_6, 200 MHz) δ ppm: 32.35, 39.77, 39.87, 39.97, 40.08, 40.18, 56.30, 110.63, 115.96, 126.04, 129.47, 130.56, 130.89, 132.66, 134.44, 134.61, 136.85, 153.45, 165.51, 191.94. LCMS (m/z): 381.20 [M^+]. Anal. calcd. for $C_{21}H_{17}ClN_2OS$: C, 66.22; H, 4.50; N, 7.35. Anal. found: C, 66.38; H, 4.49; N, 7.34.

***5-(4-chlorophenyl)-5,6-dihydroindeno[1,2-d]thiazolo[3,2-a]pyrimidine* (12B)**

Yellow crystals; Yield: 65%; m.p. 176-178ºC; Rf = 0.51 (SiO_2, ethylacetate:*n*-hexane, 3:7, v/v). IR (KBr, cm^{-1}): 3067.4 (C–H, aromatic), 3030.3 (C–H), 1697.1 (C=N), 1625.0 (C=C), 1326.7 (C–N), 729.2 (C–S), 1093.0 (C–Cl). ^{1}H NMR (DMSO-d6, 800 MHz) δppm: 4.13 (s, 3H), 7.50 (s, 1H), 7.54 (s, 1H), 7.57 (d, 2H, J = 8Hz), 7.68 (d, 1H, J = 8Hz), 7.72 (d, 1H, J = 8Hz), 7.80-7.83 (m, 4H). ^{13}C NMR (DMSO-d_6, 200 MHz) δ ppm: 32.28, 39.75, 39.86, 39.96, 40.07, 40.17, 124.17, 127.19, 128.26, 129.51, 131.91, 132.88, 134.28, 134.93, 135.55, 136.25, 137.55, 150.52, 193.77. LCMS (m/z): 339.15 [M^{+2}]. Anal. calcd. for $C_{19}H_{13}ClN_2S$: C, 67.75; H, 3.89; N, 8.32. Anal. found: C, 67.61; H, 3.90; N, 8.33.

***5-(4-chlorophenyl)-8-methoxy-5,6-dihydroindeno[1,2-d]thiazolo[3,2-a]pyrimidine* (13B)**

Light brown crystals; Yield: 60%; m.p. 184-186ºC; Rf = 0.47 (SiO_2, ethylacetate:*n*-hexane, 3:7, v/v). IR (KBr, cm^{-1}): 3058.1, 3019.1 (C–H, aromatic), 2943.5 (C–H), 1688.0 (C=N), 1622.1 (C=C), 1304.0 (C–N), 1249.4 (C–O), 765.2 (C–S), 1088.4 (C–Cl). ^{1}H NMR (DMSO-d6, 800 MHz) δppm: 3.90 (s, 3H), 4.06 (s, 3H), 7.03 (d, 1H, J = 8Hz), 7.18 (s, 1H), 7.44 (s, 1H), 7.56 (d, 2H, J = 8Hz), 7.73-7.79 (m, 4H). ^{13}C NMR (DMSO-d_6, 200 MHz) δ ppm: 32.36, 39.77, 39.87, 39.98, 40.09, 40.19, 56.30, 110.63, 115.96, 126.03, 129.47, 130.55, 130.87, 132.65, 134.43, 134.61, 136.85, 153.44, 165.50, 191.93. LCMS (m/z): 339.05 [M^{+2}]. Anal. calcd. for $C_{20}H_{15}ClN_2OS$: C, 65.48; H, 4.12; N, 7.64. Anal. found: C, 65.63; H, 4.10; N, 7.63.

***5-(4-chlorophenyl)-2-methyl-5,6-dihydroindeno[1,2-d]thiazolo[3,2-a]pyrimidine* (14B)**

Yellow crystals; Yield: 68%; m.p. 180-182ºC; Rf = 0.51 (SiO_2, ethylacetate:*n*-hexane, 3:7, v/v). IR (KBr, cm^{-1}): 3031.5 (C–H, aromatic), 2923.5 (C–H), 1695.5 (C=N), 1623.4 (C=C), 1326.9 (C–N), 729.2 (C–S), 1089.7 (C–Cl). ^{1}H NMR (DMSO-d6, 800 MHz) δppm: 4.13 (s, 6H), 7.49-7.59 (m, 3H), 7.68-7.73 (m, 2H), 7.80-7.84 (m, 4H). ^{13}C NMR (DMSO-d_6, 200 MHz) δ ppm: 32.28, 39.65, 39.86, 39.96, 40.07, 40.28, 124.17, 127.19, 128.26, 129.5, 131.9, 132.88, 134.28, 134.93, 135.55, 136.25, 137.55, 150.52, 193.77. LCMS (m/z): 349.0 $[M-H]^-$. Anal. calcd. for $C_{20}H_{15}ClN_2S$: C, 68.46; H, 4.31; N, 7.98. Anal. found: C, 68.69; H, 4.32; N, 7.99.

***5-(4-chlorophenyl)-8-methoxy-2-methyl-5,6-dihydroindeno[1,2-d]thiazolo[3,2-a]pyrimidine* (15B)** Yellow crystals; Yield: 81%; m.p. 188-190ºC; Rf = 0.66 (SiO_2, ethylacetate:*n*-hexane, 3:7, v/v). IR (KBr, cm^{-1}): 3019.2 (C–H, aromatic), 2904.3 (C–H), 1688.0 (C=N), 1620.9 (C=C), 1289.4 (C–N), 1248.5 (C–O), 765.6 (C–S), 1088.7 (C–Cl). ^{1}H NMR (DMSO-d6, 800 MHz) δppm: 3.90 (s, 5H), 4.07 (s, 4H), 7.05 (d, 1H, J = 8Hz), 7.19 (s, 1H), 7.45 (s, 1H), 7.57 (d, 2H, J = 8Hz), 7.73-7.80 (m, 3H). ^{13}C NMR (DMSO-d_6, 200 MHz) δ ppm: 32.35, 39.66, 39.87, 39.97, 40.08, 40.29, 56.30, 110.64, 115.96, 126.04, 129.47, 130.56, 130.89, 132.66, 134.44, 134.61, 136.85, 153.45, 165.51, 191.95. LCMS (m/z): 382.95 $[M^{+2}]$. Anal. calcd. for $C_{21}H_{17}ClN_2OS$: C, 66.22; H, 4.50; N, 7.35. Anal. found: C, 66.28; H, 4.51; N, 7.33.

2.1.3 SRB assay

The Hep-G2 cells derived from human liver carcinoma were purchased from the National Cell Repository NCCS, Pune, India and later cultured in the lab of ACTREC, Tata Memorial Centre, Navi Mumbai, India for in vitro testing purposes. As per the instructions, the cells were grown in Roswell Park Memorial Institute medium 1640 containing 10% fetal bovine serum. Then, 100 µL cells containing media were seeded into 96-well plates at a density of 5×103 cells/well and incubated at 37°C in a humidified atmosphere containing 5% CO2 for 24 h prior to addition of the experimental drugs. Initially, all the experimental drugs were solubilized in DMSO at 100 mg/mL and further diluted to 1.0 mg/mL using water and stored frozen prior to use. Aliquots of 100 µL (containing 90 µL of medium) of various dilutions were added to appropriate wells, resulting in the required drug concentrations of 10, 20, 40, and 80µg/mL, and were maintained at standard conditions for 48 h. For each of the experiments, a well-known anticancer drug Adriamycin (ADR) was used as a positive control at concentrations of 10, 20, 40, and 80µg/mL. The assay was terminated by the gentle

addition of 50 µL of cold 30% (w/v) trichloroacetic acid and the mixture was incubated for 60 min at 4°C. The supernatant was discarded and the plates were washed five times using tap water and then air dried. Next, SRB solution (50 µL) at 0.4% (w/v) in 1% acetic acid was added to each well and incubated for 20 min at room temperature. After staining, the unbound dye was recovered and the residual dye was removed by washing five times with 1% acetic acid and then air dried. Subsequently, the bound stain was eluted with 10 mM trizma base and the absorbance was examined at a wavelength of 540 nm on an enzyme-linked immunosorbent assay plate reader.

The growth inhibition of 50% (GI50) was calculated using the formula [(Ti−Tz)/(C−Tz)] ×100%, where Tz represents time zero growth, C is the control growth, and Ti is the test growth at four concentration levels in the presence of the drug [46, 47].

2.1.4 Molecular docking

The structures of the ligands were designed by Chem Draw Ultra 12.0, and the geometry was optimized six times through Gauss View 5.0 (trial version). In addition, the National Centre for Biotechnology Information [48] and the Protein Data Bank [49] were utilized as chemical sources to obtain the established four homological cancer protein targets, that is, IL-2 (1Z92), IL-6 (1IL6), Caspase-3 (1QX3), and Caspase-8 (1IBC). DS Visualizer software [50] was used to remove the co-crystal with the assigned target. Next, the active site was identified using the CASTp database [51]. For a particular system, validation of the docking protocol was performed using re-docking studies, where we found excellent agreement between the localization of ligands upon docking, and from the crystal structure of the assigned targets. We demonstrated the reliability and quality of the docking method in reproducing experimentally observed binding-mode-assigned targets. In addition, the docking analyses of the test set were carried out using Autodock4.1 [52] together with the Lamarkian genetic algorithm for automated flexible ligand docking, and the binding energy was estimated as negative kcal/mol. In addition, probable H-bonds and π-bonds were also assessed [53−55].

2.1.5 Prediction of ADME properties

The ADME and drug-like properties of selected ligands were predicted by employing MedChem Designer and QikProp tools. Chemical structures were optimized with LigPrep. Additionally, the percentage absorbance (% ABS) and Lipinski's violation were evaluated for this study [56].

2.1.6 MD simulation

The nature of the inhibitor used on the active site domain of IL-6 was investigated by means of MD simulation studies. The energies of dock configurations were minimized to eliminate the unfavorable atomic contacts as starting conformations for dynamic simulation in Elmar Krieger MD simulation tools (trial version) [57]. An AMBER03 force field was assigned to execute a real-time MD simulation [58]. The complex was solvated through an HOH model at density =0.997 g/L inside the 10Å simulation cell boundary and then adjusted to the physiologic pH at 7.4. Moreover, physiologic NaCl solution with 0.9% mass fraction Na+ and Cl^- ion concentration was used to maintain and neutralize the simulation cell boundary. Then, the MD simulation was run for 3,000 ps at a temperature of 298 K and 1 bar pressure to obtain snapshot (sim) trajectories. Finally, the sim trajectories were analyzed and the resulting data were plotted using Sigma Plot 11.0 tools.

2.2 RESULTS AND DISCUSSION

2.2.1 Design

These two core structural motifs are formed by the fusion of three biodynamic privileged heterosystems in such a way that one nitrogen atom occupies a bridge head position, therefore being common to both the heterocyclic rings, that is, the thiazole and the pyrimidine rings, and possessing unique structural diversity. Thiazolo[2,3-b]quinazoline and thiazolo[3,2-a]pyrimidine, as heterocyclic skeletons, exhibit a diverse range of pharmacologic activities. In view of the great medicinal importance associated with these remarkable structures, we are interested in studying MDRs with the aim of evolving an efficient and highly convergent synthetic procedure for the library of densely functionalized 5H-benzo[h]thiazolo[2,3-b]quinazoline (1A−15A) and indeno[1,2-d]thiazolo[3,2-a]pyrimidine (1B−15B) analogs in a single operation.

We initiated our study of the proposed method with 10 mol% *p*-TSA as the acidic catalyst (Scheme 5) by investigating the conditions for the reaction comprising 5-methoxy-2,3-dihydro-1H-inden-1-one (1 mmol), 4-bromobenzaldehyde (1 mmol), 4-methylthiazol-2-amine (1 mmol), and EtOH (5.0 mL) at 60°C to yield the corresponding product (4B, 51% yield) as a model in 4.5 h (entry 1). With this finding in hand, when the acidic catalyst was changed from 10% to 20% and the temperature from 60°C to 80°C, the product yield increased to 69% after 3 h reaction time (entry 4). We examined the reaction in different

organic solvents, including EtOH, methanol (MeOH), ethylacetate (EtOAc), acetonitrile (CH3CN), and toluene (PhCH3) under varied temperature conditions (Table 2.1). The proposed reaction is optimized for the amount of acidic catalyst required, as well as for temperature, to improve the yields of the desired molecules (entries 1–8), and the optimum amount was found to be 20 mol% *p*-TSA in EtOH at 80°C. The best results were obtained for 20 mol% *p*-TSA in 3 h at 80°C (entry 4, 69% yield).

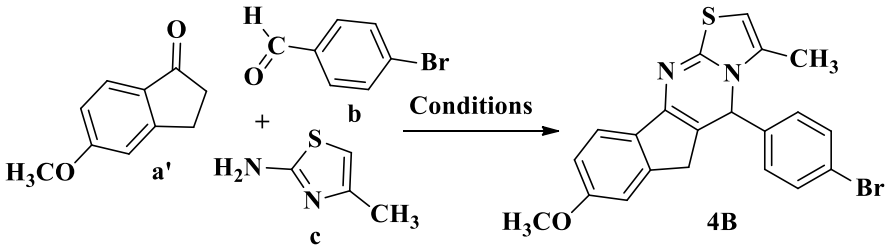

Scheme 5 Optimization of the model reaction

Note: substituted α-indanone (a′), substituted aromatic aldehydes (b) and distinctive 2-aminothiazoles (c).

Table 2.1 Optimization of catalytic amount of *p*-TSA, non-aqueous solvents and temperature in one-pot synthesis of the model reaction.[a]

Entry	*p*-TSA (mol%)	Solvents	Temp (°C)	Time (h)	Yield (%)[b]
1	10	EtOH	60	4.5	51
2	10	EtOH	80	4.0	56
3	20	EtOH	60	3.5	63
4	**20**	**EtOH**	**80**	**3.0**	**69**
5	10	MeOH	60	5.0	49
6	10	MeOH	80	4.5	54
7	20	MeOH	60	4.0	54
8	20	MeOH	80	3.5	60
9	20	EtOAc	reflux	5.0	33
10	20	CH_3CN	reflux	5.0	29
11	20	Ph-CH_3	reflux	5.0	27

Notes: [a]Reaction conditions: 5-methoxy-2,3-dihydro-1H-inden-1-one (1 mmol), 4-bromo benzaldehyde (1 mmol), 4-methylthiazol-2-amine (1 mmol), solvent (5.0 mL) and *p*-TSA.
[b]Isolated pure yield. Bold entry signifies the optimized reaction conditions.

Abbreviations: CH_3CN, acetonitrile; EtOAc, ethylacetate; EtOH, ethanol; MeOH, methanol; $PhCH_3$, toluene; *p*-TSA, *p*-toluenesulfonic acid.

In order to explore the scope of these conditions, we embarked on the synthesis of a panel of novel 5H-benzo[h]thiazolo[2,3-b]quinazoline (1A–15A) and indeno[1,2-d]thiazolo[3,2-a]pyrimidine (1B–15B) analogs bearing a bridgehead nitrogen atom from a range of substrates by the advancement of facile and efficient MDRs of highly substituted α-tetralone (a) or α-indanone (a') with some aromatic aldehydes (b) and distinctive 2-aminothiazoles (c) in EtOH in the presence of 20 mol% *p*-TSA.

The α-tetralone, 6-methoxy-1-tetralone, 7-methoxy-1-tetralone or α-indanone, 5-methoxy-1-indanone, and the substituted benzaldehydes with 4-bromo, trimethoxy, 3-hydroxy-4-methoxy (vanillin), 4-chloro were reacted with distinctive 2-aminothiazole, 4-methylthiazol-2-amine, 5-methylthiazol-2-amine to afford a library of proposed target molecules, that is, (1A–15A) and (1B–15B), respectively.

The one-pot, three-component reaction went smoothly in EtOH in the presence of *p*-TSA and gave the targeted compounds (1A–15A) and (1B–15B) in impressive yields up to 86%. The various substitutions of synthesized derivatives are given in Table 2.2A and B.

All the newly synthesized compounds were authenticated on the basis of Fourier transform infrared spectroscopy, LCMS, and 1H and 13C NMR spectral and elemental analyses.

Desired compounds have also been synthesized by a multistep synthesis involving the reaction of distinctive 2-aminothiazoles with the appropriate benzylidene-tetralones/indanones achieved by the reaction of highly substituted α-tetralone or α-indanone with different aromatic aldehydes, piperidine and glacial acetic acid in EtOH. This reaction proceeds in two steps with a comparatively longer reaction time (18–20 h) and giving moderate yields (40%–50%).

Table 2.2 Various substitutions and in vitro cytotoxicity data of synthesized derivatives against human hepatoma (Hep-G2) cell lines: A (1A–15A) and B (1B–15B)

Comp. Code	**X_1**	**X_2**	**R_1**	**R_2**	**R_3**	**Y_1**	**Y_2**	**GI_{50} µg/mL**	**LC_{50}, µg/mL**	**TGI µg/mL**
1A	-H	-H	-H	-Br	-H	-H	-H	>80	NE	NE
2A	$-OCH_3$	-H	-H	-Br	-H	-H	$-CH_3$	NE	NE	NE
3A	-H	$-OCH_3$	$-OCH_3$	$-OCH_3$	$-OCH_3$	-H	-H	NE	NE	NE
4A	-H	$-OCH_3$	$-OCH_3$	-OH	-H	-H	-H	**<10**	>80	>80
5A	$-OCH_3$	-H	-H	-Br	-H	-H	-H	>80	>80	>80
6A	$-OCH_3$	-H	$-OCH_3$	$-OCH_3$	$-OCH_3$	-H	-H	**<10**	NE	NE
7A	-H	-H	-H	-OH	-H	-H	-H	76.1	NE	NE
8A	-H	$-OCH_3$	-H	-Cl	-H	$-CH_3$	-H	>80	NE	NE
9A	$-OCH_3$	-H	-H	-Cl	-H	$-CH_3$	-H	>80	NE	NE
10A	-H	-H	-H	-Cl	-H	$-CH_3$	-H	>80	NE	NE
11A	-H	$-OCH_3$	-H	-Cl	-H	-H	-H	>80	NE	NE
12A	-H	-H	-H	-Cl	-H	-H	-H	>80	NE	NE
13A	-H	$-OCH_3$	-H	-Cl	-H	-H	$-CH_3$	>80	NE	NE
14A	$-OCH_3$	-H	-H	-Cl	-H	-H	$-CH_3$	>80	NE	NE
15A	-H	-H	-H	-Cl	-H	-H	$-CH_3$	>80	NE	NE

Comp. Code	**X**	**R_1**	**R_2**	**R_3**	**R_4**	**Y_1**	**Y_2**	**GI_{50} µg/mL**	**LC_{50}, µg/mL**	**TGI µg/mL**
1B	-H	-H	-H	-Br	-H	-H	-H	>80	NE	NE
2B	-H	-Cl	-H	-H	-H	-H	-H	>80	NE	NE
3B	-H	-H	-H	-Br	-H	-H	$-CH_3$	>80	NE	NE
4B	$-OCH_3$	-H	-H	-Br	-H	$-CH_3$	-H	>80	NE	NE
5B	-H	-H	-H	-Br	-H	$-CH_3$	-H	>80	NE	NE
6B	$-OCH_3$	-H	-H	-Br	-H	-H	-H	>80	NE	NE
7B	$-OCH_3$	-H	-H	-Br	-H	-H	$-CH_3$	>80	NE	NE
8B	-H	-H	$-OCH_3$	$-OCH_3$	$-OCH_3$	-H	-H	>80	NE	NE
9B	$-OCH_3$	-H	$-OCH_3$	$-OCH_3$	$-OCH_3$	-H	-H	>80	NE	NE
10B	-H	-H	-H	-Cl	-H	$-CH_3$	-H	>80	NE	NE
11B	$-OCH_3$	-H	-H	-Cl	-H	$-CH_3$	-H	>80	NE	NE
12B	-H	-H	-H	-Cl	-H	-H	-H	>80	NE	NE
13B	$-OCH_3$	-H	-H	-Cl	-H	-H	-H	>80	NE	NE
14B	-H	-H	-H	-Cl	-H	-H	$-CH_3$	>80	NE	NE
15B	$-OCH_3$	-H	-H	-Cl	-H	-H	$-CH_3$	>80	NE	NE
ADR								**<10**	NE	<10

Notes: *GI_{50} value of ≤ 10 µg/ml (or 1 µM) is considered to demonstrate activity in case of pure compounds (synthetic compound). Bold values indicate the active compounds.

Abbreviations: ADR, adriamycin, positive control compound; GI_{50}, concentration of drug causing 50% inhibition of cell growth; LC_{50}, concentration of drug causing 50% cell kill; NE, "not effective" even at the concentration >80 µg/ml; TGI, concentration of drug causing total inhibition of cell growth.

2.2.2 Plausible mechanism

These reactions presumably proceed through a Knoevenagel condensation between substituted α-tetralone or α-indanone and some appropriate aromatic aldehydes in the first step to construct α,β-unsaturated ketones, respectively, which undergo a Michael-type addition approach with the nucleophilic endocyclic nitrogen of the distinctive 2-aminothiazole under the maintained reaction conditions. Then, successive intramolecular cyclization occurred with the loss of a water molecule to give 5H-benzo[h]thiazolo[2,3-b] quinazolines (1A−15A) and indeno[1,2-d]thiazolo[3,2-a]pyrimidines (1B−15B).

In this setting, the domino approach and the reaction sequence of Knoevenagel condensation/Michael-type addition/intramolecular cyclization were done in a single step in a one-pot procedure in EtOH. The plausible mechanism for the reaction is delineated in Scheme 6.

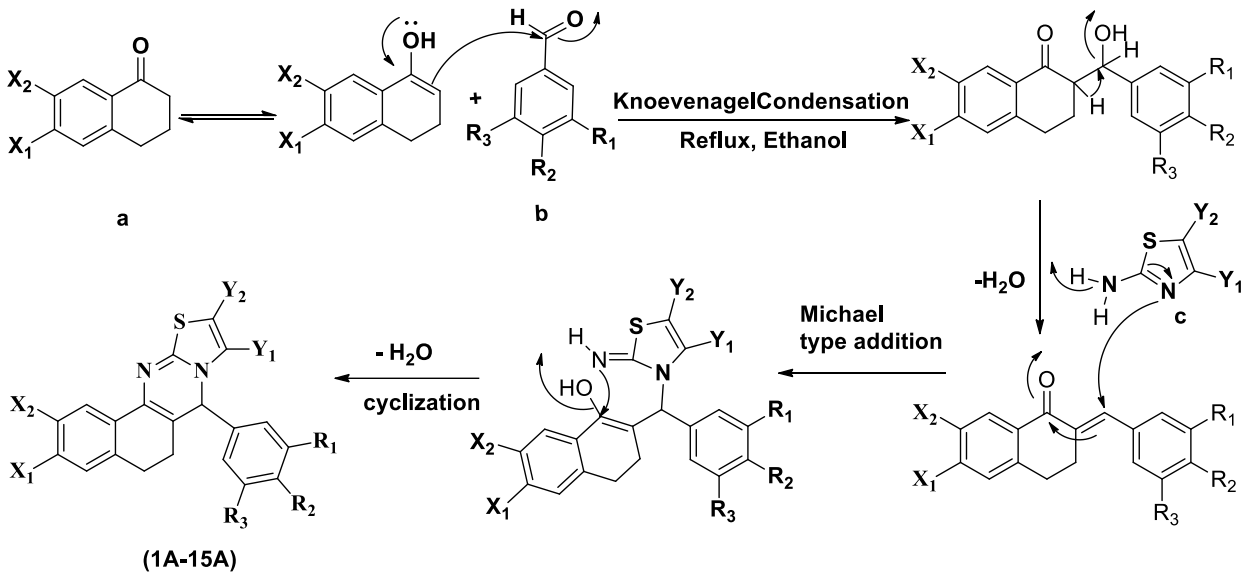

Scheme 6 Plausible scenario to account for the formation of (1A–15A) and same for the preparation of (1B–15B)

Note: substituted α-tetralone (a), substituted aromatic aldehydes (b) and distinctive 2-aminothiazoles (c).

2.2.3 In vitro antitumor screening

A library of 30 5H-benzo[h]thiazolo[2,3-b]quinazoline and indeno[1,2-d]thiazolo[3,2-a] pyrimidine derivatives were screened against Hep-G2 cells. The inhibition activities (GI50) of the synthetic compounds 1A–15A, 1B–15B, and ADR on Hep-G2 cells are summarized in Table 2.2A and B. The effects of treatment with the most active members (4A and 6A) of this study and with ADR on Hep-G2 are shown by the plotted growth curve (Figure 2.1) and the microscopic images (Figure 2.2).

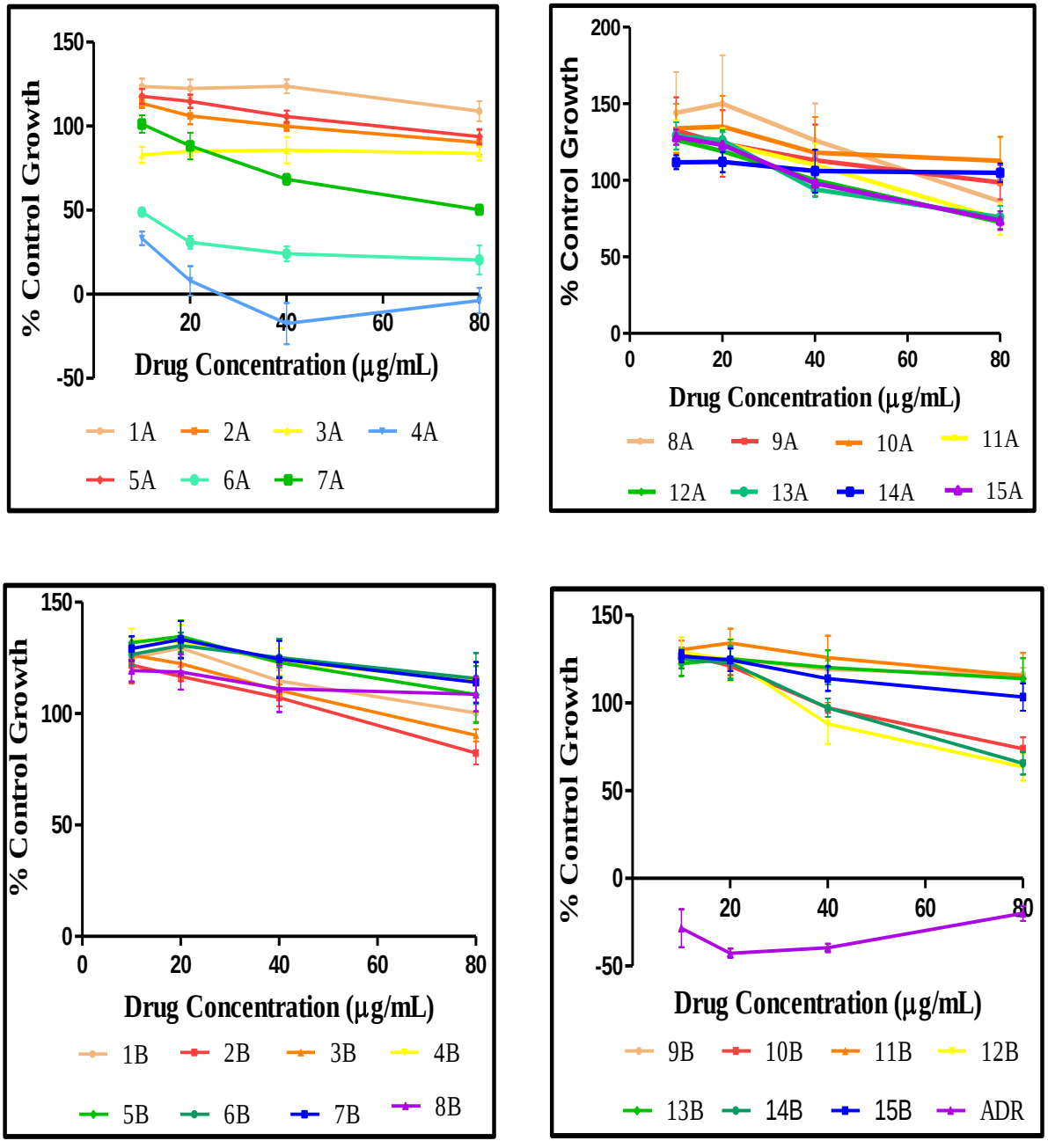

Figure 2.1 Growth Curve of (1A–15A and 1B–15B): Human Hepatoma Cell Line (Hep-G2).
Abbreviation: ADR, Adriamycin.

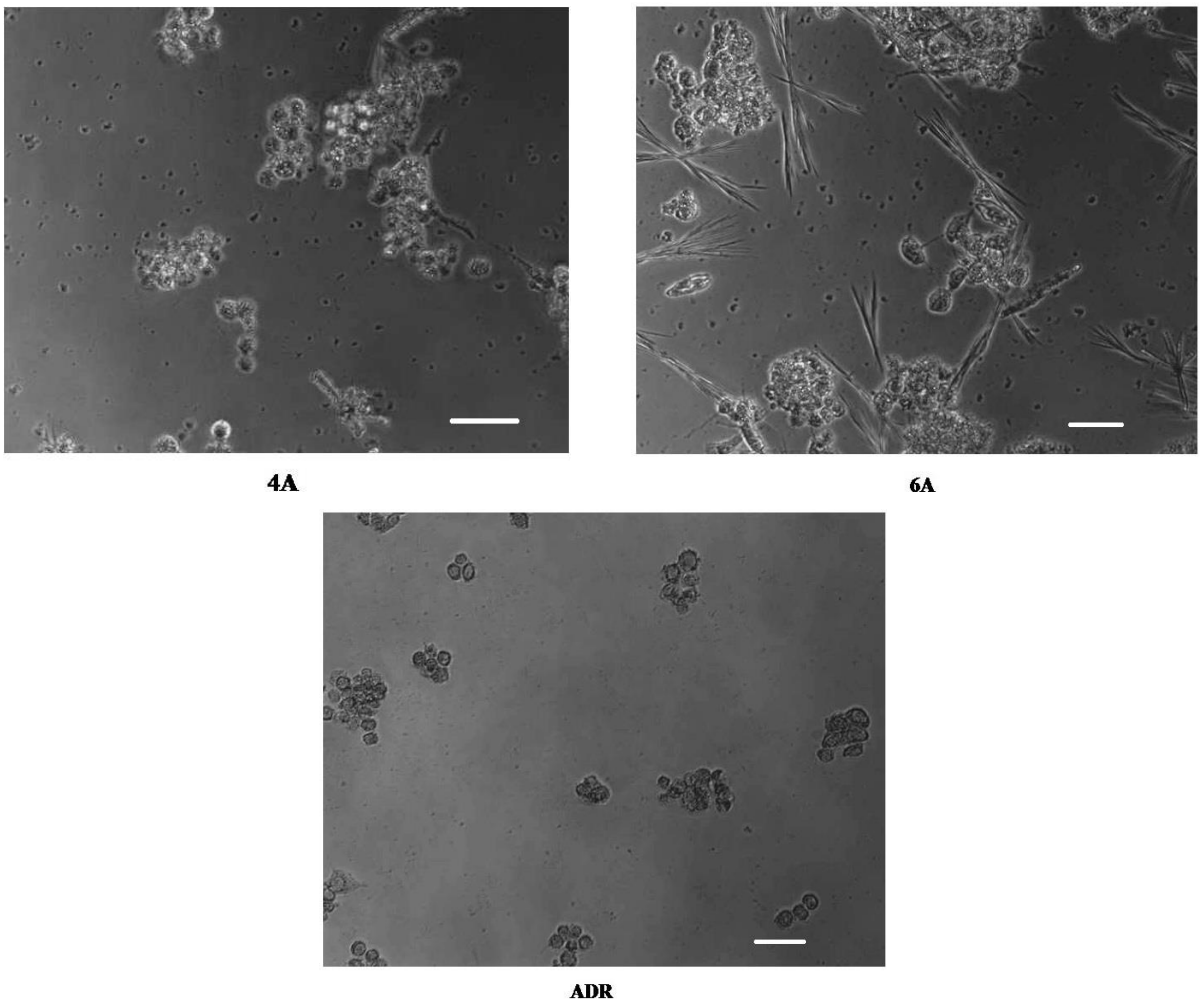

Figure 2.2 Microscopic pictures showing the effect of treatments with the active compounds (A) 4A and (B) 6A and the reference drug (C) ADR on Hep-G2 human liver cancer cell line.
Note: Scale bar 50 μm.
Abbreviation: ADR, Adriamycin.

Close examination of the activity data (Table 2.2A and B) revealed that the presence of –OH and –OCH3 groups in the phenyl ring, preferably at the R1, R2, and R3 positions, in conjugation with the introduction of the –OCH3 group in the tetralone ring at X1 or X2 is crucial for inhibitory activity. Substitution of 3-methoxy-4-hydroxy on the phenyl ring and 6-methoxy on the tetralone ring led to compound 4A, while substitutions of 3,4,5-trimethoxy on the phenyl ring and 7-methoxy on the tetralone ring led to compound 6A with better cytotoxicity (GI50 ,10 μg/mL). In contrast, substitutions with –Br, –Cl, and –OH groups on the phenyl ring at the R2 position were ineffective against Hep-G2 cells. The methyl substitution on the thiazole ring did not contribute to producing inhibitory activity.

Replacement of the tetralone ring with the indanone ring system, that is, 1B–15B, reduced the anticancer activity against Hep-G2 human liver cancer cell lines.

The growth curve of the in vitro findings suggested that the percentage growth inhibition values of the potent compounds 4A and 6A was ≤50% at 10 μg/mL concentration, but they did not move toward a negative value. Therefore, it might be expected in future that both compounds could lead to the death of cancerous cells while minimizing that of normal cells.

2.2.4 Molecular docking studies

Computational analysis was performed using various well-known liver cancer targets, specifically IL-2, IL-6, Caspase-3, and Caspase-8, through Autodoc 4.1, together with Lamarkian genetic algorithm for automated docking of flexible ligands. Molecular docking poses of both the potent compounds 4A and 6A with the related targets IL-2, IL-6, Caspase-3, and Caspase-8 are presented in Figure 2.3 which indicates the interactions of amino acids with ligands, H-bonds, and π-bonds as well as the bond lengths. The docking affinities (kcal/mol), numbers of H-bonds and π-bonds, and the interactions of amino acids of the potent members with them are given in Table 2.3.

Compounds 4A and 6A exhibited strong affinity (binding interaction energy ranged from -6.1 to -7.87 kcal/mol), while others showed good binding affinity with preferred molecular targets. Compound 4A displayed excellent affinity with IL-6 (-7.87 kcal/mol, 2H and 4π-bonds), IL-2 (-7.68 kcal/mol, 5π-bonds), Caspase-3 (-6.69 kcal/mol, 1H and 7π-bonds), and Caspase-8 (-6.48 kcal/mol, 1π-bond). A similar pattern was observed for compound 6A with IL-2 (-7.63 kcal/mol, 1H and 1π-bonds), IL-6 (-7.43 kcal/mol, 2H and 4π-bonds), and Caspase-8 (-6.76 kcal/mol, 1H and 5π-bond), but with less affinity for Caspase-3 (-6.14 kcal/mol, 1H and 6π-bonds).

Moreover, both the active members of the present study have strong affinity binding to IL-2, Caspase-3, Caspase-8, and the binding energies, particularly for the IL-6 receptor site, are predominantly high (from -7.43 to -7.87 kcal/mol). Accordingly, it might be assumed that the promising cytotoxic properties of these compounds, which were indicated by the in vitro antitumor activity on Hep-G2 cells, might be better mediated through an IL-6-dependent mechanism (Table 2.3).

Interleukin-2 (IL-2):

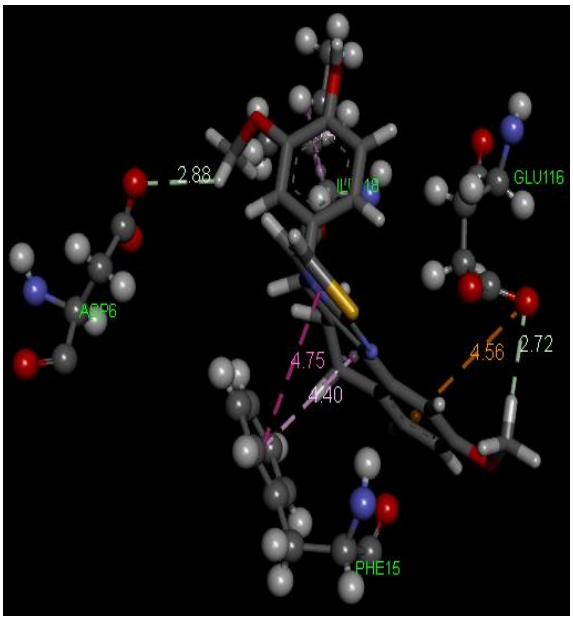

4A

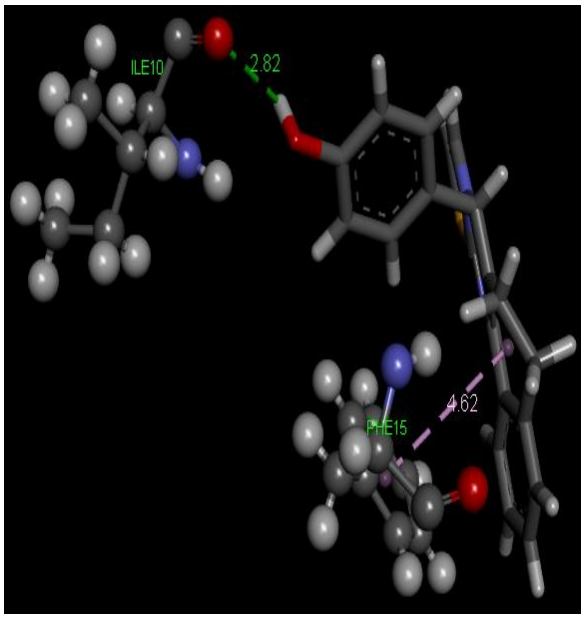

6A

Interleukin-6 (IL-6):

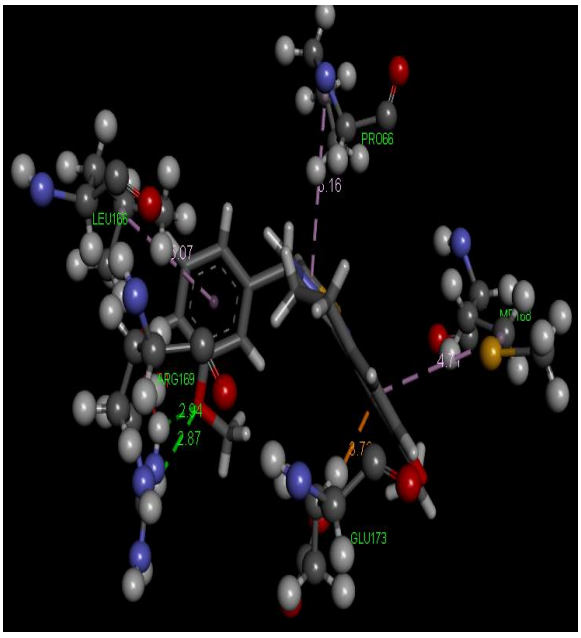

4A

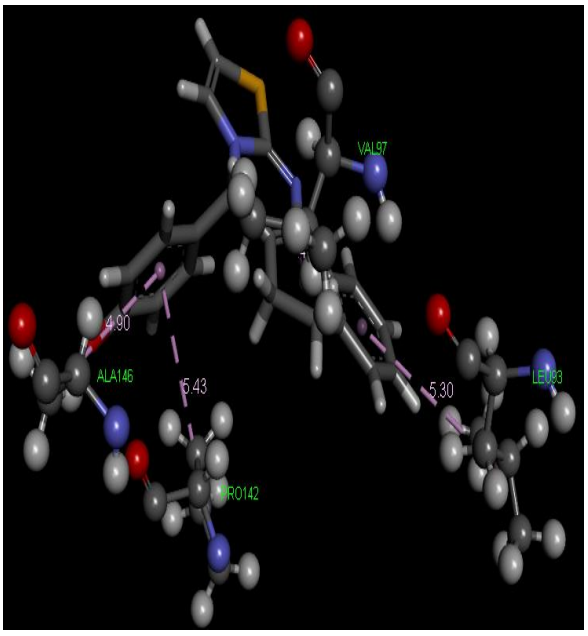

6A

Caspase-3:

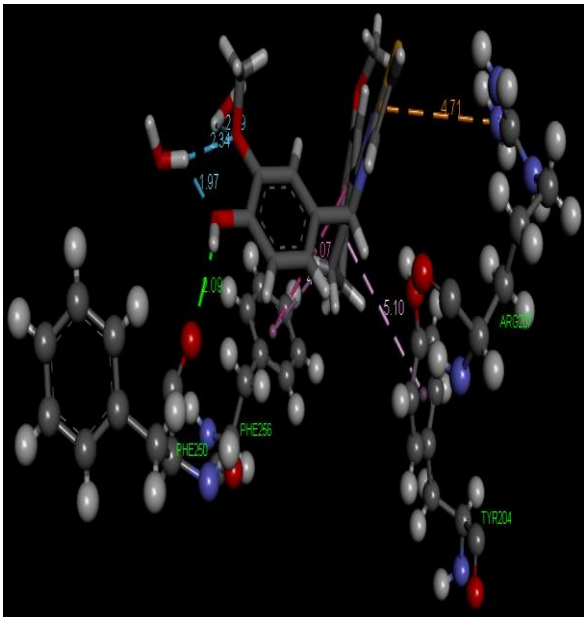

4A

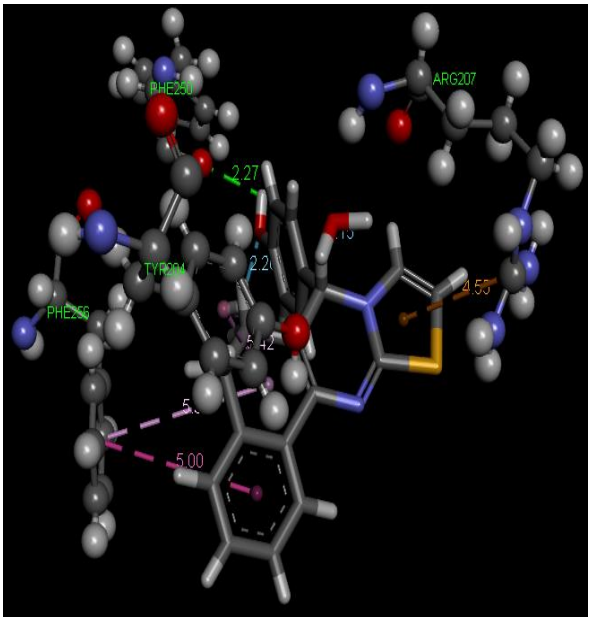

6A

Caspase-8:

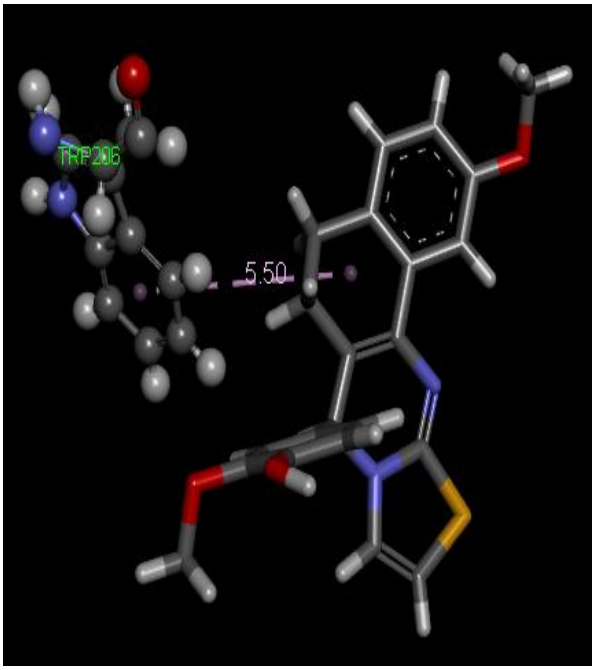

4A

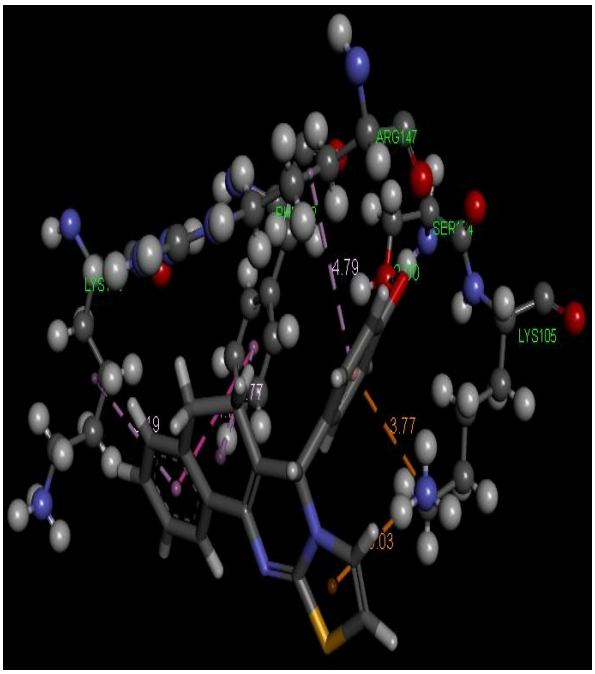

6A

Figure 2.3 Docking images of active compounds, 4A & 6A for IL-2, IL-6, Caspase-3 and Caspase-8

Abbreviation: IL, interleukin.

Table 2.3 Docking affinity of active compounds with assigned anticancer receptors

Ligands	Receptors	Binding affinity [kcal/ mol]	Amino acids involved in interaction	H-bonds	π-bonds
4A	IL-2	-7.680	ARG A 38 THR A 41 ASP B 6 ALA B 13 THR B 14 PHE B 15 LYS B 16 TYR B 20 GLU B 106 THR B 115 GLU B 116 ARG B 117 ILE B 118 TYR B 119 PHE B 121	0	5
	IL-6	-7.871	ASN A 62 LEU A 63 PRO A 66 LYS A 67 MET A 68 ALA A 69 PHE A 75 LEU A 166 ARG A 169 SER A 170 GLU A 173 PHE A 174 SER A 177	2	4
	Caspase-3	-6.695	THR A 62 SER A 65 TYR A 204 TRP A 206 ARG A 207 SER A 209 PHE A 250 SER A 251 PHE A 256 HOH A 645 HOH A 684 HOH A 696 HOH A 708 HOH A 733 HOH A 736	1	7
	Caspase-8	-6.480	SER A 65 TYR A 204 TRP A 206 ARG A 207 ASN A 208 SER A 209 TRP A 214 GLU A 248 SER A 249 PHE A 250 SER A 251	0	1
6A	IL-2	-7.630	ARG A 38 THR A 41 ASP B 6 GLU B 9 PHE B 15 LYS B 16 ALA B 17 TYR B 20 GLU B 113 THR B 115 GLU B 116 ARG B 117 ILE B 118 TYR B 119 PHE B 121	1	1
	IL-6	-7.438	GLU A 43 THR A 44 LYS A 47 SER A 48 MET A 50 ARG A 105 PHE A 106 GLU A 107 SER A 108 GLN A 157 TRP A 158 ASP A 161 THR A 164	0	3
	Caspase-3	-6.142	SER A 65 TYR A 204 TRP A 206 ARG A 207 ASN A 208 SER A 209 TRP A 214 SER A 249 PHE A 250 SER A 251 PHE A 256 HOH A 645 HOH A 665 HOH A 684 HOH A 696 HOH A 736	1	6
	Caspase-8	-6.760	SER A 63 ARG A 64 SER A 65 TYR A 204 SER A 205 TRP A 206 ARG A 207 ASN A 208 SER A 209 TRP A 214 GLU A 248 SER A 249 PHE A 250 SER A 251	1	5

2.2.5 Prediction of ADME properties

A study of pharmacokinetic parameters was carried out utilizing QikProp version 4.5 tools to predict the ADME properties of both series (1A–15A) and (1B–15B) and the ranges for the calculated properties of all members, along with their average values are summarized in Table 2.4. In addition, we also calculated % ABS, number of H-bond acceptors (n–OH), number of H–bond donors (n-OHNH), octanol/water partition coefficients (QPlogPo/w), and Lipinski's violation.

Interestingly, it was found that the % ABS obtained for all members was 100% and the QPlogPo/w prediction was found to be within the accepted range of -2.0 to 6.5. Moreover, all members followed the violated Lipinski parameters.

Table 2.4- Pharmacokinetic parameters important for oral bioavailability and protein binding parameters of synthesized compounds

Comp.	**% ABS**	**MW**	**Volume**	**Donor HB**	**Acceptor HB**	**Lipinski's violation**	**QPlogPo/w**
Rule	**>80% is high <25% is poor**	**<500**	**500.0 – to 2000.0**	**<5**	**<10**	**≤1**	**–2.0 to 6.5**
1A	100	395.316	1041.638	0	1	1	6.493
2 A	100	439.369	1168.198	0	1.75	1	6.799
3 A	100	436.525	1261.8	0	4	1	6.007
4 A	100	392.472	1138.921	1	3.25	1	5.196
5 A	100	425.342	1105.697	0	1.75	1	6.476
6 A	100	436.525	1261.747	0	4	1	6.006
7 A	100	332.419	1011.802	1	1.75	1	5.108
8 A	100	394.92	1041.638	0	1	1	6.493
9 A	100	394.92	1159.867	0	1.75	1	6.724
10 A	100	364.892	1065.077	0	1	1	6.576
11 A	100	380.891	1097.431	0	1.75	1	6.402
12 A	100	350.865	1033.256	0	1	1	6.419
13 A	100	394.918	1159.867	0	1.75	1	6.724
14 A	100	394.918	1159.815	0	1.75	1	6.724
15 A	100	364.892	1095.69	0	1	1	6.741
1B	100	381.289	972.937	0	1	1	6.036
2 B	100	336.838	942.479	0	1	1	5.672
3 B	100	395.316	1037.84	0	1	1	6.374
4 B	100	425.342	1080.745	0	1.75	1	6.247
5 B	100	395.316	1016.635	0	1	1	6.264
6 B	100	411.315	1037.038	0	1.75	1	6.018
7 B	100	425.342	1101.954	0	1.75	1	6.357
8 B	100	392.472	1122.39	0	3.25	1	5.516

9 B	100	422.498	1177.838	0	4	1	5.445
10 B	100	350.865	1008.558	0	1	1	6.191
11 B	100	380.891	1072.663	0	1.75	1	6.174
12 B	100	336.838	964.548	0	1	1	5.961
13 B	100	366.864	1028.656	0	1.75	1	5.943
14 B	100	350.865	1029.454	0	1	1	6.3
15 B	100	380.891	1093.555	0	1.75	1	6.282

2.2.6. MD simulation

MD simulation was performed on the active inhibitor 4A with IL-6 to explore the binding poses in depth. Compound 4A displayed high binding affinity (low docking energy) and stable complex for IL-6 receptor. Therefore, we decided to investigate the influence of compound 4A on the active site of IL-6 receptor.

The stability of the system under simulation was assessed using the root-mean-square deviation (RMSD) of atomic positions of the backbone atoms, relative to the starting structures. The binding energy versus time plot indicates the change in conformation and, therefore, the binding energy, with respect to time. As shown in Figures 2.4 and 2.5, the RMSD, the binding energy, and the potential energy of IL-6 with compound 4A, including the complex, were computed using MD trajectory frames. Furthermore, we monitored the structural stability of the backbone structure throughout the process through a graphic profile.

We observed a dramatic fluctuation in RMSD at 1,000 ps (time), whereas no significant fluctuations were observed after 1,500 ps (time), and it achieved an almost steady state, indicating the stability of the backbone structure with the ligand at about 1,500 ps time in the MD simulation.

The binding energy and the potential energy of the complex were estimated as a function of time, which indicated that the potential energy (kJ/mol) did not show further fluctuations after 100 ps, whereas the average complex binding energy was observed to be about -0.9 kg/mol. The fluctuations in the residue of the backbone structure are illustrated in Figure 2.4.

In summary, we examined these data, where we found the structural stability of compound 4A with the active site domain of IL-6 receptor.

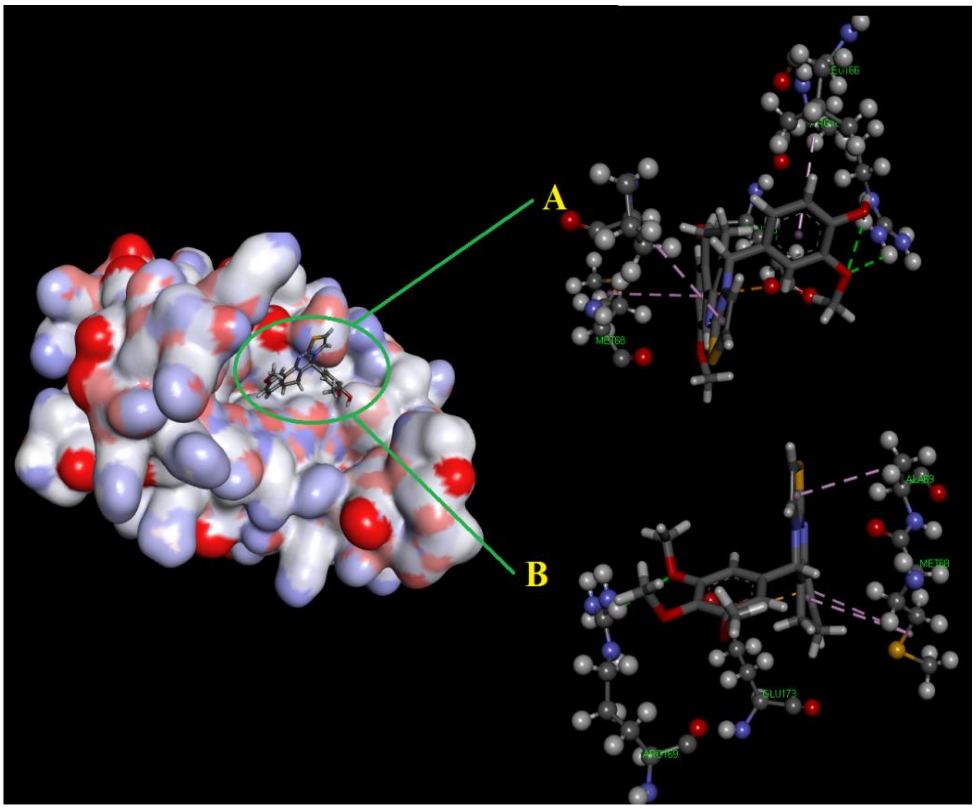

Figure 2.4 Docking complex of 4Awith the IL-6 receptor.

Notes: Structural conformational changes before MD simulation (A) and after MD simulation (B): Back bone of active site domain complex, which shows the contraction of ligand with amino acids residue.

Abbreviations: IL, interleukin; MD, molecular dynamic.

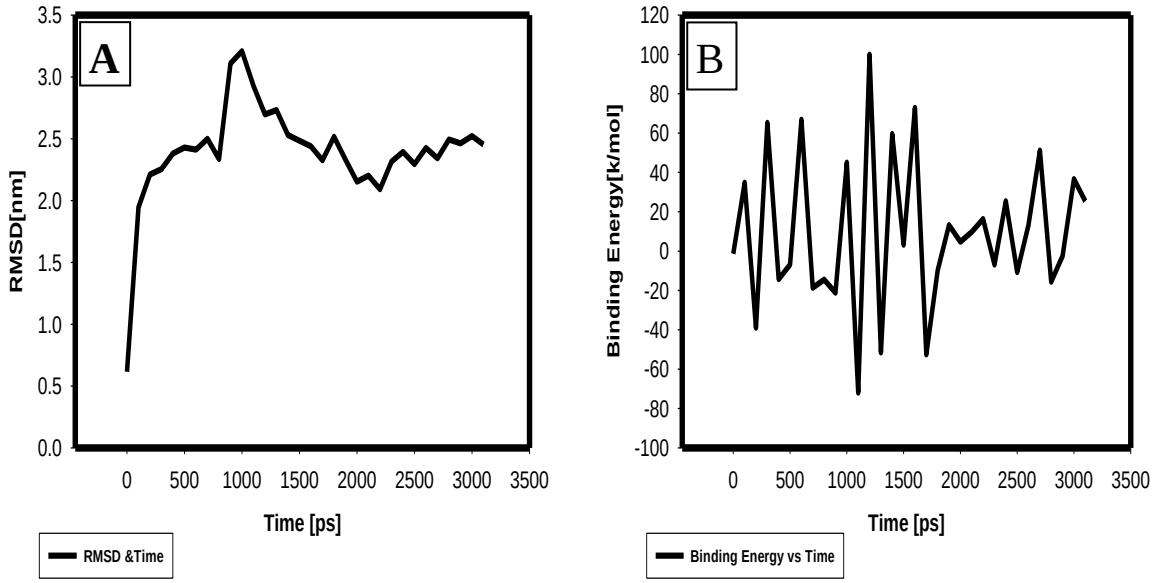

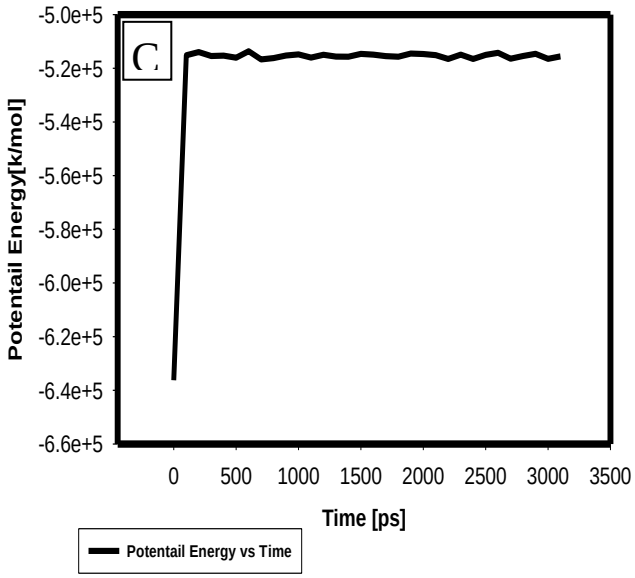

Figure 2.5 The stability profile of ligand and protein complex under the MD simulation.

Notes: (**A**) Average RMSD versus time graph that shows the convergence of simulated structure toward an equilibrium state with respect to the reference structure (initial structure). (**B**) Potential energy of complex versus time graph that shows the stability of ligand and protein complex and (**C**) binding energy of complex versus time graph that also shows the stability of ligand and protein complex.

Abbreviations: MD, molecular dynamic; RMSD, root-mean-square deviation.

2.3 REFERENCES

[1] Silvana Grasso, Nicola Micale, Anna-Maria Monforte, Pietro Monforte, Santina Polimeni, Maria Zappala. Synthesis and in vitro antitumour activity evaluation of 1-aryl-1H,3H-thiazolo[4,3-b]quinazolines. Eur. J. Med. Chem. 2000;35:1115 – 1119.

[2] Hou Z, Zhou N, He B, Yang Y, Yu X. Study on the interaction between thiazolopyrimidine analogues and bovine serum albumin. Spectrochim Acta Part A: Mol. Biomol. Spectrosc. 2011;79:1931-1935.

[3] Keshari AK, Singh AK, Saha S. Bridgehead nitrogen thiazolo[3,2-a]pyrimidine: a privileged structural framework in drug discovery. Mini Rev Med Chem. Epub 2017 Feb 16.

[4] Singh P, Kumari K, Dubey M, Vishvakarma VK, Mehrotrac GK, Pandey ND, Chandra R. Ionic liquid catalyzed synthesis of 7-phenyl-1,4,6,7-tetrahydro-thiazolo[5,4-d]pyrimidine-2,5-diones. C. R. Chimie. 2012;15:504–510.

[5] Qi X, Xiang H, Yang C. Synthesis of functionalized chromeno[2,3 b]pyrrol-4(1H) ones by silver-catalyzed cascade reactions of chromones/thiochromones and isocyanoacetates. Org Lett. 2015;17(22):5590–5593.

[6] Nagaraju A, Ramula BJ, Shukla G, et al. A facile and highly convergent approach to thiazolo[3,2-a]pyridines via one-pot multicomponent domino reaction under metal-free and solvent-free conditions. Tetrahedron. 2015;71(21):3422–3427.

[7] Kumar M, Sharma K, Sharma DK. Diversity oriented one-pot three-component sequential synthesis of annulated benzothiazoloquinazolines. Org Med Chem Lett. 2012;2(1):10.

[8] Kuramoto M, Sakata Y, Terai K, et al. Preparation of leukotriene B(4) inhibitory active 2- and 3-(2-aminothiazol-4-yl)benzo[b]furan derivatives and their growth inhibitory activity on human pancreatic cancer cells. Org Biomol Chem. 2008;6(15):2772–2781.

[9] Misra RN, Xiao HY, Kim KS, et al. N-(cycloalkylamino)acyl-2-aminothiazole inhibitors of cyclin-dependent kinase 2. N-[5-[[[5-(1,1-dimethylethyl)-2-oxazolyl]methyl]thio]-2-thiazolyl]-4-piperidinecarbox-amide (BMS-387032), a highly efficacious and selective antitumor agent. J Med Chem. 2004;47(7):1719–1728.

[10] Patel AB, Chikhalia KH, Kumari P. An efficient synthesis of new thiazolidin-4-one fused s-triazines as potential antimicrobial and anticancer agents. J Saudi Chem Soc. 2014;18(5):646–656.

[11] Rahman MU, Jeyabalan G, Saraswat P, Parveen G, Khan S, Yar MS. Quinazolines and anticancer activity: a current perspective. Synth Commun. 2016;47(5):379–408.

[12] Monchaud D, Allain C, Teulade-Fichou MP. Development of a fluorescent intercalator displacement assay (G4-FID) for establishing quadruplex-DNA affinity and selectivity of putative ligands. Bioorg Med Chem Lett. 2016;26(18):4842–4845.

[13] Chen X, Du Y, Sun H, Wang F, Kong L, Sun M. Synthesis and biological evaluation of novel tricyclic oxazine and oxazepine fused quinazolines. Part 1: erlotinib analogs. Bioorg Med Chem Lett. 2014;24(3):884–887.

[14] Zahedifard M, Faraj FL, Paydar M, et al. Synthesis of apoptotic new quinazolinone-based compound and identification of its underlying mitochondrial signalling pathway in breast cancer cells. Curr Pharm Des. 2015;21(23):3417–3426.

[15] Chandregowda V, Kush AK, Chandrasekara Reddy G. Synthesis and in vitro antitumor activities of novel 4-anilinoquinazoline derivatives. Eur J Med Chem. 2014;44(7):3046–3055.

[16] Alagarsamy V, Raja Solomon V, Dhanabal K. Synthesis and pharmacological evaluation of some 3-phenyl-2-substituted-3H-quinazolin-4-one as analgesic, anti-inflammatory agents. Bioorg Med Chem. 2007;15(1):235–241.

[17] Nandy P, Vishalakshi MT, Bhat AR. Synthesis and antitubercular activity of Mannich bases of 2-methyl-3H-quinazolin-4-ones. Indian J Heterocycl Chem. 2006;15(3):293–294.

[18] Georgey H, Abdel-Gawad N, Abbas S. Synthesis and anticonvulsant activity of some quinazolin-4-(3H)-one derivatives. Molecules. 2008;13(10):2557–2569.

[19] Verhaeghe P, Azas N, Gasquet M, et al. Synthesis and antiplasmodial activity of new 4-aryl-2-trichloromethylquinazolines. Bioorg Med Chem Lett. 2008;18(1):396–401.

[20] Ismail MA, Barker S, Abau el-Ella DA, Abouzid KA, Toubar RA, Todd MH. Design and synthesis of new tetrazolyl- and carboxybiphenylylmethyl quinazoline derivatives as angiotensin II AT1 receptor antagonists. J Med Chem. 2006;49(5):1526–1535.

[21] Malamas MS, Millen J. Quinazoline acetic acids and related analogues as aldose reductase inhibitors. J Med Chem. 1991;34(4):1492–1503.

[22] Roopan SM, Sompalle R. Synthetic chemistry of pyrimidines and fused pyrimidines: a review. Synth Commun. 2016;46(8):645–672.

[23] Al-Omary FA, Hassan GS, El-Messery SM, El-Subbagh HI. Substituted thiazoles V. Synthesis and antitumor activity of novel thiazolo[2,3-b]quinazoline and pyrido[4,3-d]thiazolo[3,2-a]pyrimidine analogues. Eur J Med Chem. 2012;47(1):65–72.

[24] Lin R, Johnson SG, Connolly PJ, et al. Synthesis and evaluation of 2,7-diamino-thiazolo[4,5-d]pyrimidine analogues as anti-tumor epidermal growth factor receptor (EGFR) tyrosine kinase inhibitors. Bioorg Med Chem Lett. 2009;19(8):2333–2337.

[25] Kolb S, Mondesert O, Goddard ML, et al. Development of novel thiazolopyrimidines as CDC25B phosphatase inhibitors. Chem Med Chem. 2009;4(4):633–648.

[26] Geist JG, Lauw S, Illarionova V, et al. Thiazolopyrimidine inhibitors of 2-methylerythritol 2,4-cyclodiphosphate synthase (IspF) from mycobacterium tuberculosis and plasmodium falciparum. Chem Med Chem. 2010;5(7):1092–1101.

[27] Zhao D, Chen C, Liu H, et al. Biological evaluation of halogenated thiazolo[3,2-a]pyrimidin-3-one carboxylic acid derivatives targeting the YycG histidine kinase. Eur J Med Chem. 2014;87:500–507.

[28] Badawey E, Rida SM, Hazza AA, Fahmy HTY, Gohar YM. Potential anti-microbials. II. Synthesis and in vitro anti-microbial evaluation of some thiazolo[4,5-d]pyrimidines. Eur J Med Chem. 1993;28(2):97–101.

[29] Bekhit AA, Fahmy HT, Rostom SA, Baraka AM. Design and synthesis of some substituted 1H-pyrazolyl-thiazolo[4,5-d]pyrimidines as anti-inflammatory-antimicrobial agents. Eur J Med Chem. 2003;38(1):27–36.

[30] Kuppast B, Spyridaki K, Lynch C, Hu YS, Liapakis G. Synthesis of new thiazolo[4,5-d] pyrimidines as corticotropin releasing factor modulators. Med Chem. 2015;11(1):50–59.

[31] Furrer H, Granzer E, Wagner R. A new class of potent hypolipemic agents raising high-density lipoproteins. Synthesis, reactions and pharmacological properties. Eur J Med Chem. 1994;29:819–829.

[32] Rida SM, Habib NS, Badawey EA, Fahmy HT, Ghozlan HA. Synthesis of novel thiazolo[4,5-d]pyrimidine derivatives for antimicrobial, anti-HIV and anticancer investigation. Die Pharm. 1996;51(12):927–931.

[33] Fahmy HT, Rostom SA, Saudi MN, Zjawiony JK, Robins DJ. Synthesis and in vitro evaluation of the anticancer activity of novel fluorinated thiazolo[4, 5-d]pyrimidines. Arch Pharm. 2003;336(4–5):216–225.

[34] Jeanneau-Nicolle E, Benoit-Guyod M, Namil A, Leclerc G. New thiazolo[3,2-a] pyrimidine derivatives, synthesis and structure-activity relationships. Eur J Med Chem. 1992;27(2):115.

[35] Varano F, Catarzi D, Vincenzi F, et al. Design, synthesis and pharmacological characterization of 2-(2 furanyl)thiazolo[5,4-d]pyrimidine-5,7-diamine derivatives: New

highly potent A2A adenosine receptor inverse agonists with antinociceptive activity. J Med Chem. 2016;59(23):10564–10576.

[36] Gali R, Banothu J, Porika M, Velpula R, Hnamte S. Indolylmethylene benzo[h]thiazolo[2,3-b]quinazolinones: Synthesis, characterization and evaluation of anticancer and antimicrobial activities. Bioorg Med Chem Lett. 2014;24(17):4239–4242.

[37] Gupta R, Chaudhary RP. X-ray, NMR and DFT studies on benzo[h]thiazolo[2,3-b] quinazoline derivatives. J Mol Struct. 2013;1049:189–197.

[38] Sakram B, Sonyanaik B, Ashok K, Rambabu S, Johnmiya SK. Benzo[h]thiazolo[2,3-b] quinazolines by an efficient *p*-toluenesulfonic acid-catalyzed one-pot two-step tandem reaction. Res Chem Intermed. 2016;42(3):1699–1705.

[39] Velpula R, Banothu J, Gali R, Sargam Y, Bavantula R. One-pot and solvent-free synthesis of 3-(9-hydroxy-3-methoxy-7-aryl-6,7,9,10-tetrahydro-5H-benzo[h]thiazolo [2,3-b]quinazolin-9-yl)-2H-chromen-2-ones and their antibacterial evaluation. Turk J Chem. 2015;39:620–629.

[40] Gupta R, Chaudhary RP. Synthesis, spectroscopic characterization and DFT studies on the novel indeno-thiazolopyrimidine heterocyclic system. J Sulfur Chem. 2014;35(1):86–97.

[41] Youssef MM, Amin MA. Microwave assisted synthesis of some new thiazolopyrimidine, thiazolodipyrimidine and thiazolopyrimidothiazolopyrimidine derivatives with potential antioxidant and antimicrobial activity. Molecules. 2012;17(8):9652–9667.

[42] Mohareb RM, Al-Omran F, Azzam RA. Heterocyclic ring extension of estrone: Synthesis and cytotoxicity of fused pyran, pyrimidine and thiazole derivatives. Steroids. 2014;84:46–56.

[43] Al-Omary FA, Hassan GS, El-Messery SM, El-Subbagh HI. Substituted thiazoles V. Synthesis and antitumor activity of novel thiazolo[2,3-b]quinazoline and pyrido[4,3-d] thiazolo[3,2-a]pyrimidine analogues. Eur J Med Chem. 2012;47(1):65–72.

[44] Valderrama JV, Ríos D, Muccioli GG, Calderon PB, Brito I, Benites J. Hetero-annulation reaction between 2-acylnaphthoquinones and 2-aminobenzothiazoles. A new synthetic route to antiproliferative benzo[g]benzothiazolo[2,3-b]quinazoline-7,12-quinones. Tetrahedron Lett. 2015;56(36):5103–5105.

[45] Rizzo S, Bartolini M, Ceccarini M, Piazzi L, Gobbi S. Targeting Alzheimer's disease: Novel indanone hybrids bearing a pharmacophoric fragment of AP2238. Bioorg Med Chem. 2010;18(5):1749–1760.

[46] Vanicha V, Kanyawim K. Sulforhodamine B colorimetric assay for cytotoxicity screening. Nat Protoc. 2006;1(3):1112–1116.

[47] Skehn P, Storeng R, Scudiero A, et al. New colorimetric cytotoxicity assay for anticancer drug screening. J Natl Cancer Inst. 1990;82(13):1107–1112.

[48] National Center for Biotechnology Information, National Library of Medicine, National Institutes of Health. Available from: https://www.ncbi.nlm.nih.gov/protein/. Accessed January 25, 2017.

[49] RCSB Protein Data Bank. A structural view of biology. Available from: http://www.rcsb.org/pdb/home/home.do. Accessed January 25, 2017.

[50] Dassault systemes. DS Visualizer. Available from: http://accelrys.com/products/collaborative-science/biovia-discovery-studio/visualization-download.php. Accessed January 27, 2017.

[51] CASTp. Computed atlas of surface topography of proteins. Available from: http://sts.bioe.uic.edu/castp/. Accessed January 27, 2017.

[52] AutoDock 4.1. Available from: http://autodock.scripps.edu/. Accessed December 19, 2016.

[53] De Boer EC, De Jong WH, Steerenberg PA, et al. Induction of urinary interleukin-1 (IL-1), IL-2, IL-6, and tumour necrosis factor during intravesical immunotherapy with bacillus Calmette–Guérin in superficial bladder cancer. Cancer Immunol Immunother. 1992;34(5):306–312.

[54] Du J, Yang H, Zhang D, et al. Structural basis for the blockage of IL-2 signaling by therapeutic antibody basiliximab. J Immunol. 2010;184(3):1361–1368.

[55] Romanowski MJ, Scheer JM, O'Brien T, McDowell RS. Crystal structures of a ligand-free and malonate-bound human caspase-1: implications for the mechanism of substrate binding. Structure. 2004;12(8):1361–1371.

[56] Lagorce D, Sperandio O, Galons H, Miteva MA, Villoutreix BO. FAF-drugs2: free ADME/tox filtering tool to assist drug discovery and chemical biology projects. BMC Bioinformatics. 2008;9:396.

[57] Krieger E, Darden T, Nabuurs SB, Finkelstein A, Vriend G. Making optimal use of empirical energy functions: force-field parameterization in crystal space. *Proteins*. 2004;57(4):678–683.

[58] Best RB, Buchete NV, Hummer G. Are current molecular dyanamics force fields too helial? *Biophys J*. 2008;95(1):L07–L09.

3. INTRODUCTION

Toxicity testing of novel compounds is important for the drug development process. Acute oral toxicity studies are performed to evaluate the degree to which substances are toxic for animals, humans or the environment, to analyse the mechanism of toxic chemicals, and to develop new or improved tests for the specific types of chemically induced effects.

Acute oral toxicity study of both 4A and 6A was performed as per revised Organization for Economic Cooperation and Development (OECD) guidelines 423 [1]. Both 4A and 6A were dissolved in 0.25% carboxymethyl cellulose (CMC) and administered orally at the dose of 5 and 10 mg/kg body weight to albino Wistar rats for 15 days (n=10) and the animals were observed every day for any toxic manifestations (Figure 3.1).

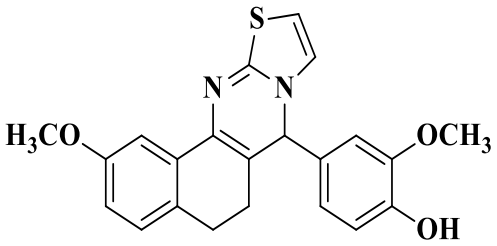

4A

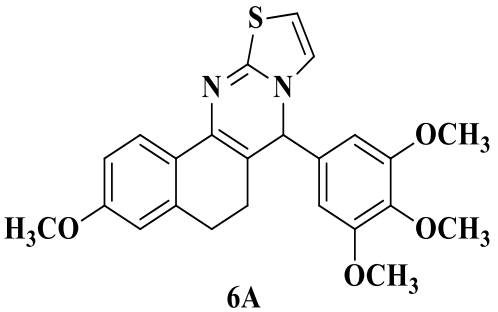

6A

Figure 3.1 Chemical structures of **4A** (2-methoxy-4-(2-methoxy-6,7-dihydro-5H-benzo[h] thiazolo[2,3-b]quinazolin-7-yl)phenol) and **6A** (3-methoxy-7-(3,4,5-trimethoxyphenyl)-6,7-dihydro-5H-benzo[h]thiazolo[2,3-b]quinazoline).

3.1 MATERIALS AND METHODS

3.1.1 Chemicals and reagents

NDEA was obtained from Sigma Aldrich, Bengaluru, India. Sodium citrate, disodium hydrogen phosphate, trichloroacetic acid and potassium dihydrogen phosphate were procured from SD Fine Chemicals, Mumbai, India. And other reagents used in this study, were of analytical grade.

3.1.2 Procurement and acclimatization of animals

Healthy male Wistar albino rats, weighing 80-120 g, were obtained from central animal house facility of S. D. College of Pharmacy & Vocational Studies, Muzaffarnagar, Uttar Pradesh, India and were housed in polypropylene cages with rice husks for bedding. The

experiment was performed as per The Committee for the Purpose of Control and Supervision of Experiments on Animals (CPCSEA) guidelines for laboratory animals and ethics, Department of animal welfare, Government of India (Approval No. SDCOP&VS/AH/CPCSEA/01/0038/R1). Animals were acclimatized under standard laboratory conditions (at 25±5˚C; relative humidity of 44–56%; 12 h light: dark cycle) with free access of standard rat chow and water *ad libitium.*

3.1.3 Acute toxicity protocol

Acute oral toxicity study of 4A and 6A compounds were performed at doses of 5 and 10 mg/kg body (n=10, rats each group) weight according to the OECD guidelines of the testing of chemicals [2]. 4A and 6A were dissolved in 0.25% carboxymethyl cellulose (CMC) and administered orally to albino Wistar rats for 15 days and the animals were observed every day for any toxic manifestation. Later, blood was collected in 2 mL eppendorf tube from the retro-orbital of rats and centrifuged at 5,000 rpm (4ºC) for 10 min to separate the serum and stored at -20ºC until analysis. Livers were dissected out and rinsed with ice cold saline and stored at -20ºC for further studies.

Various biological parameters such as AST and ALT; bilirubin and biliverdin; and various biochemical parameters (SOD, CAT, PC, GSH, TBARS) were measured during the experiment.

3.1.4 Measurements of body weight

The body weight of each animal from the each group was measured using a sensitive balance, one before the commencement of dosing and one on the day of sacrifice.

3.1.5 Estimation of oxidative stress parameters

3.1.5.1 Tissue malonaldehyde (MDA)

The measurement of MDA was carried out according to previously literatures [3]. 1.0 mL of 10% (w/v) tissue homogenate, 0.5 mL of 0.8% thiobarbituric acid and 0.5 mL of 30% trichloroacetic acid were used collectively in a falcon tube and enclosed with aluminium foil. After that, the tubes were kept in a shaking water bath for 30 min at 80ºC. Then, it was cooled for 15 min and centrifuged at 3000 rpm for 15 min.

Absorbance was measured spectrophotometrically at 540 nm against blank and tissue samples. The amount of MDA present in a sample was calculated according to the following equation:

$$\text{nM of MDA/}\mu\text{g of protein} = (V \times \text{OD at 540 nm})/(0.56 \times \text{protein concentration}).$$

Where, V is final volume of the test solution.

3.1.5.2 Tissue protein carbonyl (PC)

PC assay was carried out according to the method given in the previous literature with slight modifications [4]. 10% tissue homogenate was prepared in distilled water. 150 µL of tissue homogenate was poured in eppendorf tube and precipitated by adding 500 µL of 10% trichloracetic acid. After that, the tubes were centrifuges at 13,000 rpm for 2 min and supernatant was discarded.

Later, the cell pellets were incubated with 500 µL of 0.2% 2,4-dinitrophenylhydrazine with constant vortexing at every 5 min interval for 1h. Next, supernatant was removed and cell pellets were washed with 500 µL ethanol: ethyl acetate (1:1) solution three times. Later, pellets were dissolved in 600 µL Guanidine Hydrochloride (6M) and absorbance was recorded at 360nm. Similar procedure was performed for preparing Blanks solution where cells were absent. The PC content was calculated as follows:

$$\text{PC (}\mu\text{g/mg of protein)} = (\text{A360sample} - \text{A360sample blank})/\text{mg of protein}$$

3.1.5.3 Tissue glutathione (GSH)

GSH assay was carried out according to method prescribed in the previous literature with slight modifications [5]. 0.2 mL of 10% (w/v) tissue homogenate was added in eppendorf tube and 1.8 mL distilled water added to it. At the same time, precipitating solution was prepared by mixing 0.2 g ethylenediaminetetraacetic acid disodium salt, 1.67 g of glacial metaphosphoric acid, and 30 g sodium chloride in 100 mL distilled water.

Further, this precipitating solution was added to the above mixture. The mixture was then allowed to stand for 5 min and filtered. To 2 mL of filtrate, 8.0 mL of 0.3 M phosphate solution and 1.0 mL of 0.4% w/v 5,5'-dithio-bis-2-nitrobenzoic acid were added and centrifuged at 13000 rpm for 1 min. Similar procedure was performed for preparing Blanks solution where cells were absent. Then, the optical density (OD) was recorded at 412 nm.

The total protein content of each sample was measured using the Bradford reagent and bovine serum albumin (BSA) was used as a standard. The tissue GSH content was calculated as follows:

GSH (μM/μg of protein) = (310.4 × Ei× OD at 412 nm)/μg of protein.

Where, Ei is the correction factor (0.542)

3.1.5.4 Tissue superoxide dismutase (SOD)

Determination of SOD in the test samples were carried out according to method prescribed in the previous literature with slight modifications [6]. 100 μL of 10% cytosolic supernatant was prepared with tris–hydrochloric acid buffer (pH = 8.5) and final volume was adjusted up to 3.0 mL with the same buffer. Lastly, 25 μL of pyrogallol was added and change in absorbance was recorded at 420 nm at one min interval for 3 mins. Similar procedure was performed for preparing blanks solution where cells were absent.

One unit of SOD is expressed as the amount of enzyme required causing 50% inhibition of pyrogallol auto-oxidation per 3 mL of assay mixture and is given by the formula:

Unit of SOD/μg or protein = [100 × [(A-B)/(A×50)]]/μg of protein.

Where, A = Change in absorbance per min in control and B = Change in absorbance per min in test sample.

3.1.5.5 Tissue catalase (CAT)

CAT enzyme estimation was carried out according to procedure which was explained previously [3]. 10% (w/v) tissue homogenate was prepared in 50 mM phosphate buffer and centrifuged at 10000 rpm for 20 mins. 50 μL of supernatant was added to a tube containing 2.9 mL of 19 mM solution of hydrogen peroxide (H_2O_2) prepared in potassium phosphate buffer. Disappearance of H_2O_2 was monitored at 1 min interval for 3 mins at 240 nm. CAT activity was calculated as follows:

nM of H_2O_2/min/μg of protein = (ΔA/min × volume of assay) / (0.0719 × volume of sample × μg of protein).

3.1.6 Biochemical estimations

3.1.6.1 Aspartate aminotransferase (AST) and alanine aminotransferase (ALT)

AST and ALT were estimated in serum using a commercially available kit from Transia Biomedicals Ltd., Baddi, and Himachal Pradesh, India. According to the manufacturer's protocol, 100 µl serum samples added 100 µl of working reagent and measured the absorbance at 340nm at regular intervals of 1 min for 3 mins [7].

$$\text{Activity of ALT or AST (U/mL)} = \Delta A340/\text{min} \times 1768.$$

3.1.6.2 Tissue Bilirubin

Bilirubin in liver was measured as per the following procedure published earlier in the literature with slight modifications [8, 9]. All the tissue samples were thawed and homogenized in phosphate buffer saline (8.0 g sodium chloride, 0.2 g potassium chloride, 0.2 g potassium dihydrogen phosphate, 1.15 g disodium hydrogen phosphate, 0.372 g ethylene diaminetetraacetic acid disodium salt, pH 7.4). 500 µL of tissue homogenate (10%) was added to 2.0 mL of 1.5% butylatedhydroxy toluene in acetone:ethanol (1:1) in a eppendorf tube.

Simultaneously, fresh diazo reagent was prepared by mixing 300 µL of 10% sodium nitrite and 8.0 mL of 2M *p*-toluene sulfonic acid, then combining 4.0 mL of this mixture with 2.0 mL of 2.1% *p*-iodoaniline in glacial acetic acid, kept at room temperature for 2.0 min. Then the solution was diluted with distilled water (10 mL) and 200 µL of 1.5M ammonium sulfamate. This working diazo reagent was kept on ice for 5 min and 500 µL was added to each sample homogenates. Diazo blank reagent was freshly prepared by combining 2 mL of *p*-toluene sulfonic acid and 5.0 mL of 10% ascorbic acid, followed by addition of 2.1% *p*-iodoaniline in glacial acetic acid and 2.0 mL of n- butyl acetate, mixed and used immediately.

Finally, all the tubes were incubated for 1 hour on ice in dark. After incubation, freshly prepared 3.0 mL of 1% ascorbic acid in 0.1 M sodium chloride was added to each vial. All the vials were shaken vigorously, kept for 1.0 min and centrifuged at 2400 rpm for 10 min. The absorbance of the upper organic phase was taken at 530 nM wavelength. The content of bilirubin was calculated as follows:

$$A_{530}\text{sample} - A_{530}\text{blank} = \Delta A_{530}\text{Test}$$

3.1.6.3 Tissue biliverdin

Estimation of biliverdin was performed as per the method prescribed in the previous literature with slight modifications [8, 9]. Tissue samples were homogenized in phosphate buffer saline as per described in the previous section. 500 µL of tissue homogenate (10%) was combined with 500 µL of 10 M glacial acetic acid, 400 µL of 40 mM ascorbic acid, 500 µL of double distilled water and 100 µL of 200 mM barbituric acid. Samples were incubated in a water bath at 95°C in dark and then samples were extracted with butanol, vortexed and centrifuged. The upper organic layer was carefully removed and extracted with 2.5 mL 2M sodium hydroxide. The absorbance of upper layer was taken at 535 nM wavelength. The content of biliverdin was calculated as follows:

$$A_{535}\text{sample} - A_{535}\text{blank} = \Delta A_{535}\text{Test}$$

3.2 RESULTS

3.2.1 Body weight variation

The body weight variation was not more prominent in both doses 5 mg/kg and 10 mg/kg rats as compared to normal control rats after oral administration of 4A and 6A for 15 days.

Table 3.1 Effects of 4A and 6A on body weight and after oral administration of 5 and 10 mg/kg for 15 days.

Groups	Initial body weight (gm)	Final body weight (gm)	Weight gain (gm)	Percentage growth
NC	107.33±10.08	144.50±2.46	37.17±6.72	25.72
4A(5)	108.67±12.54	136.83±13.27*	28.17±1.47	20.58
4A(10)	109.17±10.06	140.50±5.04*	31.33±3.02*	22.30
6A(5)	106.80±6.95	140.61±4.11*	33.81±1.92*	24.05
6A(10)	107.98±4.81	140.56±6.18**	32.58±1.94**	23.18

Data represented as mean±SD (n=10). Statistically significant differences were observed between normal control and test groups [Unpaired student T-test (*p<0.001, **p<0.01)]. Abbreviations: normal control (NC), 4A 5 mg/kg {4A (5)}, 4A 10 mg/kg {4A (10)}, 6A 5 mg/kg {5A (5)}, 6A 10 mg/kg {6A (5)}.

3.2.2 Physiological and biochemical parameters in liver and various enzyme levels in serum

The effect of 4A and 6A on the changes in body weight of rats was illustrated in Table 3.1. After 15 days of exposure with 4A and 6A, a slight increase in body weight was observed in all animal groups. No mortality and behavioural changes were observed up to 15 days. Both compounds were safe at 10 mg/kg dose for 15 days.

Various biological parameters such as AST and ALT; bilirubin and biliverdin; and various biochemical parameters (SOD, CAT, PC, GSH, TBARS) were measured during this study. We observed various enzyme levels i.e. alanine aminotransferase (ALT) and aspartate aminotransferase (AST) in serum; bilirubin and biliverdin in liver tissue during acute toxicity studies of both compounds (Figure 3.2 & 3.3).

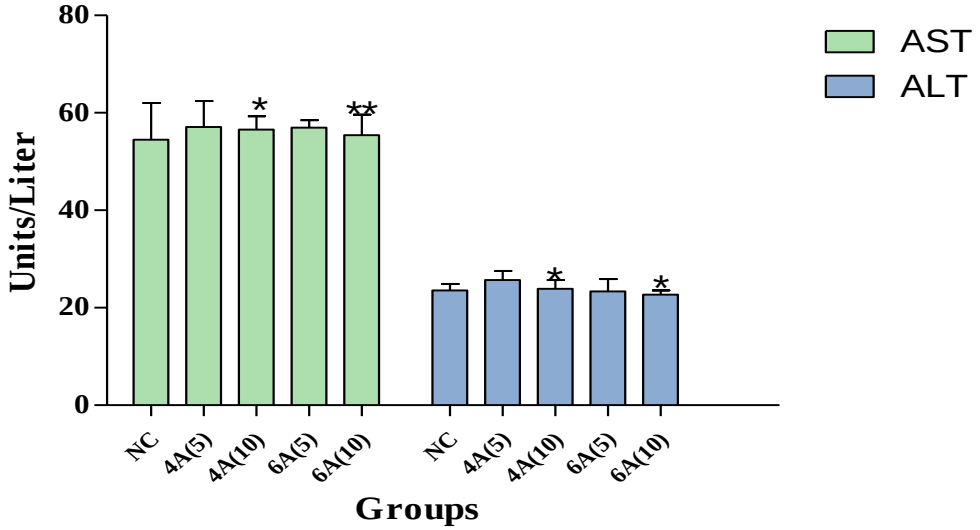

Figure 3.2 Effects of 4A and 6A on enzyme levels in serum after 5 mg/kg and 10 mg/kg doseadministration for 15 days treatment. Data represented as mean±SD (n=10). Statistically significant differences were observed between normal control and test groups [Unpaired student T-test (*p<0.001, **p<0.01)]. Abbreviations: normal control (NC), 4A 5 mg/kg {4A(5)}, 4A 10 mg/kg {4A(10)}, 6A 5 mg/kg {5A(5)}, 6A 10 mg/kg {6A(5)}.

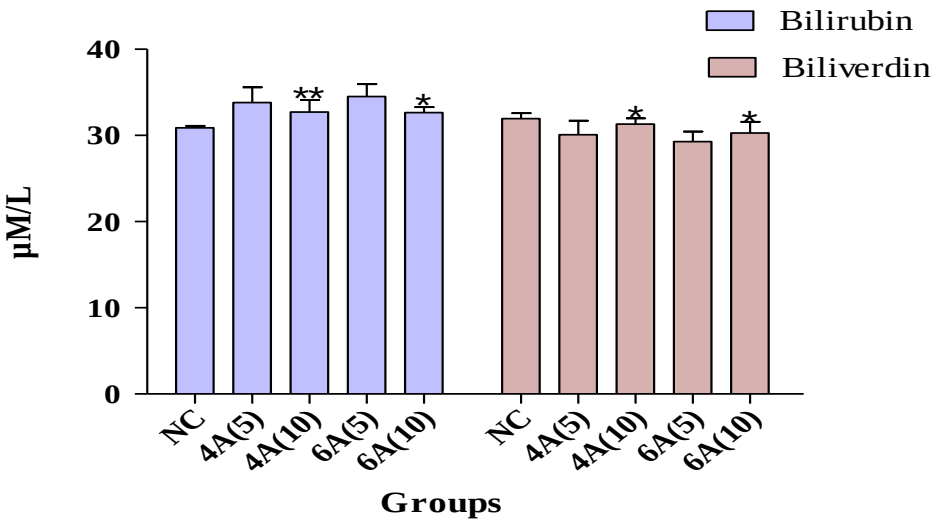

Figure 3.3 Effects of 4A and 6A on catabolic by-product (bilirubin and biliverdin) after 10 mg/kg dose administration for 15 days treatment. Data represented as mean±SD (n=10). Statistically significant differences were observed between normal control and test groups [Unpaired student T-test (*p<0.001, **p<0.01)]. Abbreviations: normal control (NC), 4A 5 mg/kg {4A (5)}, 4A 10 mg/kg {4A (10)}, 6A 5 mg/kg {5A (5)}, 6A 10 mg/kg {6A (5)}.

During oxidative stress parameter studies, we observed that there was no remarkable impact on SOD level between 4A, 6A tests and NC (~ 0.20 μM) groups. In the case of CAT and GSH levels, both compounds showed similar trend to NC. Further the tissue malondialdehyde (MDA) and PC formations were also measured to evaluate the toxic effects of 4A and 6A into the rats liver tissue. The MDA and PC levels were similar to NC. The results collectively suggested that there were no significant changes in any of these parameters following 4A and 6A treatments (dose 5 and 10 mg/kg) as compared to normal control. (Table 3.2)

Table 3.2 Effects of 4A and 6A on oxidative stress parameters after oral administration of 5 mg/kg and 10 mg/kg for 15 days.

Groups	SOD (U/mg of Protein)	CAT (mM H_2O_2 Decomposed/ min/mg of Protein)	GSH (μM/mg of protein)	TBARS (nM of MDA/mg of protein)	PC(μM/mg of Protein)
NC	0.34±0.01	6.07±0.55	16.48±0.53	0.31±0.04	0.12±0.01
4A(5)	0.35±0.02	6.78±0.25*	18.92±0.67	0.33±0.03	0.13±0.04
4A(10)	0.32±0.03*	5.41±0.68	17.04±0.49*	0.33±0.04*	0.15±0.02
6A(5)	0.27±0.01	6.70±0.31*	18.06±0.31*	0.34±0.01	0.16±0.01
6A(10)	0.30±0.02**	6.67±0.24	19.98±0.38**	0.36±0.02*	0.18±0.02

Data represented as mean±SD (n=10). Statistically significant differences were observed between normal control and test groups [Unpaired student T-test (*p<0.001, **p<0.01)]. Abbreviations: normal control (NC), 4A 5 mg/kg {4A (5)}, 4A 10 mg/kg {4A (10)}, 6A 5 mg/kg {5A (5)}, 6A 10 mg/kg {6A (5)}.

Results obtained from acute oral toxicity studies implied that both compounds were safe up to 10 mg/kg body weight dose in albino Wistar rats. Therefore, we decided to perform anti-HCC activity at a dose of 10 mg/kg body weight.

3.3 DISCUSSION

A previous screening study (in-vitro and molecular modelling screening) showed that 4A and 6A compounds possessed the potent cytotoxic activity against Hep-G2 human hepatocellular carcinoma cells. Therefore, it is logical to speculate that targeted compounds might be alternatives for the treatment of HCC in vivo. Based on the findings as explained above, 4A and 6A compounds were subjected to assess the safe and effective serum concentration in albino Wistar rats. In acute toxicity study, oral administration of 4A and 6A was well tolerated in rats at doses of 5 and 10 mg/kg and also we were not observed any significant reduction in body weight gain persisted over the 15 days. Various enzymes for instance ALT and AST in serum; bilirubin and biliverdin were evaluated in rat's liver tissues. These enzyme levels are usually raised during liver injury, other organs tissue damages or in toxic condition [10-12]. Interestingly, we found that the level of these enzymes were normal after the treatment with tested compounds 4A and 6A.

Additionally, we performed various biochemical parameters for instance SOD, CAT, PC, GSH, and TBARS to observe the mechanism of toxicity during oral administration of 4A and 6A at the dose tested. In this way, we were not observed any significant changes in the levels of these different biochemical parameters in treated rats compared to untreated rats (NC). Therefore, we concluded that both the compounds 4A and 6A are safe. All these findings suggested that 4A and 6A can be further administered in HCC rats to evaluate the potency against HCC condition.

REFERENCES

[1] Guideline O. For the testing of chemicals, guidance document on acute oral toxicity. Environmental health and safety monograph series on testing and assessment 2008: 1-27.

[2] Tice RR, Agurell E, Anderson D et al. Single cell gel/comet assay: Guidelines for in vitro and in vivo genetic toxicology testing. Environ Mol Mutagen. 2000;35:206-221.

[3] Lodhi RL, Maity S, Kumar P, Saraf SA, Kaithwas G, Saha S. Evaluation of mechanism of hepatotoxicity of leflunomide using albino wistar rats. Afr. J. Pharmacy Pharmacol. 2013;7:1625-1631.

[4] Saha S, Chan DSZ, Lee CY, Wong W, New LS, Chui WK, Yap CW, Chan ECY, Ho HK. Pyrrolidinediones reduce the toxicity of thiazolidinediones and modify their anti-diabetic and anti-cancer properties. Eur. J. Pharmacol. 2012;697:13-23.

[5] Saha S, New LS, Ho HK, Chui WK, Chan ECY. Direct toxicity effects of sulfoconjugated troglitazone on human hepatocytes. Toxicol. Let. 2010;195:135-141.

[6] Greenwald RA. Handbook of methods for oxygen radical research. Free Radic. Biol. Med. 1987;3:161.

[7] Kushwaha PS, Raj V, Singh AK, Keshari AK, Saraf SA, Mandal SC, Yadav RK, Saha S. Antidiabetic effects of isolated sterols from ficus racemosa leaves. RSC Adv. 2015;5:35230-35237.

[8] Makos BK and Youson JH. Tissue levels of bilirubin and biliverdin in the sea lamprey, Petromyzon marinus L., before and after biliary atresia. Comp Biochem Physiol A Physiol. 1988;**91**(4):701-710.

[9] Puppalwar P, Goswami K, Dhok A. Review on—Evolution of Methods of Bilirubin Estimation. IOSR-JDMS.2012;1(3):17-28.

[10] Makos BK and Youson JH. Tissue levels of bilirubin and biliverdin in the sea lamprey, Petromyzon marinus L., before and after biliary atresia. Comp Biochem Physiol A Physiol. 1988;91(4):701-710.

[11] Kowsalya R, Kaliaperumal J, Vaishnavi M, Namasivayam E. Anticancer activity of Cynodon dactylon L. root extract against diethyl nitrosamine induced hepatic carcinoma. South Asian J Cancer. 2015;4:83-87.

[12] Pradeep K, Mohan CV, Gobianand K, Karthikeyan S. Silymarin modulates the oxidant-antioxidant imbalance during diethylnitrosamine induced oxidative stress in rats. Eur J Pharmacol. 2007;560:110–116.

4. INTRODUCTION

Chronic exposure to chemical carcinogens leads to several biochemical and genetic variations in the cells. N-nitrosodiethylamine (NDEA), a known most toxic and environmental hepatic carcinogen, has been used as tumour inducer in various hepatic cancer models. Also, it has been shown to be mutagenic and genotoxic [1]. Cytochrome P450 enzyme dependent NDEA metabolism produces reactive oxygen species (ROS) and also other free radicals, which may be responsible for its tumorigenic activity [2, 3] Currently, NDEA-induced hepatocellular carcinoma (HCC) in rats is extensively used as a standard experimental model to investigate the different stages of hepatocarcinoma [4].

Dysregulated cell proliferation and solid tumor generation are generally encountered in several cancers including HCC. The mechanism of cancer development is mainly due to the activation of oncogenes and inactivation of tumour suppressor genes (TSG) [4, 5]. HCC is one of the most common malignancies with high prevalence and poor prognosis and second leading cause of cancer-associated deaths, worldwide [6, 7]. Its rate of incidence is dramatically increasing in developing countries, due to increased underlying hepatic conditions, for instance, alcoholic liver disease, non-alcoholic fatty liver disease (NAFLD), hepatitis B & C infection. Worldwide mortality rate of all other leading cancers (such as lung, breast and prostate cancers) are declining, whereas death rate of liver cancer is increased by 2.8% in men and 3.4% in women each year [8, 9]. Approximately 748,000 new cases (9.2% of all new global cancer cases) of HCC are being diagnosed every year, worldwide [10].

As per reports, chemotherapy with standard cytotoxic agents such as doxorubicin, cisplatin or 5-fluorouracil, shows below 10% response rate without a clear benefit in overall survival [11, 12]. In addition, these are poorly tolerated in patients as a result of systemic toxicities and their associated adverse effects [13]. In fact, one of the most challenging applications in the emerging field of HCC treatment is to develop new therapeutic strategies for solid tumors with negligible or lesser cytotoxicity to the normal cells.

Functionalized thiazolo[2,3-b]quinazoline scaffold have long been studied and served as a versatile building blocks in the emerging field of synthetic medicinal chemistry [14, 15]. This privileged structural motif is known for its wide range of biological activities [16-19]

including anticancer [20], antiinflammatory [21], antituberculosis [22], anticonvulsant [23], antimalarial [24], antihypertensive [25], anti-diabetic [26] etc.

In chapter 2, we described *p*-toluenesulfonic acid (*p*-TSA)-promoted syntheses, molecular modelling and in vitro antitumor activity of 5H-benzo[h]thiazolo[2,3-b] quinazoline (1A-15A) and indeno[1,2-d]thiazolo[3,2-a]pyrimidine (1B-15B) analogs against human hepatoma (Hep-G2) cells where compounds 4A and 6A (Figure 1) were found as potent inhibitors among the series [27].

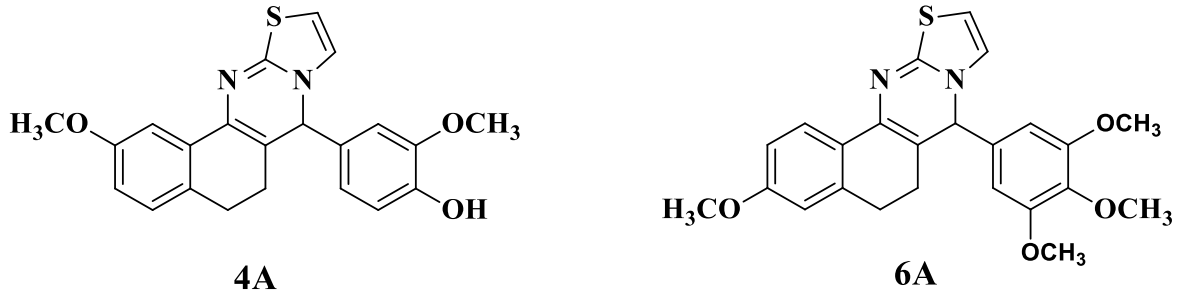

Figure 4.1 Chemical structures of **4A** (2-methoxy-4-(2-methoxy-6,7-dihydro-5H-benzo[h] thiazolo[2,3-b]quinazolin-7-yl)phenol) and **6A** (3-methoxy-7-(3,4,5-trimethoxyphenyl)-6,7-dihydro-5H-benzo[h]thiazolo[2,3-b]quinazoline):

In continuation to our effort to develop novel therapeutic strategies for HCC treatment, we investigated the in vivo antitumor activity involving the role of oxidative stress parameters and inflammatory mediators in NDEA-induced HCC using male albino Wistar rats. The molecular mechanism underlying the antitumor effects of 4A and 6A was explored by observing the gene expression levels through the real-time quantitative reverse-transcribed polymerase chain reaction (qRT-PCR) analysis. Later, Proton nuclear magnetic resonance (^{1}H-NMR)-based serum metabolomics were performed to analyse the effects of 4A and 6A against HCC- induced metabolic alterations.

4.1 MATERIALS AND METHODS

4.1.1 Materials

N-nitrosodiethylamine (NDEA), Glutathione (GSH) and 2,4-dinitrophenylhydrazine (DNPH) were acquired from Sigma-Aldrich, USA. ALT and AST kits were purchased from the Transasia Biomedicals Pvt. Ltd., Baddi, India. Interleukins (IL-2, IL-6) were commercially procured from Sigma-Aldrich, USA and (IL-1β and IL-10) from Genetex Biotech Asia Pvt. Ltd, New Delhi, India. All the chemicals and solvents were of analytical grades with 99%

purity and in house distilled water was used throughout the experiment. Test compounds 4A and 6A were synthesised previously by our research group [27].

4.1.2 Experimental animals

Healthy male Wistar albino rats, weighing 80-120 g, were obtained from central animal house facility of S. D. College of Pharmacy & Vocational Studies, Muzaffarnagar, Uttar Pradesh, India and were housed in polypropylene cages with rice husks for bedding. The experiment was performed as per CPCSEA guidelines for laboratory animals and ethics, Department of animal welfare, Government of India (Approval No. SDCOP&VS/AH/CPCSEA/01/0038/R1). Animals were acclimatized under standard laboratory conditions (at 25±5˚C; relative humidity of 44–56%; 12 h light: dark cycle) with free access of standard rat chow and water *ad libitium.*

4.1.3 Experimental design

All the experimental Wistar rats were randomly distributed into 5 groups of 8 animals each (n=8) and the groups were classified as Group I (Normal Control): 0.25% CMC (2 mL/kg); Group II (Carcinogen Control): NDEA (100 mg/kg, i.p. every week for 6 weeks) [28-30]; Group III (Positive Control): NDEA+5-FU (10 mg/kg, i.p. for 15 days after the dose of NDEA administration); Group IV (4A): NDEA+4A (10 mg/kg, orally for 15 days after the dose of NDEA administration); Group V (6A): NDEA+6A (10 mg/kg, orally for 15 days after the dose of NDEA administration).

The abovementioned protocol to induce HCC was adopted from various literatures [31, 32]. After adaptive inhabitation to experimental conditions for initial one week, all experimental animals of group II to V were administrated with NDEA. After the dose of NDEA administration for 6 weeks, 5-FU, 4A and 6A were given for 15 days as a curative agent against liver injury, mentioned in group III, IV and V respectively.

At the end of experimental period, animals were sacrificed by cervical decapitation and livers were excised immediately, rinsed in ice-cold saline and stored at -80°C for further histological studies and molecular level investigations. The serum was also collected, processed and stored for further bio-chemical analysis.

4.1.4 Estimation of various physiological parameters

To estimate the body weight variation, rats were weighed at the initial and final days of experiment and % weight gain calculated to observe the cytotoxic effects between treated and untreated group. Liver weight, number and percentage incidence of carcinogenic nodules of liver were calculated.

4.1.5 Estimation of serum enzyme levels and biochemical examination in liver

Serum enzymes, including aspartate aminotransferase (AST), alanine aminotransferase (ALT), lactate dehydrogenase (LDH) and creatine phosphokinase (CK), were measured using commercially available kit. The oxidative stress parameters like catalase (CAT) [33], protein carbonyl (PC) [34], superoxide dismutase (SOD) [35], glutathione (GSH) [36] and thiobarbituric acid reactive substances (TBARS) [33] were also estimated in liver tissue in the similar way as described previously in chapter 3. The total protein concentration of each sample was measured using the Bradford reagent and the bovine serum albumin (BSA) was used as a standard.

4.1.6 Estimation of catabolic by-products in hepatic tissue: Bilirubin and biliverdin

Conjugated bilirubin and biliverdin in liver were measured as per the previously explained in chapter 3 [37].

4.1.7 Estimation of cytokines in hepatic tissue

Elevated levels of interleukin-1β (IL-1β), IL-2, IL-6, and IL-10 inflammatory mediators were assayed as per the instructions provided by the manufacturers. Rat IL-1β, IL-2, IL-6, and IL-10 ELISA kit was based on standard sandwich enzyme-linked immune-sorbent assay technology.

4.1.8 Histopathological studies and scanning electron microscopy (SEM) of hepatic tissue

Liver tissues from each group were assessed for their morphological changes using eosin and hematoxylin staining. The tissues were conserved in 10% formalin for overnight. Subsequently, the tissues were superseded by 70% isopropanol overnight. Afterward, the tissues rinsed with isopropanol at various concentrations (70, 90 and 100%) and dehydrated further by 100% xylene. The tissue samples were then fixed in beeswax and 5 μM longitudinal tissue sections were sliced by using microtome. Finally, the tissues were fixed

and stained by eosin and hematoxylin dyes and examined under a microscope (magnification 40 X).

For SEM analysis, 2-4 mm liver tissue samples were collected and fixed in 2.5% glutaraldehyde for 2-6 h at 4ºC for primary fixation. After that, the samples were cleaned with 0.1M phosphate buffer for 15 min at 4ºC. Later, 1% osmium tetroxide was used as a post-fixation for 2 h at 4ºC. Again, the samples were washed in 0.1 M phosphate buffer for 3 times at 15 min interval and kept at 4ºC. Afterward, these samples were dehydrated with acetone at various concentrations (30, 50, 70, 90, 95 and 100%). All specimens were air dried at room temperature and critical point drying (31.5ºC at 1100 psi). Finally, tissue samples were mounted on to the aluminum stubs with adhesive tape and observed for the morphological changes using a scanning electron microscope (JEOL JSM-6490LV) [38].

4.1.9 Real-time quantitative reverse-transcribed polymerase chain reaction (qRT-PCR) analysis

To determine the expression of mRNA for the different genes, 10 mg of tissue samples of each group was taken in a tube and total RNA was extracted using TriZol reagent and RNeasy mini kit was employed to purify the RNA. cDNA reactions were prepared utilizing GeneSure first strand cDNA synthesis kit (Genetix Biotech Asia Pvt. Ltd., New Delhi, India) for quantitative PCR. Finally, Real-time PCR was carried out in Agilent Stratagene Mx3000P series (Applied Biosystems, Foster City, USA) using Sybr$^{@}$ green PCR master mix. The mRNA was normalized with housekeeping control β-actin. ΔCt values were normalized with untreated control samples for all compounds ($\Delta Ct = Ct_{\text{gene of interest}} - Ct_{\text{house keeping gene}}$). Relative changes in the expression level of one specific gene were calculated in terms of $2\text{-}\Delta\Delta Ct$ ($\Delta\Delta Ct = \Delta Ct_{test} - \Delta Ct_{control}$) [34].

The primer sequences were as follows: GAPDH, 5'-TGATGGGTTTCCCATTGATGA-3' (forward) and 5'-TGATTCTACCCACGGCAAGTT-3' (reverse)[39]; IL-6, 5' TCAATGAGGAGACTTGCCTG-3' (forward), 5'-GATGAGTTGTCATGTCCTGC-3' (reverse) [40].

4.1.10 ^{1}H-NMR based serum metabolic profiling

4.1.10.1 Sample Preparation and NMR instrumentation

An aliquot of serum (250 µL) from each sample and 250 µL of 0.9% of an aqueous saline solution (50 mM concentration, pH 7.4 in D_2O) were taken in 2 mL eppendrof tube and

centrifuged at 10,000 rpm for 5 min. The supernatant was transferred to a 5 mm NMR tubes (Wilmad Glass, USA) for data recording. 0.1% v/v TSP (Sodium salt of 3-trimethylsilyl-(2,2,3,3-d4)-propionic acid) as external standard, was mixed in NMR tube.

The NMR spectra of prepared samples were generated at 298K on a Bruker Biospin Avance-III 800 MHz NMR spectrometer, operating at proton frequency of 800.21 MHz. The spectrometer is equipped with CryoProbe with maximum gradient-strength output of 53 G/cm. 1D ^{1}H NMR spectra were recorded using the Carr–Purcell–Meiboom–Gill (CPMG) pulse sequence in Topspin-2.1 (Bruker NMR data Processing Software) with pre-saturation of the water peak via irradiating it perpetualy during the recycle delay (RD) of 5 sec. Each CPMG spectrum consisted of the accumulation of 128 scans and lasted for approximately 15 minutes. A total spin–spin relaxation time of 60 ms (n=300 and 2τ=200 δs) with a line broadening factor of 0.3 Hz was applied to remove broad signals from triglycerides, proteins, cholesterols and phospholipids. Diffusion time of 120 ms was used to enervate the signals of low molecular weight compounds without affecting the lipid signals.

All the acquired NMR spectra were processed using Topspin-2.1 (Bruker NMR data Processing Software) and standard Fourier Transformation (FT) procedure for phase and baseline correction. Prior to FT, each Free Induction Decays (FIDs) were zero-filled to 4096 data points and a sine-bell apodisation function/tapering function was applied. After FT, the chemical shifts were referenced internally to methyl doublet of L-lactate (at δ=1.33 ppm). All the recorded spectra were visually analysed for their acceptability and subjected to multivariate statistical analysis to identify the altered metabolic pattern.

4.1.10.2 Spectral Assignment

To identify the distinct allocation of various peaks in the CPMG ^{1}H NMR spectra, two-dimensional NMR (2D NMR) spectra were recorded for selected samples including ^{1}H-^{1}H total correlation spectroscopy (TOCSY) and ^{1}H-^{13}C heteronuclear single quantum correlation (HSQC). The chemical shifts were identified and assigned at a good extent by comparing them with the chemical shifts available with the software Chenomx 8.1 (Chenomx Inc., Edmonton, Canada). The remaining peaks in the CPMG ^{1}H NMR spectra were allocated using the previously existing databases available as HMDB (The Human Metabolome Database) and other literature reports [41-43].

4.1.10.3 Multivariate data analysis

All the acquired NMR spectra were corrected manually for phase and baseline aberration in Topspin 2.1 (Bruker NMR data Processing Software). The CPMG (δ 0.5−8.5 ppm) spectra were then binned into 0.01 ppm wide integrated spectral buckets with the help of AMIX package (Version 3.8.7, Bruker, Bio Spin). The regions containing the resonance from residual *water* (*δ 4.7-5.1* ppm), were excluded to avoid the effects of imperfect water suppression. The binned data were then obtained from AMIX after mean centring and normalization, which was executed by dividing each data point by the sum of all data points present in the sample, to compensate for the differences in concentration of metabolites among individual serum samples.

The data were scaled up using unit variance where identical weight was given to all variables. The resulting data matrices were exported into Microsoft Office Excel 2010 and used for multivariate analysis via open access web-based metabolomic data processing tool, named MetaboAnalyst 3.0 (http://ww.metaboanalyst.ca/) and Unscrambler X Software (Version 10.3, CAMO USA, Norway). Principal component analysis (PCA) was first performed on both the CMPG and sets to identify the outliers.

To further demonstrate the separation between samples belonging to different groups, supervised partial least squares-discriminant analysis (PLS-DA) was performed to identify the metabolites significantly contributing to group differentiation. Model quality was assessed with R^2, indicating the validity of models against over fitting, and Q^2, indicating the predictive ability. Potential metabolites markers were extracted from PLS-DA loading plots and the scores of variable importance on projection (VIPs). The statistical significance of these metabolites was calculated by Student's t-test (p value less than 0.05).

4.1.11 Statistical data analysis

Statistical data analysis was performed using Graph Pad Prism 5.0 (San Diago, CA, USA). All results were expressed as mean ± standard deviation (SD). The data was analysed by one-way ANOVA (analysis of variances) followed by Bonferroni multiple comparison test. Statistical significance differences were considered with respect to Carcinogen control (*p<0.001, **p<0.01, ***p<0.05).

4.2 RESULTS

4.2.1 Estimation of physiological and biochemical parameters in liver tissue and various enzyme levels in serum

In the in-vivo study, we initially analyzed the defensive efficiency of 4A, 6A and 5-FU through various physiological parameters like body weight, liver weight, number and percentage incidence of carcinogenic nodules in liver of experimental groups of animals, respectively. The body weight and liver weight variation were more prominent in NDEA-administered (Group II) rats as compared to the normal control (Group I) rats; conversely, treatment with 4A and 6A normalized the impact to a certain extent (Table 1).

And the similar observations were noted for carcinogenic nodule no. per animal and % incidence of carcinogenic nodules in liver. The test compounds and 5-FU were significantly ($p < 0.05$) lowered the NDEA-induced carcinogenic nodules and % incidence as compared to group II (Table 2). As mentioned above, the administration of 4A, 6A and 5-FU normalized these parameters to a certain level. Interestingly, the impact of 4A was nearly similar to the standard chemotherapeutic drug, 5-FU.

Table 4.1 Effects of 4A and 6A on body weight and liver weight in hepatocellular carcinoma after oral administration of 10 mg/kg for 15 days.

Groups	Initial body weight (gm)	Final body weight (gm)	Weight gain (gm)	Percentage growth	Liver weight (gm)
NC	97.33±10.08	144.50±2.46	47.17±6.72	33	7.17±0.20
CC	105.67±13.74	116.83±12.09	11.17±1.47	10	10.69±0.82
PC	101.17±10.06	130.50±5.04*	29.33±3.02*	22	7.58±0.31*
4A	100.33±6.95	131.39±4.11*	31.33±1.92*	24	8.00±0.16**
6A	102.17±4.81	130.61±6.18*	24.83±1.94*	19	8.83±0.11**

Data represented as mean±SD (n=8). Statistically significant differences were observed between carcinogen control and test groups [one way-ANOVA followed by Bonferroni multiple comparison test (*p<0.001, **p<0.01)]. Abbreviations: normal control (NC), carcinogen control (CC), positive control (PC).

Table 4.2 Effects of 4A and 6A on carcinogenic nodules incidence in hepatocellular carcinoma after oral administration of 10 mg/kg for 15 days.

Groups	No. of animal bearing nodules/ total animals	% Incidence of nodules[a]	Total no. of nodules	No. of nodules per animal[b]
NC	0/6	0	0	0
CC	6/6	100	41	7
PC	3/6	50	7	1
4A	4/6	66.67	11	2
6A	5/6	83.33	22	4

[a](Number of nodules bearing rats/total number of rats in each group) ×100.
[b](Total number of tumour/number of tumour bearing rats in each group).

Abbreviations: normal control (NC), carcinogen control (CC), positive control (PC).

Table 4.3 Effects of 4A and 6A on oxidative stress parameters in hepatocellular carcinoma after oral administration of 10 mg/kg for 15 days.

Groups	SOD (U/mg of Protein)	CAT (mM H_2O_2 Decomposed/ min/mg of Protein)	GSH (µM/mg of protein)	TBARS (nM of MDA/mg of protein)	PC(µM/mg of Protein)
NC	0.34±0.02	6.07±0.55	16.48±0.53	0.31±0.04	0.12±0.01
CC	0.15±0.01	1.78±0.25	8.92±0.67	0.53±0.03	1.13±0.04
PC	0.30±0.04*	5.41±0.68*	13.04±0.49*	0.33±0.04**	0.15±0.02*
4A	0.27±0.03*	3.70±0.31*	11.06±0.31*	0.34±0.01**	0.16±0.01*
6A	0.20±0.02**	2.67±0.24**	9.98±0.38**	0.36±0.02**	0.28±0.02**

Data represented as mean±SD (n=8). Statistically significant differences were observed between carcinogen control and test groups [one way-ANOVA followed by Bonferroni multiple comparison test (*$p<0.001$, **$p<0.01$)]. Abbreviations: normal control (NC), carcinogen control (CC), positive control (PC).

Table 4.3 depicts the reduction of oxidative stress markers (SOD, CAT, GSH, TBARS and PC) after drug treatment and the status of hepatic antioxidant potential was investigated in NDEA-exposed groups to explore the functional correlation between oxidative stress and cancer progression.

We observed that the GSH concentration was greatly reduced in NDEA-exposed rats which on treatment with 5-FU, 4A and 6A efficiently increased the GSH content towards normal (Table 4.3). Besides this, we noticed that the levels of SOD and CAT enzymes were reduced up to 50% and 70% respectively after NDEA exposure while a minor reduction in these enzymatic activities was observed in 4A and 6A treated groups with respect to control.

In contrast, a significant increase in MDA and PC formation was appeared in HCC rats but these formations were most efficiently regained after 5-FU, 4A, and 6A treatment. Figure 2 indicates the level of serum liver marker enzymes such as AST, ALT, LDH and CK in normal control and experimental animals. NDEA-induced carcinogenic control (Group II) animals exhibit almost two folds increase ($p<0.01$) in the levels of these enzymes when compared to normal control (Group I). However, treatment with test compounds 4A and 6A showed their ability in the maintenance of these enzymatic activities.

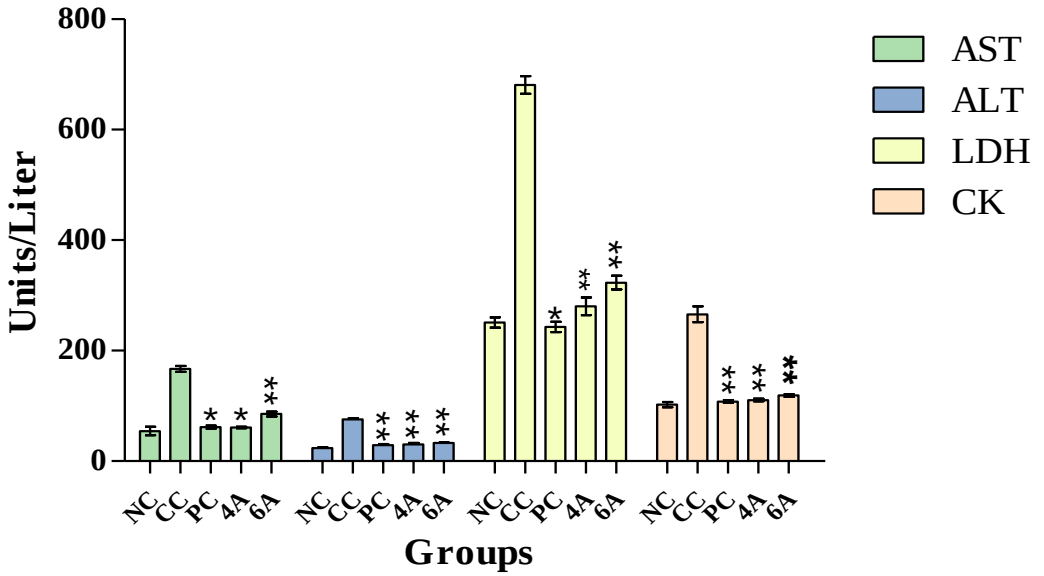

Figure 4.2 Effects of 4A and 6A on enzyme levels in serum after 10 mg/kg dose administration for 15 days treatment. Data represented as mean±SD (n=8). Statistically significant differences were observed between carcinogen control and test groups [one way-ANOVA followed by Bonferroni multiple comparison test (*p<0.001, **p<0.01)]. Abbreviations: normal control (NC), carcinogen control (CC), positive control (PC).

4.2.2 Estimation of catabolic by-products (bilirubin and biliverdin) in hepatic tissue

4A and 6A treated (groups IV and V, respectively) rats reflect significant ($p<0.01$) normalization of the catabolic pigments in liver tissues as compared to carcinogenic control group (Group II) which, in turn, exhibits almost two folds significant ($p<0.001$) elevation as compared to normal control, indicating the toxic nature of NDEA (Figure 4.3).

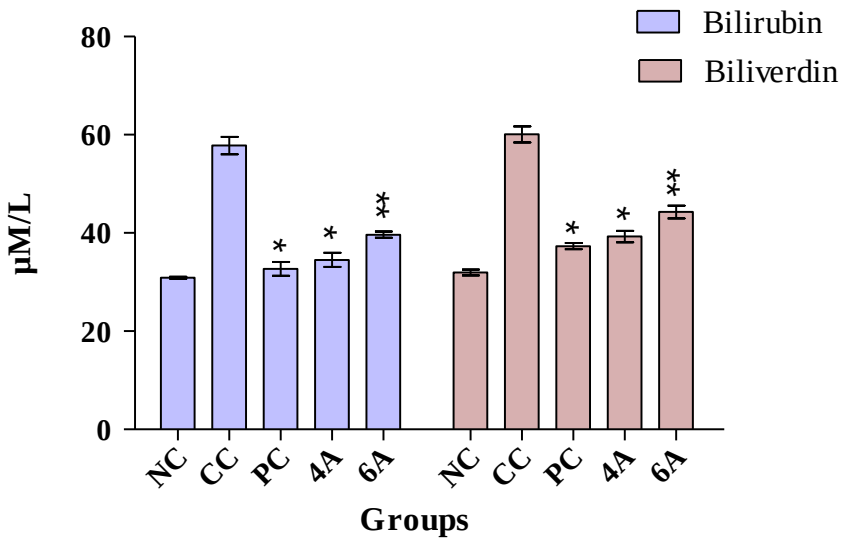

Figure 4.3 Effects of 4A and 6A on catabolic by-product (bilirubin and biliverdin) after 10 mg/kg dose administration for 15 days treatment. Data represented as mean±SD (n=8). Statistically significant differences were observed between carcinogen control and test groups [one way-ANOVA followed by Bonferroni multiple comparison test (*p<0.001, **p<0.01)]. Abbreviations: normal control (NC), carcinogen control (CC), positive control (PC).

4.2.3 Effect of 4A and 6A on IL-1β, IL-2, IL-6, and IL-10 levels

To further characterize the effects of 4A and 6A in the inflammatory events, we investigated the tissue concentration of the specific inflammatory cytokines viz: IL-1β, IL-2, IL-6, and IL-10 by ELISA. The concentration of these cytokines in rat hepatic tissue was increased significantly by 2-3 folds after NDEA treatment as compared to normal control. Both the test compounds and 5-FU significantly suppressed the abnormally high concentration of these mediators in tumour tissues. Treatment with 4A and 6A (10 mg/kg) attenuated the increased levels of IL-1β, IL-2, IL-6, and IL-10 with pronounced effect on IL-6. Compound 4A treated group showed inhibition of IL-6 level as well as other cytokines level (p<0.001), more similar to 5-FU (Table 4.4).

Table 4.4 Effects of 4A and 6A on IL-2, IL-6, IL-10 and IL-1β in hepatic carcinogenic tissue after oral administration of 10 mg/kg for 15 days.

Groups	IL-2 (Pg/ml)	IL-6 (Pg/ml)	IL-10 (Pg/ml)	IL-1β (Pg/ml)
NC	134.03±10.08	39.23±2.46	58.13±6.72	42.50±4.19
CC	330.60±13.74	124.18±12.09	113.31±8.47	110.22±8.49
PC	160.19±10.06*	57.06±5.04*	66.33±6.02*	57.53±5.86*
4A	192.73±6.95*	62.10±4.11*	70.15±10.12*	70.90±10.68**
6A	269.00±4.81**	73.88±6.18**	80.79±1.94**	84.34±2.03**

Data represented as mean±SD (n=8). Statistically significant differences were observed between carcinogen control and test groups [one way-ANOVA followed by Bonferroni multiple comparison test (*p<0.001, **p<0.01)]. Abbreviations: normal control (NC), carcinogen control (CC), positive control (PC).

4.2.4 Impact of the test compound on IL-6 gene expression

Our findings suggest that NDEA-alone administration dramatically elevated the IL-6 levels compared to untreated group (group I). However, 5-FU, 4A and 6A treatment significantly normalized the elevated levels of IL-6. The efficacy of 4A and 6A at 10 mg/kg dose was nearly equivalent to commercially available chemotherapeutic drug 5-FU, and 4A was found to be potent than 6A (Figure 4.4).

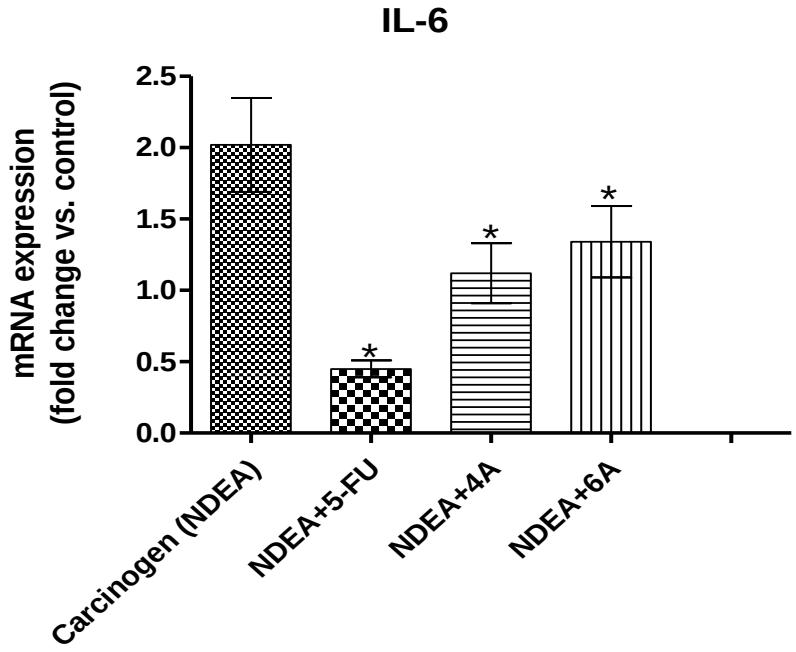

Figure 4.4 Gene expression levels of pro-inflammatory cytokine IL-6 after 4A and 6A administration in NDEA treated rats. Data represented as mean±SD (n=8). Statistically significant differences were observed between carcinogen control and test groups [Paired T-test, (*p<0.001)].

4.2.5 Morphology, histopathology and SEM analysis

Morphological changes were observed using intact liver of various groups. There was a clear visual difference in the numbers of carcinogenic nodules between 4A, 6A and NDEA-administered groups.

Histological changes of hepatic tissue were observed in various treated groups compared to normal control. Hepatic tissues analysis exhibited loss of architecture and the presence of enlarged hepatocytes in carcinogen control (CC) than normal control. The NDEA-administered groups also exhibited irregular sinusoids and degenerated tumour cells. The rats treated with 4A and 6A (10 mg/kg) showed cells with architecture more or less similar to normal control (Figure 4.5) and the effects were similar to 5-FU.

SEM analysis also followed the similar patterns where loss of architecture and degenerated tumour cells were less prominent in drugs 4A, 6A and 5-FU treated rats as compared to NDEA-exposed groups (Figure 4.5).

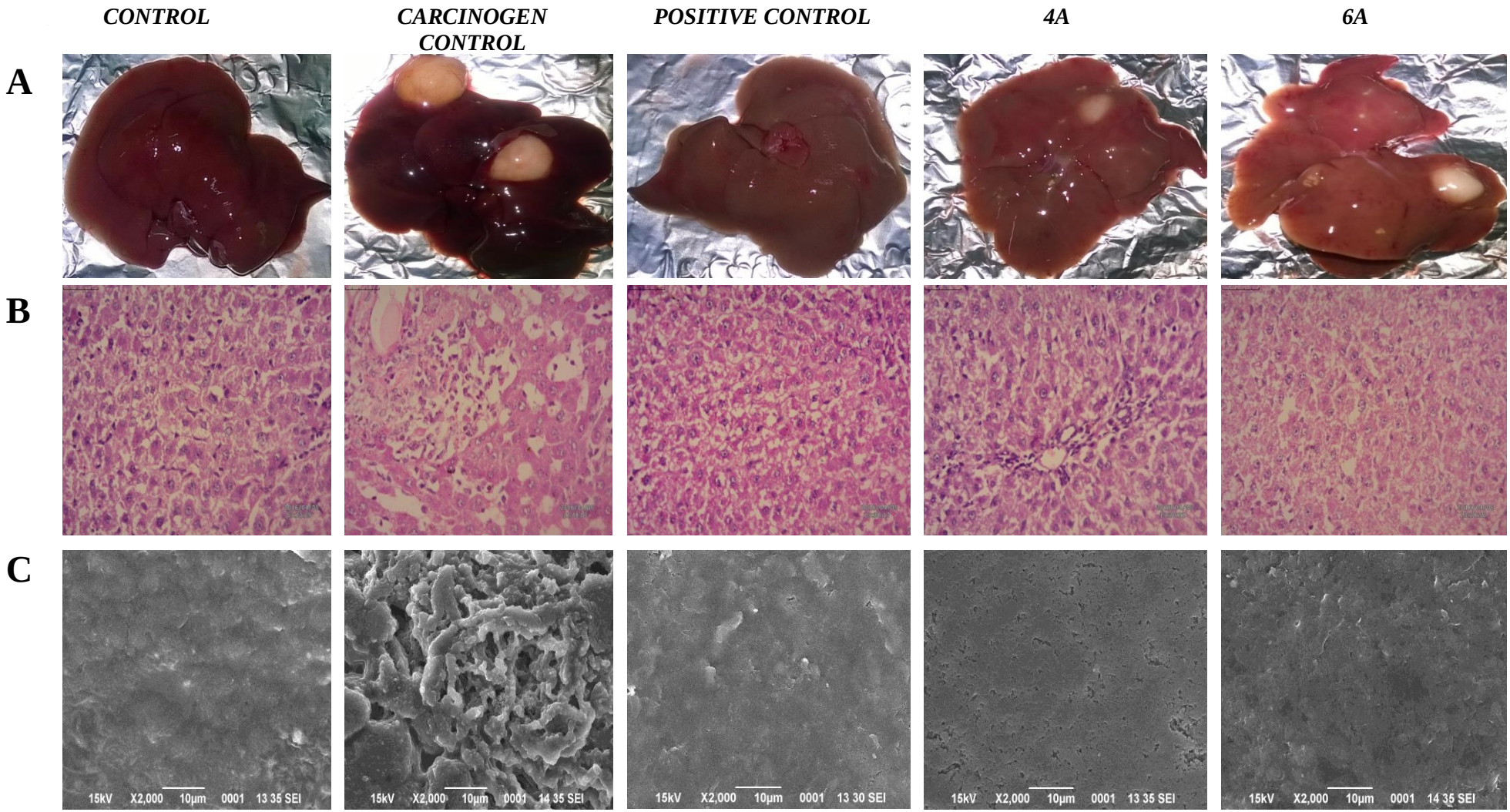

Figure 4.5 The hepatic pathological changes in NDEA-induced rats. Carcinogenic nodules were prominent in NDEA group which was absent or reduced significantly after 5-FU, 4A and 6A administration. A- Intact liver, B- Histopathological changes (40X, Scale bar 50 µm), C- Scanning electron microscopic photomicrographs of the liver tissues (2000X). Abbreviations: normal control (NC), carcinogen control (CC), positive control (PC).

4.2.6 ^{1}H-NMR based metabolomics

4.2.6.1 Metabolic effects of 4A and 6A in NDEA-induced HCC rats

An acquired NMR data from the serum samples of all groups were analysed using SIMCA-P software, version 11.0 (Umetrics AB, Umea, Sweden) where chemometric methods including principal components analysis (PCA) and orthogonal partial least squares-discriminant analysis (OPLS-DA) were performed to examined the metabolic alterations in an unsupervised and supervised manner, respectively.

PCA model was applied to authenticate the analytical quality system performance to discern outliers. OPLS-DA model was useful to obtain a summary of set of samples and to discriminate the variables that are responsible for variation among all the groups. The OPLS-DA model was optimized through two variables i.e. Q^2 and R^2Y. Score plots obtained from 1D ^{1}H CPMG NMR spectra (Figure 4.6) (from OPLS-DA and S plots) exhibited reasonable separation among all groups (Figure 4.7 and 4.8).

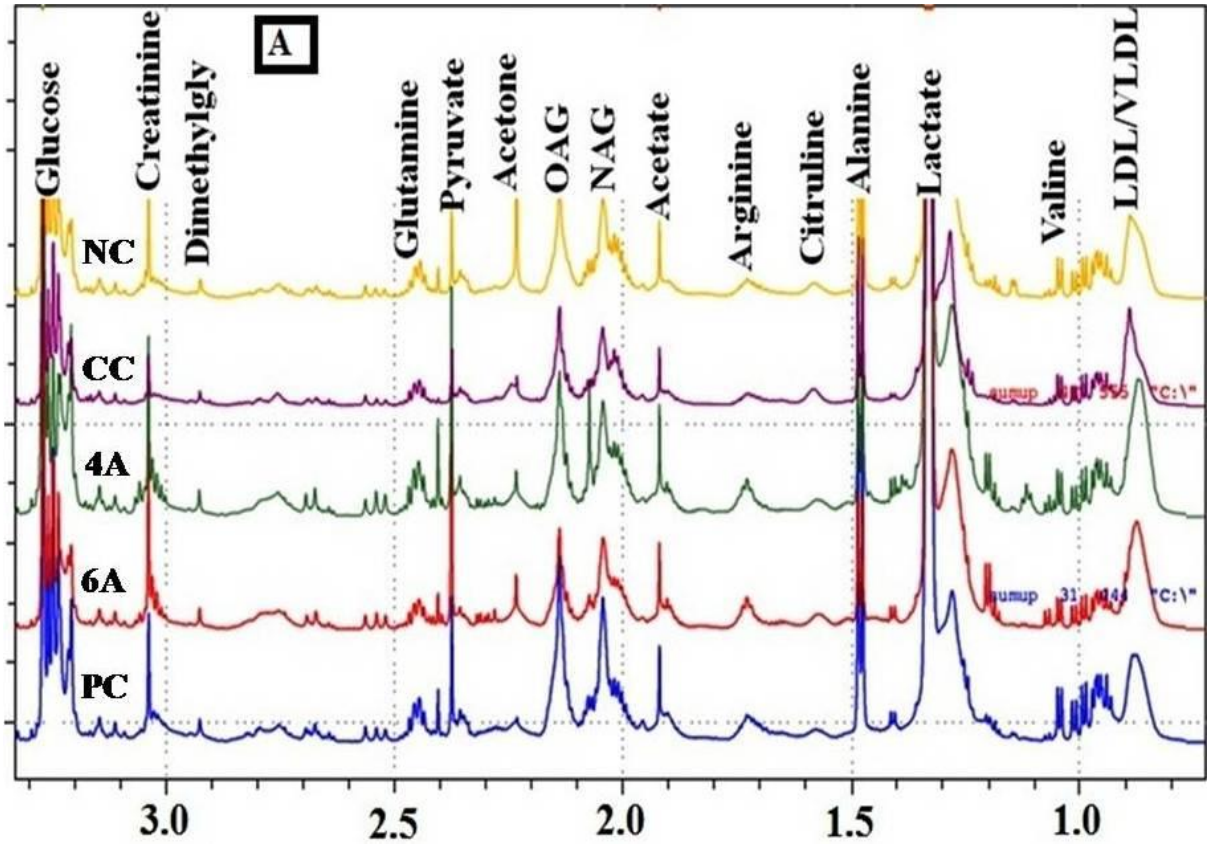

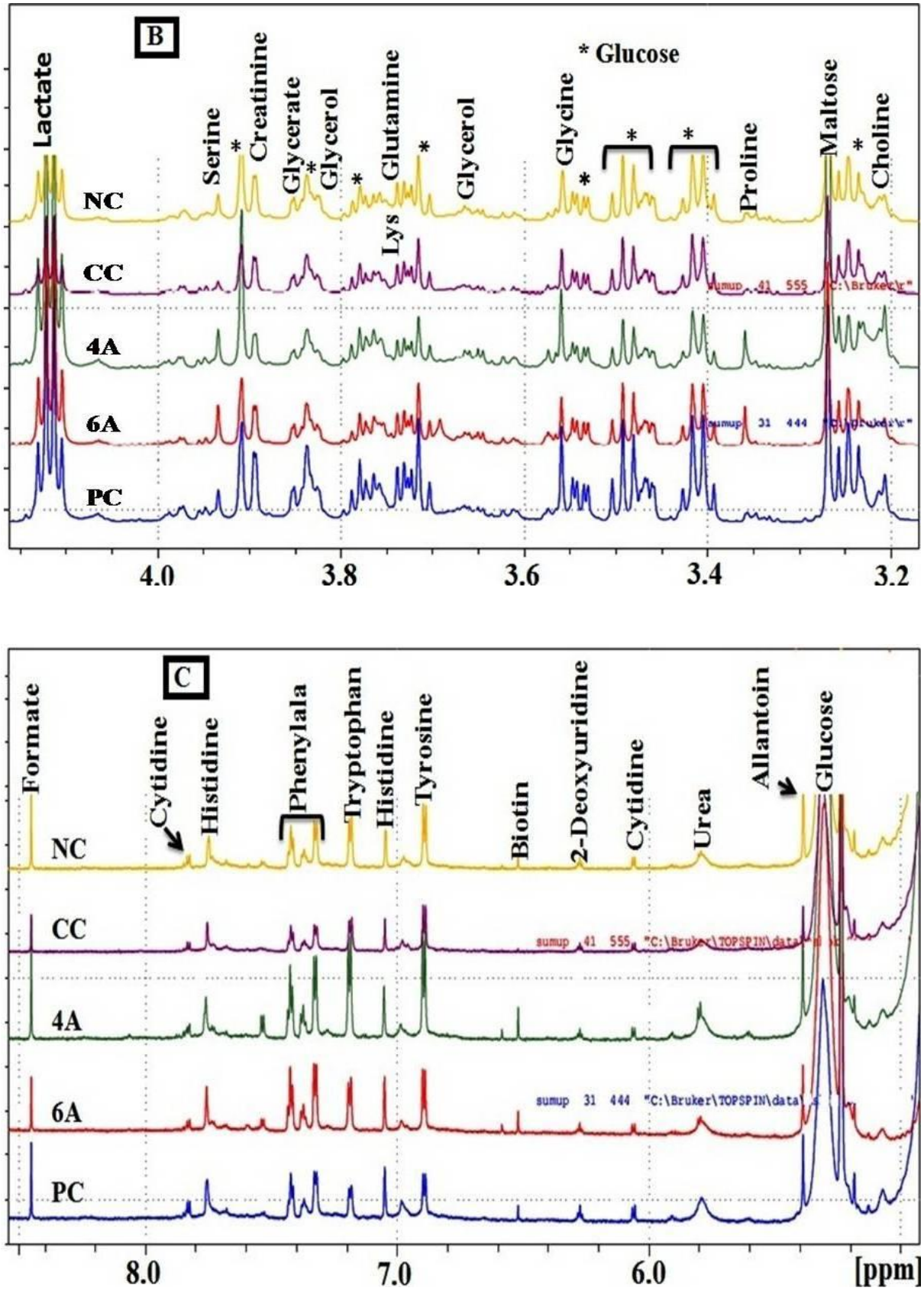

Figure 4.6 Representative 1D ^{1}H CPMG NMR spectra of rat serum obtained from different groups [Normal control (NC), NDEA (CC), NDEA+5-FU- 10mg/kg (PC), NDEA+4A-10

mg/kg (4A) and NDEA+6A-10 mg/kg (6A)]. The peaks annotated in the figure show the assignments of serum metabolites **A:** 0 - 3.0 ppm, **B:** 3.2 - 4.0 ppm and **C:** 5.0 - 8.0 ppm. The abbreviations used are: LDL/VLDL: low/very-low density lipoproteins; OAG: O-acetyl glycoprotein; NAG: N-acetyl glycoprotein.

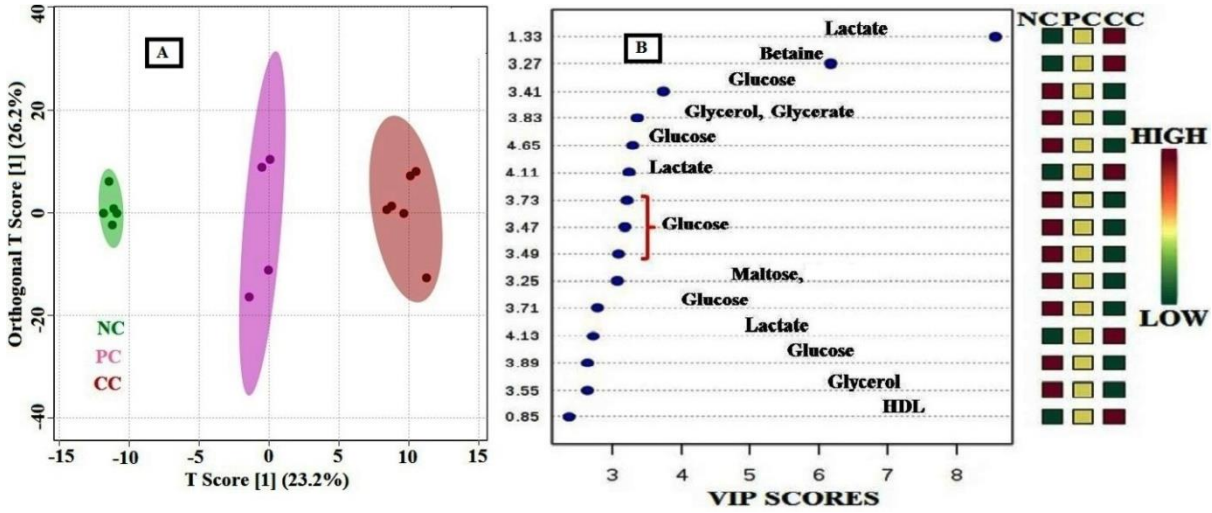

Figure 4.7 The combined and pairwise OPLS-DA analysis: **(A)** 2D OPLS-DA analysis of 1D ^{1}H CPMG NMR spectra score plot derived from combined analysis comprising of all the groups: normal control (NC), carcinogen control (CC), positive control (PC) 5-FU, 10 mg/kg (i.p.), pairwise analysis. **(B)** The potential discriminatory metabolite entities identified from VIP scores derived from PLS-DA modelling of complete data matrix and resulting VIP scores for top 20 metabolite entities are shown in increasing order of VIP score values to highlight their discriminatory potential.

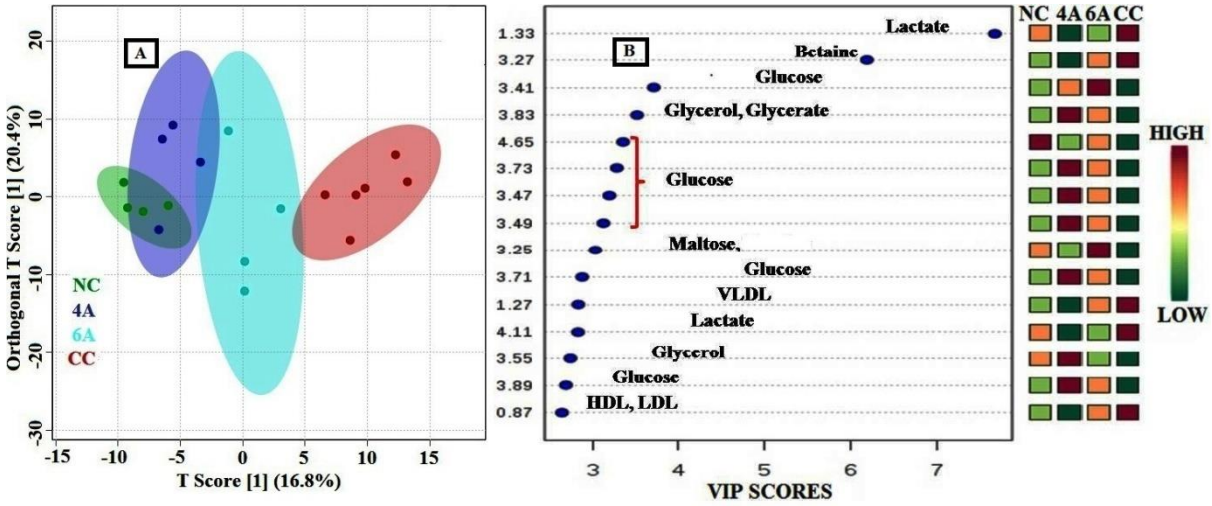

Figure 4.8 The combined and pairwise OPLS-DA analysis: **(A)** 2D OPLS-DA analysis of 1D ^{1}H CPMG NMR spectra score plot derived from combined analysis comprising of all the groups: normal control (NC), carcinogen control (CC), 4A and 6A = 10 mg/kg.

(B) pairwise analysis. The potential discriminatory metabolite entities identified from VIP scores derived from PLS-DA modelling of complete data matrix and resulting VIP scores for top 20 metabolite entities are shown in increasing order of VIP score values to highlight their discriminatory potential.

The various metabolites were carefully chosen when the statistically major threshold of variable influence on projection (VIP) values achieved from the OPLS-DA model was greater than 1.0. Meanwhile, the two-tailed Student's t-test *p*-values less than 0.05 ($p < 0.05$) was considered statistically significant. Log2 fold change (FC) was employed to demonstrate how these selected differential metabolites varied among all the groups of animals.

The datasets of these differentially expressed metabolites (log2-scaled) were introduced into MetaboloAnalyst 3.0 for the generation of heat map and multivariate statistics. The areas (AUC) under the receiver operating characteristic curves (ROC) were constructed to evaluate the effectiveness of potential biomarkers. In the MetaboAnalyst analysis, the results were considered statistically significant when p-value is less than 0.05 (Figure 4.9).

4.2.6.2 Metabolic changes during carcinogenic condition with treatments

On the basis of PLS-DA data, both the combined and pair wise analysis revealed $R^2 = 0.70$, $Q^2Y \geq 0.90$, indicating the significant metabolic changes in NDEA, 4A and 6A treated groups. The key observation of serum metabolic alterations between the untreated and NDEA-exposed groups together with their chemical shifts (δ) values, variable importance on projection (VIP) score and p-value are illustrated in Figure 4.7 and 4.8. There were significant elevated levels of Lactate, HDL, LDL, VLDL, tryptophan, tyrosine, creatinine, arginine and decreased levels of glucose, maltose, betaine, leucine, glycerate, glycerol, valine, carnosine, in NDEA treated group. Representative box-cum-whisker plots also supported the significant alterations in the above mentioned metabolites profile (Figure 4.9). All these metabolites were successfully retrieved after the administration of 4A and 6A, particularly at 10 mg/kg dose.

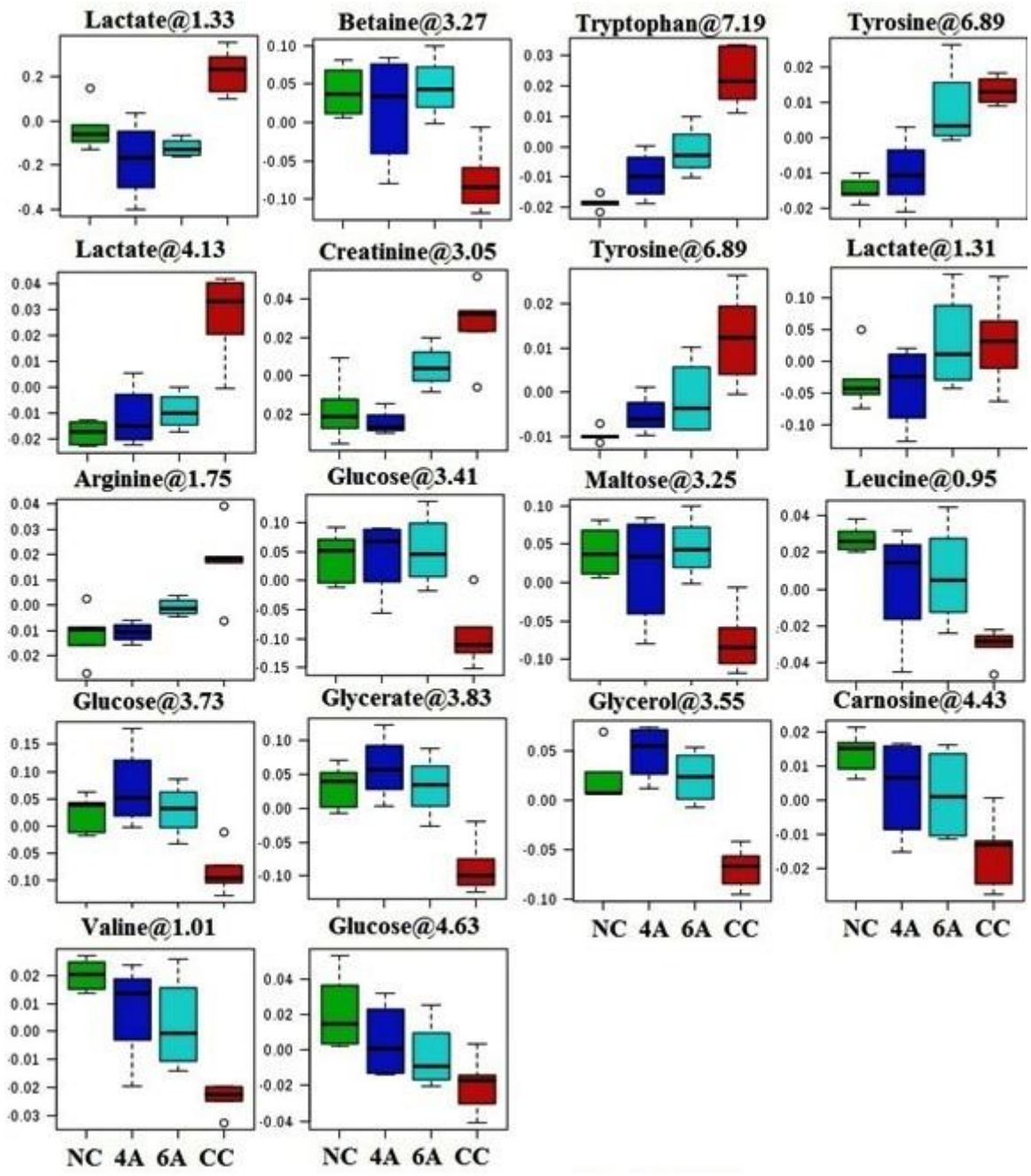

Figure 4.9 Metabolic effects of 4A and 6A treatment: the box-cum-whisker plots are showing relative variations in quantitative profiles of serum metabolites relevant in the context of the pathophysiology of hepatocellular carcinoma.

The metabolite highlighted in green colour are the metabolites whose p-value was found not to be significant ($p>0.05$). In the box plots, the boxes denote interquartile ranges, horizontal line inside the box denote the median, and bottom and top boundaries of boxes are 25th and 75th percentiles, respectively.

Lower and upper whiskers are 5th and 95th percentiles, respectively. Where: normal control (NC), carcinogen control (CC) = NDEA, positive control (PC), 4A and 6A = 10 mg/Kg.

4.3 DISCUSSION

Liver is a vital organ, playing an imperative role in various physiological and defensive mechanisms and regulating intermediary metabolism in the body [44]. According to literatures, chemotherapy against HCC has no any survival benefits for patients. The clinical outcome of HCC treatment remains limited and unsatisfactory due to systemic toxicities and other side effects [13, 45]. Considering these consequences, chemotherapeutic agents may be used in lower dose as well as higher dose but the higher dosages provide better efficacy profile while the lower dosages give better safety profile. Therefore, these are never-ending balancing act [12, 46]. It is, therefore, urgent to develop probable therapeutic agents for better efficacy as well as safety profile to sustain the clinical benefits in cancerous patients.

The synthesised compounds 4A and 6A, which displayed excellent anti-proliferative activity on Hep-G2 cells with GI_{50} < 10 μg/mL and in silico studies revealed that 4A and 6A have impressive binding energy with crucial hydrogen bond and π–bonds to various HCC biomarkers like IL-2, IL-6, caspase-3 and caspase-8 [27]. The in-vivo investigation was carried out to evaluate the ameliorative effects of NDEA-induced hepatocellular carcinogenesis in albino Wistar rats by 5H-benzo[h]thiazolo[2,3-b] quinazolines and the role of specific cytokines, oxidative and metabolic stress manifestations during cancer progression. Overall, these findings first time clearly suggested the hepatoprotective effect of 4A and 6A against NDEA-induced HCC and its ability to bind with important markers more significantly.

In contrary, NDEA-exposed groups showed decrease in body weight, increase in liver weight and higher number of carcinogenic nodules which indicates critical HCC condition in rats. However, chemo-drugs treatment with 4A, 6A and 5-FU significantly regained the various biochemical parameters near to normal. Exposure of animals to 4A, 6A and 5-FU after NDEA administration significantly normalized the reduced weight, increased % incidence of carcinogenic nodules and enhanced the protective action of 4A and 6A against carcinogen-induced metabolic alterations in hepatic cells.

Further, oxidative stress associated biochemical processes diminished the GSH, SOD and CAT levels and conversely, the formation of MDA and PC were induced in carcinogen-injected rats. Hence, alterations of these parameters confirmed the onset of hepatic oxidative

stress and correlation of transformed cells during cancerous conditions. The formation of excess reactive oxygen species (ROS) occurs during the various stages of metabolic biotransformation of NDEA exposure and leads to carcinogenesis by upregulation of several biochemical, intracellular signaling pathways, and gene expression [47]. Endogenous anti-oxidative defence system like, GSH is a free radical scavenger and both the SOD and CAT are antioxidant enzymes which inactivate hydrogen peroxide and dismutase superoxides, respectively [48]. Previously, it was reported that there was a decrease in the activities of enzymatic antioxidants during HCC conditions [49]. Cancerous cells have been reported to sequester vital antioxidants from the systemic circulation, in order to achieve the demands of developing solid tumours [50].

Treatment with 4A and 6A revealed preventive action to retrieve the levels of GSH, SOD and CAT near to normal and enhanced the anti-oxidative physiological processes. The levels of MDA and PC were attenuated significantly in drug treatment groups as compared to NDEA-exposed HCC rats. Bilirubin and biliverdin are the catabolic by-products of RBCs and the elevated levels of these biomarkers indicate hepatic disease state. During this study, it was observed that the levels of bilirubin and biliverdin were elevated in carcinogen-exposed group, whereas 4A and 6A treatment significantly attenuated the levels of these two specific markers [37].

Moreover, various enzymes like ALT, AST, LDH and CK are notably increased in human serum with liver metastases of HCC [51]. Similar observations were noted in NDEA-exposed rats and the levels were brought down to normalcy with 5-FU, 4A and 6A drug treatments and predominantly, the impact of 4A is comparable to standard 5-FU.

In addition, intact liver architecture, histopathology and SEM analysis were assessed to analyse the morphological changes associated to NDEA administration and drug treatment. Both histology and SEM analyses revealed that degenerated tumour cells, loss of architecture, and tumoral vacuoles were formed in NDEA-induced rats as previously reported [9]. The histological investigation of the rats treated with 4A, 6A and 5-FU showed cells with architecture more or less similar to control (group I), representing the hepatoprotective activity of the compounds in cancerous condition. In the SEM analysis, we also observed degenerated necrotic tissues in carcinogen exposed rats, which were regularized to a great extent in 4A and 6A treatment groups.

The serum cytokines are key mediators for several pathological and physiological modulations involving inflammation and cancer progression. Further, recent studies indicate that expression of inflammatory mediators like IL-1β, IL-2, IL-6 and IL-10 are involved in initiation and progression of HCC conditions [52]. As per several reports, the regulation of expression and secretion of various cytokines and their receptors have been already described in patients with severe liver conditions [53, 54]. For example, circulating blood interleukins-1β (IL-1β), IL-2, IL-6, and IL-10 concentrations were increased in patients with hepatic cancers [52-55].

In consequent with this information related to potential biomarkers, we wanted to know whether 4A and 6A may be active against these HCC specific inflammatory cytokines. The investigation further proved via various ELISA assays where we observed that all these inflammatory cytokines were elevated in NDEA-exposed rats. In addition, the levels of cytokines regularised after the treatment with 4A, 6A and 5-FU, indicating that both the test compounds exhibited anti-HCC property via inhibition of IL-1β, IL-2, IL-6 and IL-10 over expression at cancer sites. Both the test compounds manifested potential inhibition with IL-6 rather than IL-1β, IL-2 and IL-10. Similar pattern was also observed in quantitative RT-PCR analysis. The level of IL-6 gene expression was spectacularly decreased with NDEA-exposed rats (group II) and returned to normal control with 4A, 6A and 5-FU treatments which strongly supported potent anti-HCC activity of 4A. Interleukin 6 (IL-6) is a pleiotropic four-helical cytokine that modulates the inflammation-associated cancers by activating the phosphorylation of STAT3 to promote tumor initiation, invasion and metastasis [56, 57]. However, increased levels of IL-6 have been reported to be related to HCC prognosis with elevated cancer risk [58].

^{1}H NMR based metabolomics were further implemented to evaluate whether 4A and 6A have ability to restore the metabolic perturbations in NDEA-exposed HCC progression. OPLS-DA score plots using MetaboAnalyst [59] were derived from 1D ^{1}H CPMG NMR spectral data of rat serum samples of all groups and the carcinogen-exposed HCC rat serum samples were clearly demonstrated the significant metabolic alterations in cancerous conditions.

The decreasing level of glucose and increasing level of lactate were observed in carcinogen-exposed rats which are consisted with earlier findings [60, 61]. These findings were fully supported the War-burg effect and may be linked with higher amount of glucose consumption by cancerous tissues and followed by formation of lactic acid as by-product [61,

62]. We found that 4A, 6A and 5-FU treatment regularized the imbalance of above metabolites. In this way, we noticed significant elevated levels of lipoproteins and lipids in HCC rats compared to normal and these are involved to transport hydrophobic lipid molecules in circulation or ECF.

Next, lipids are also used for production of energy for instance β-oxidation, therefore, the elevated level could be due to the consequences of energy requirement for cell membrane synthesis and rapid proliferation [63]. Moreover, betaine and glycerol were down regulated in HCC condition. These metabolites are mainly involved in metabolism of choline. 4A and 6A administration regained the concentrations of these altered metabolites to normal level further providing evidence of anti-cancer activity of 4A and 6A [64]. The depleted level of leucine is in accordance with the previous report on human HCC [65]. Arginine (semi-essential amino acid in humans) is critical for the human cancers growth. It is also involved in protein synthesis as well as diverse aspects of tumor metabolism including the synthesis of nitric oxide, proline, glutamate, polyamines and nucleotides. Elevated level of arginine was found in carcinogen exposed as compared to drug-treated rat serum samples [66].

Furthermore, serum creatinine, an important intermediate in the energy metabolism, was significantly increased in NDEA-induced HCC rats compared to normal control and might be associated with increase in energy demand due to cancer proliferations. Tyrosine was also upregulated in NDEA-induced HCC rats which might be due to increased catabolism [64, 67]. Administration of chemically synthesized anticancer compounds (4A and 6A) remarkably attenuated all these metabolites markers, exhibiting hepatoprotective action of 4A and 6A against NDEA-exposed HCC. Overall, the impact of 4A and 6A was more prominent at 10 mg/kg dose that was comparable to the reference chemotherapeutic 5-FU.

4.4 REFERENCES

[1] Velu P, Vijayalakshmi A, Iyappan P, Indumathi D. Evaluation of antioxidant and stabilizing lipid peroxidation nature of Solanum xanthocarpum leaves in experimentally diethylnitrosamine induced hepatocellular carcinogenesis. Biomed Pharmacother. 2016;84:430–437.

[2] Heindryckx F, Colle I, Vlierberghe HV. Experimental mouse models for hepatocellular carcinoma research. Int J Exp Pathol. 2009;90(4):367–386.

[3] Raghunandhakumar S, Paramasivam A, Senthilraja S, et al. Thymoquinone inhibits cell proliferation through regulation of G1/S phase cell cycle transition in N-nitrosodiethylamine-induced experimental rat hepatocellular carcinoma. Toxicol Lett. 2013;223(1):60-72.

[4] Kumara M, Verma V, Nagpal R, et al. Effect of probiotic fermented milk and chlorophyllin on gene expressions and genotoxicity during AFB1-induced hepatocellular carcinoma. Gene. 2011;490:54–59.

[5] Kawajiri K, Fujii-Kuriyama Y. P450 and human cancer. Jpn J Cancer Res. 2005;82:1325–1335.

[6] Gupta P, Bansal MP, Koul A. Evaluating the effect of lycopene from Lycopersicum esculentum on apoptosis during NDEA induced hepatocarcinogenesis. Biochem Biophys Res Commun. 2013;434:479–485.

[7] World Health Organization. Cancer fact sheet, February 2017. Available from: http://www.who.int/mediacentre/factsheets/fs297/en/. Accessed on May 19, 2017.

[8] Hashim D, Boffetta P, Vecchia LC, et al. The global decrease in cancer mortality: trends and disparities. Ann Oncol. 2016;27(5):926–933.

[9] Chacko S, Samanta S. A novel approach towards design, synthesis and evaluation of some Schiff base analogues of 2-aminopyridine and 2-aminobezothiazole against hepatocellular carcinoma. Biomed Pharmacother. 2017;89:162–176.

[10] Kew MC. Hepatocellular carcinoma: epidemiology and risk factors. J Hepatocell Carcinoma. 2014;1:115–125.

[11] Marin JJG, Castano B, Martinez-Becerra P, et al. Chemotherapy in the treatment of primary liver tumours. Cancer Ther. 2008;6:711–728.

[12] Park SH, Lee Y, Han SH, Kwon SY, et al. Systemic chemotherapy with doxorubicin, cisplatin and capecitabine for metastatic hepatocellular carcinoma. BMC Cancer. 2006;6:1471–1476.

[13] Okada S. Cancer chemoprevention as adjuvant therapy for hepatocellular carcinoma. Jpn J Clin Oncol. 2001;31:357–358.

[14] Qin X, Lv Y, Liu P, et al. Novel morpholin-3-one fused quinazoline derivatives as EGFR tyrosine kinase inhibitors. Bioorg Med Chem Lett. 2016;26:1571–1575.

[15] Vodnala S, Bhavani AKD, Kamutam R, Naidu VGM, Promila, Prabhakar C. DABCO-catalyzed one-pot three component synthesis of dihydropyrano[3,2-c]chromene substituted quinazolines and their evaluation towards anticancer activity. Bioorg Med Chem Lett. 2016;26:3973–3977.

[16] Rahman MU, Jeyabalan G, Saraswat P, Parveen G, Khan S, Yar MS. Quinazolines and anticancer activity: a current perspective. Synth Commun. 2016;47(5):379–408.

[17] Monchaud D, Allain C, Teulade-Fichou MP. Development of a fluorescent intercalator displacement assay (G4-FID) for establishing quadruplex-DNA affinity and selectivity of putative ligands. Bioorg Med Chem Lett. 2016;26(18):4842–4845.

[18] Chen X, Du Y, Sun H, et al. Synthesis and biological evaluation of novel tricyclic oxazine and oxazepine fused quinazolines. Part 1: erlotinib analogs. Bioorg Med Chem Lett. 2014;24(3):884–887.

[19] Zahedifard M, Faraj FL, Paydar M, et al. Synthesis of apoptotic new quinazolinone-based compound and identification of its underlying mitochondrial signalling pathway in breast cancer cells. Curr Pharm Des. 2015;21(23):3417–3426.

[20] Chandregowda V, Kush AK, Reddy CG. Synthesis and in vitro antitumor activities of novel 4-anilinoquinazoline derivatives. Eur J Med Chem. 2014;44(7):3046–3055.

[21] Alagarsamy V, Solomon RV, Dhanabal K. Synthesis and pharmacological evaluation of some 3-phenyl-2-substituted-3H-quinazolin-4-one as analgesic, anti-inflammatory agents. Bioorg Med Chem. 2007;15(1):235–241.

[22] Nandy P, Vishalakshi MT, Bhat AR. Synthesis and antitubercular activity of Mannich bases of 2-methyl-3H-quinazolin-4-ones. Indian J Heterocycl Chem. 2006;15(3):293–294.

[23] Georgey H, Abdel-Gawad N, Abbas S. Synthesis and anticonvulsant activity of some quinazolin-4-(3H)-one derivatives. Molecules. 2008;13(10):2557–2569.

[24] Verhaeghe P, Azas N, Gasquet M, et al. Synthesis and antiplasmodial activity of new 4-aryl-2-trichloromethylquinazolines. Bioorg Med Chem Lett. 2008;18(1):396–401.

[25] Ismail MA, Barker S, Abau-el-Ella DA, Abouzid KA, Toubar RA, Todd MH. Design and synthesis of new tetrazolyl- and carboxybiphe-nylylmethyl quinazoline derivatives as angiotensin II AT1 receptor antagonists. J Med Chem. 2006;49(5):1526–1535.

[26] Malamas MS, Millen J. Quinazoline acetic acids and related analogues as aldose reductase inhibitors. J Med Chem. 1991;34(4):1492–1503.

[27] Keshari AK, Singh AK, Raj V, et al. *p*-TSA-promoted syntheses of 5H-benzo[h]thiazolo[2,3-b]quinazoline and indeno[1,2-d]thiazolo[3,2-a]pyrimidine analogs: molecular modeling and in vitro antitumor activity against hepatocellular carcinoma. Drug Des Devel Ther. 2017;11:1623–1642.

[28] Matsuzaki T, Murase N, Yagihashi A, et al. Liver Transplantation for Diethylnitrosamine-Induced Hepatocellular Carcinoma in Rats. Transplant Proc. 1992;24(2):748–751.

[29] Shiota G, Harada K, Ishida M, et al. Inhibition of hepatocellular carcinoma by glycyrrhizin in diethylnitrosamine-treated mice. Carcinogenesis. 1999;20:59-63.

[30] Furuta K, Sato S, Miyake T, et al. Anti-tumor effects of cimetidine on hepatocellular carcinomas in diethylnitrosamine-treated rats. Oncol Rep. 2008;19(2):361-368.

[31] Imamoto R, Okano JI, Sawada S, et al. Null anticarcinogenic effect of silymarin on diethylnitrosamine-induced hepatocarcinogenesis in rats. Exp Ther Med. 2014;7(1):31-38.

[32] Mukherjee D, Ahmad R. Glucose-6-phosphate Dehydrogenase Activity During N′-nitrosodiethylamine-induced Hepatic Damage. Achiev Life Sci. 2015;9:51–56.

[33] Lodhi RL, Maity S, Kumar P, et al. Evaluation of mechanism of hepatotoxicity of leflunomide using albino wistar rats. Afr J Pharm Pharmacol. 2013;17:1625–1631.

[34] Saha S, Chan DSZ, Lee CY, et al. Pyrrolidinediones reduce the toxicity of thiazolidinediones and modify their anti-diabetic and anti-cancer properties. Eur J Pharmacol. 2012;697:13–23.

[35] Kushwaha PS, Raj V, Singh AK, et al. Antidiabetic effects of isolated sterols from *Ficus racemosa* leaves. RSC Adv. 2015;5:35230-35237.

[36] Keshari AK, Kumar G, Kushwaha PS, et al. Isolated flavonoids from *Ficus racemosa* stem bark possess antidiabetic, hypolipidemic and protective effects in albino Wistar rats. J Ethnopharmacol. 2016;181:252–262.

[37] Makos BK and Youson JH. Tissue levels of bilirubin and biliverdin in the sea lamprey, Petromyzon marinus L., before and after biliary atresia. Comp Biochem Physiol A Physiol. 1988;91(4):701-710.

[38] Ong MM, Latchoumycandane C, Boelsterli UA. Troglitazone-induced hepatic necrosis in an animal model of silent genetic mitochondrial abnormalities. Toxicol Sci. 2007;97:205-213.

[39] Peinnequin A, Mouret C, Birot O, et al. Rat pro-inflammatory cytokine and cytokine related mRNA quantification by real-time polymerase chain reaction using SYBR green. BMC Immunol. 2004;5:1-10.

[40] Schaefer N, Tahara K, Websky VM, et al. Role of resident macrophages in the immunologic response and smooth muscle dysfunction during acute allograft rejection after intestinal transplantation. Transpl Int. 2008;21:778-791.

[41] Wishart DS, Jewison T, Guo AC, et al. HMDB 3.0-The human metabolome database in 2013. Nucleic acids Res. 2013;41:801-807 .

[42] Nicholson JK, Foxall PJ, Spraul M, Farrant RD, Lindon JC. 750 MHz ^{1}H and ^{1}H-^{13}C NMR spectroscopy of human blood serum. Anal Chem. 199;67:793-811.

[43] Guleria A, Bajpai NK, Rawat A, Khetrapal CL, Prasad N, Kumar D. Metabolite characterisation in peritoneal dialysis effluent using high resolution ^{1}H and ^{1}H ^{13}C NMR spectroscopy. Magn Reson Chem. 2014;52:475-479.

[44] Sahani S. Evaluation of hepatoprotective efficacy of APCL-A polyherbal formulation in vivo in rats. Ind Drug. 1998;36:628–632.

[45] Rossi L, Zoratto F, Papa A, et al. Current approach in the treatment of hepatocellular carcinoma. World J Gastrointest Oncol. 2010;2:348–359.

[46] Ueda H, Fukuchi H, Tanaka C. Toxicity and efficacy of hepatic arterial infusion chemotherapy for advanced hepatocellular carcinoma. Oncol Lett. 2012;3:259–263.

[47] Newman DJ. Natural products as leads to potential drugs: an old process or the new hope for drug discovery. J Med Chem. 2008;51:2589–2599.

[48] Saha S. Hepatotoxicity of thiazolidinedione antidiabetic drugs: a structural toxicity relationship study. Ph.D. Thesis. National University of Singapore. 2010.

[49] Kweon S, Park KA, Choi H. Chemopreventive effect of garlic powder diet in diethylnitrosamine-induced rat hepatocarcinogenesis. Life Sci. 2003;7:2515–2526.

[50] Pradeep K, Mohan CV, Gobianand K, Karthikeyan S. Silymarin modulates the oxidant-antioxidant imbalance during diethylnitrosamine induced oxidative stress in rats. Eur J Pharmacol. 2007;560:110–116.

[51] Kowsalya R, Kaliaperumal J, Vaishnavi M, Namasivayam E. Anticancer activity of Cynodon dactylon L. root extract against diethyl nitrosamine induced hepatic carcinoma. South Asian J Cancer. 2015;4:83-87.

[52] Wu H, Li N, Jin R, et al. Cytokine levels contribute to the pathogenesis of minimal hepatic encephalopathy in patients with hepatocellular carcinoma via STAT3 activation. Sci Rep. 2016;6:1-9.

[53] Montoliu C, Piedrafita B, Serra MA, et al. IL-6 and IL-18 in blood may discriminate cirrhotic patients with and without minimal hepatic encephalopathy. J Clin Gastroenterol. 2009;43:272–279.

[54] Onal IK, Akdogan M, Oztas E, et al. Does interleukin-18 play a role in the pathogenesis of hepatic encephalopathy? Hepatogastroenterology. 2011;8:497–502.

[55] Luo M, Li L, Yang EN, Dai CY, Liang SR, Cao WK. Correlation between interleukin-6 and ammonia in patients with overt hepatic encephalopathy due to cirrhosis. Clin Res Hepatol Gastroenterol. 2013;37:384–390.

[56] Chang Q, Daly L, Bromberg J. The IL-6 feed-forward loop: a driver of tumorigenesis. Semin Immunol. 2014;26:48-53.

[57] Germain D, Frank DA. Targeting the cytoplasmic and nuclear functions of signal transducers and activators of transcription 3 for cancer therapy. Clin Cancer Res. 2007;13:5665-5669.

[58] Othman MS, Aref AM, Mohamed AA, Ibrahim WA. Serum Levels of Interleukin-6 and Interleukin-10 as Biomarkers for Hepatocellular Carcinoma in Egyptian Patients. ISRN Hepatol. 2013;2013:1-9.

[59] Xia J, Sinelnikov IV, Han B, Wishart DS. MetaboAnalyst 3.0-making metabolomics more meaningful. Nucleic Acids Res. 2015;43:1-7.

[60] Sahdev AK, V Raj, Singh AK, et al. Ameliorative effects of pyrazinoic acid against oxidative and metabolic stress manifested in rats with dimethylhydrazine induced colonic carcinoma, Cancer Biol Therapy. 2017:1-10. doi:10.1080/15384047.2017.1310341.

[61] Wang H, Wang L, Zhang H, et al. ^{1}H NMR-based metabolic profiling of human rectal cancer tissue. Mol Cancer. 2013;12:1-12.

[62] Gribbestad IS, Petersen SB, Fjøsne HE, Kvinnsland S, Krane J. ^{1}H NMR spectroscopic characterization of perchloric acid extracts from breast carcinomas and non-involved breast tissue. NMR Biomed. 1994;7:181–194.

[63] Liu Y, Hong Z, Tan G et al. NMR and LC/MS-based global metabolomics to identify serum biomarkers differentiating hepatocellular carcinoma from liver cirrhosis. Int J Cancer. 2014;135:658–668.

[64] Huang Q, Tan Y, Yin P, et al. Metabolic characterization of hepatocellular carcinoma using nontargeted tissue metabolomics. Cancer Res. 2013;73(16):4992-5002.

[65] Gao H, Lu Q, Liu X et al. Application of 1H NMR-based metabonomics in the study of metabolic profiling of human hepatocellular carcinoma and liver cirrhosis. Cancer Sci. 2009;100:782–785.

[66] Delage B, Fennell DA, Nicholson L, et al. Arginine deprivation and argininosuccinate synthetase expression in the treatment of cancer. Int J Cancer. 2010;126:2762–2772

[67] Fages A, Duarte-Salles T, Stepien M et al. Metabolomic profiles of hepatocellular carcinoma in a European prospective cohort. BMC Med. 2015;13:1–14.

5. Summary and Conclusion

Hepatocellular carcinoma, especially in the later stages, is a major problem in the clinic and serious complication of cirrhosis or other chronic liver disease. At present, the treatment strategies are limited and there is a clear need for new therapies. Only a few medications are available in the market for the treatment of HCC, possession of contraindication and side effects are the biggest unacceptability for the patient. Therefore, the main objective of my research work is to design, synthesis and evaluation of novel 5H-benzo[h] thiazolo[2,3-b]quinazoline (1A–15A) and indeno[1,2-d]thiazolo[3,2-a]pyrimidine (1B–15B) analogs for the treatment of HCC. Recent studies have delineated the underlying mechanism and discovered novel drug-like small molecules that show promising effects for the treatment of HCC.

These novel synthesized molecules are an untapped resource for novel therapeutic strategies against HCC. Therefore, the current research focused on:

- Design and develop advanced one-pot as well as two-step synthetic routes to novel drug-like molecules
- Applying molecular modelling studies and in vitro evaluation
- Also applying SAR study to uncover and design novel drug-like molecules and
- Finally, in vivo antitumor activity together with proton NMR-based metabolomic studies to optimize the promising drug candidates.

We have successfully devised a highly proficient and operationally simple metal-free, one-pot MDR for obtaining a series of novel, hitherto unreported, 5H-benzo[h]thiazolo[2,3-b]quinazoline (1A–15A) and indeno[1,2-d]thiazolo[3,2-a]pyrimidine (1B–15B) analogs displaying potent anticancer activity against Hep-G2 cells as an alternative approach for the treatment of HCC. Considering this library of novel compounds, we concluded that 5H-benzo[h]thiazolo[2,3-b] quinazoline, along with a substituted phenyl ring (hydrophobic side chain) establishes an important pharmacophoric structure, and the R1, R2, and R3 positions of the phenyl ring, as well as the X1 and X2 positions of the tetralone ring system, are the key reactive sites that could be modified with various groups to elicit greater antitumorigenic potential.

We have also demonstrated that substitutions with more electronegative groups (–OH, –OCH3) on the hydrophobic side chain directly linked to thiazolo[2,3-b]quinazoline led to active members 4A and 6A, eliciting enhanced antitumorigenic activity, with GI50, 10

μg/mL, which was confirmed by docking analyses. Additionally, 3-methoxy-4-hydroxyphenyl–substituted 5H-benzo[h]thiazolo[2,3-b]quinazoline led to 4A, which displayed excellent antitumorigenic activity among a library of 30 novel synthesized compounds with values of GI50,10 μg/mL.

This approach, using a one-pot, multicomponent reaction sequence involving a domino Knoevenagel condensation/Michael-type addition followed by an intramolecular cyclization, where the desired molecules are obtained in a one-flask domino manner with atom and step economy in impressive yields (up to 86%) from readily available and low-priced starting materials, is a resource-effective and desirable route. Additionally, the target compounds were also synthesized by conventional two-step reactions, which were compared with this novel approach on the basis of obtained yields (40%–50%).

Various computational approaches demonstrated effective oral absorption and protein binding. These compounds, therefore, might be stable in some form of pharmaceutical dosage. Additionally, MD simulation supported our hypothesis regarding the stability of compound 4A with IL-6 protein during the simulation run. The results from the MD simulation run of the active inhibitor showed very less fluctuation with the active site domain of IL-6 and it achieved an almost steady state. We concluded that the compounds would be bound stably to IL-6.

In this way, next, acute oral toxicity study of both 4A and 6A was carried out to find out the safety profile in albino Wistar rats. Oral administration of 4A and 6A was well tolerated in rats at doses of 5 and 10 mg/kg and also we were not observed any significant reduction in body weight gain persisted over the 15 days. The results obtained from this study implied that both compounds were safe up to 10 mg/kg body weight dose in rats. Therefore, we further decided to perform in vivo anti-HCC activity at a dose of 10 mg/kg body weight in albino Wistar rats.

The results of in vivo investigation suggest that 4A and 6A exerted a chemo-preventive effects against experimentally NDEA-induced in vivo HCC in albino Wistar rats and this effect could be attributed to an increased antioxidant profile, restored liver-specific enzymes and decreased expression of oncogenes. Correlations of inflammatory cytokine levels with biochemical markers of HCC were also observed. Effectual treatment with 4A and 6A reflected reduction in the development of carcinogenic hepatic nodules and restored the

normal histological architecture of system. 4A and 6A alter the inflammatory signature to reduce significantly the overexpression of IL-6 and attenuate carcinogenic condition.

Additionally, metabolic profiling established that 4A and 6A have the ability to normalize several metabolites that were significantly disturbed in NDEA-exposed rats, supporting the anticancer activities of 4A and 6A for preventing the endogenous metabolic disorders associated with NDEA-induced liver carcinogenesis. However, various physiological and morphological changes, oxidative parameters, liver marker enzymes, cytokines and proton-NMR based serum metabolite profiles were assessed to evaluate the antitumor effect of 4A and 6A against NDEA-induced HCC.

While considering all the research findings together, it may be concluded that the newly developed method is both more useful and more profitable in each and every aspect, compared with the conventional route. Due to the importance of these two core structural motifs, that is, 5H-benzo[h]thiazolo[2,3-b]quinazoline and indeno[1,2-d]thiazolo[3,2-a]pyrimidine, especially in the areas of pharmaceutical and medicinal chemistry, we suggest that the protocols that we have outlined should open up new avenues of investigation, with enormous implications for achieving diversity in chemical synthesis. And our research findings also reveal that the antitumor effect of compound 4A is more prominent than 6A. Finally, this study provides evidences toward the potency of both 4A and 6A treatment in the amelioration of NDEA-exposed HCC in albino Wistar rats through IL-6 downregulation along with oxidative and metabolic stress reduction and suggests that they can be considered for a range of therapeutic interventions of hepatic cancer in future.

Drug Design, Development and Therapy

Dovepress
open access to scientific and medical research

Open Access Full Text Article

ORIGINAL RESEARCH

p-TSA-promoted syntheses of 5H-benzo[h]thiazolo[2,3-b]quinazoline and indeno[1,2-d]thiazolo[3,2-a]pyrimidine analogs: molecular modeling and in vitro antitumor activity against hepatocellular carcinoma

Amit K Keshari[1]
Ashok K Singh[1]
Vinit Raj[1]
Amit Rai[1]
Prakruti Trivedi[2]
Balaram Ghosh[2]
Umesh Kumar[3]
Atul Rawat[3]
Dinesh Kumar[3]
Sudipta Saha[1]

[1]Department of Pharmaceutical Sciences, Babasaheb Bhimrao Ambedkar University, Vidya Vihar, Raebareli Road, Lucknow, Uttar Pradesh, [2]Department of Pharmacy, Birla Institute of Technology & Science Pilani, Hyderabad Campus, Hyderabad, Telangana State, [3]Centre of Biomedical Research (CBMR), Sanjay Gandhi Post-Graduate Institute of Medical Sciences Campus, Raebareli Road, Lucknow, Uttar Pradesh, India

Abstract: In our efforts to address the rising incidence of hepatocellular carcinoma (HCC), we have made a commitment to the synthesis of novel molecules to combat Hep-G2 cells. A facile and highly efficient one-pot, multicomponent reaction has been successfully devised utilizing a *p*-toluenesulfonic acid (*p*-TSA)-catalyzed domino Knoevenagel/Michael/intramolecular cyclization approach for the synthesis of novel 5H-benzo[h]thiazolo[2,3-b]quinazoline and indeno[1,2-d]thiazolo[3,2-a]pyrimidine analogs bearing a bridgehead nitrogen atom. This domino protocol constructed one new ring by the concomitant formation of multiple bonds (C–C, C–N, and C=N) involving multiple steps without the use of any metal catalysts in one-pot, with all reactants efficiently exploited. All the newly synthesized compounds were authenticated by means of Fourier transform infrared spectroscopy, liquid chromatography–mass spectrometry, proton nuclear magnetic resonance spectroscopy, and carbon-13 nuclear magnetic resonance spectroscopy, together with elemental analysis, and their antitumor activity was evaluated in vitro on a Hep-G2 human cancer cell line by sulforhodamine B assay. Computational molecular modeling studies were carried out on cancer-related targets, including interleukin-2, interleukin-6, Caspase-3, and Caspase-8. Two compounds (4A and 6A) showed growth inhibitory activity comparable to the positive control Adriamycin, with growth inhibition of 50% <10 μg/mL. The results of the comprehensive structure–activity relationship study confirmed the assumption that two or more electronegative groups on the phenyl ring attached to the thiazolo[2,3-b]quinazoline system showed the optimum effect. The in silico simulations suggested crucial hydrogen bond and π–π stacking interactions, with a good ADMET (absorption, distribution, metabolism, excretion, and toxicity) profile and molecular dynamics, in order to explore the molecular targets of HCC which were in complete agreement with the in vitro findings. Considering their significant anticancer activity, 4A and 6A are potential drug candidates for the management of HCC.

Keywords: thiazolo[3,2-a]pyrimidine and thiazolo[2,3-b]quinazoline, hepatocellular carcinoma, domino reactions, interleukins, caspases, molecular docking, ADMET, dynamics, multi-component reactions, metal-free

Introduction

One in six human deaths globally is due to multifaceted disease, such as cancer. Liver cancer accounted for 788,000 deaths in 2015 and is the second most common cause of cancer-related deaths, worldwide. The most prevalent primary liver cancer

Correspondence: Sudipta Saha
Department of Pharmaceutical Sciences, Babasaheb Bhimrao Ambedkar University, Vidya Vihar, Raebareli Road, Lucknow 226025, Uttar Pradesh, India
Tel +91 80 9074 7008
Email sudiptapharm@gmail.com

submit your manuscript | www.dovepress.com
Dovepress
http://dx.doi.org/10.2147/DDDT.S136692

Drug Design, Development and Therapy

Dovepress
open access to scientific and medical research

Open Access Full Text Article

ORIGINAL RESEARCH

5H-benzo[h]thiazolo[2,3-b]quinazolines ameliorate NDEA-induced hepatocellular carcinogenesis in rats through IL-6 downregulation along with oxidative and metabolic stress reduction

Amit K Keshari[1]
Ashok K Singh[1]
Umesh Kumar[2]
Vinit Raj[1]
Amit Rai[1]
Pranesh Kumar[1]
Dinesh Kumar[2]
Biswanath Maity[2]
Sneha Nath[3]
Anand Prakash[3]
Sudipta Saha[1]

[1]Department of Pharmaceutical Sciences, Babasaheb Bhimrao Ambedkar University, [2]Centre of Biomedical Research, SGPGIMS Campus, [3]Department of Biotechnology, Babasaheb Bhimrao Ambedkar University, Lucknow, India

Abstract: 5H-benzo[h]thiazolo[2,3-b]quinazoline scaffold is known to have an antitumor effect on certain types of malignancies; however, its effect on hepatocellular carcinoma (HCC) remains unclear. Previously, we reported *p*-toluenesulfonic acid-promoted syntheses, molecular modeling and in vitro antitumor activity of 5H-benzo[h]thiazolo[2,3-b]quinazoline against human hepatoma (Hep-G2) cells where compounds **4A** and **6A** were found to be potent inhibitors among the series. In continuation to our previous effort to develop novel therapeutic strategies for HCC treatment, here we investigated the in vivo antitumor activity and the mechanism underlying the effects of **4A** and **6A** in N-nitrosodiethylamine (NDEA)-induced HCC using male Wistar rats. NDEA was administered weekly intraperitoneally at a dose of 100 mg/kg for 6 weeks. Various physiological and morphological changes, oxidative parameters, liver marker enzymes and cytokines were assessed to evaluate the antitumor effect of **4A** and **6A**. In addition, proton nuclear magnetic resonance-based serum metabolomics were performed to analyze the effects of **4A** and **6A** against HCC-induced metabolic alterations. Significant tumor incidences with an imbalance in carcinogen metabolizing enzymes and cellular redox status were observed in carcinogenic rats. Tumor inhibitory effects of **4A** and **6A** were noted by histopathology and biochemical profiles in NDEA-induced hepatic cancer. Compounds **4A** and **6A** had a potential role in normalizing the elevated levels of inflammatory mediators such as interleukin-1β (IL-1β), IL-2, IL-6 and IL-10. At molecular level, the real-time quantitative reverse-transcribed polymerase chain reaction analysis revealed that **4A** and **6A** attenuated the *IL-6* gene overexpression in hepatic cancer. Further, orthogonal partial least squares discriminant analysis scores plot demonstrated a significant separation of **4A** and **6A**-treated groups from carcinogen control group. Both the compounds have potential to restore the imbalanced metabolites due to HCC, signifying promising hepatoprotective activities. All these findings suggested that **4A** and **6A** could be potential drug candidates to treat HCC.

Keywords: 5H-benzo[h]thiazolo[2,3-b]quinazoline, N-nitrosodiethylamine, NDEA, hepatocellular carcinoma, HCC, interleukins, ^{1}H-NMR based metabolomics

Introduction

Chronic exposure to chemical carcinogens leads to several biochemical and genetic variations in the cells. N-nitrosodiethylamine (NDEA), a known toxic and environmental hepatic carcinogen, has been used as a tumor inducer in various hepatic cancer models. Also, it has been shown to be mutagenic and genotoxic.[1] Cytochrome P450 enzyme-dependent NDEA metabolism produces reactive oxygen species (ROS) and

Correspondence: Sudipta Saha
Department of Pharmaceutical Sciences, Babasaheb Bhimrao Ambedkar University, Vidya Vihar, Raebareli Road, Lucknow, Uttar Pradesh 226025, India
Tel +91 80 9074 7008
Email sudiptapharm@gmail.com

submit your manuscript | www.dovepress.com
Dovepress
http://dx.doi.org/10.2147/DDDT.S143075

Bridgehead Nitrogen Thiazolo[3,2-a]pyrimidine: A Privileged Structural Framework in Drug Discovery

Author(s): Amit K. Keshari, Ashok K. Singh, Sudipta Saha*.

Journal Name: Mini-Reviews in Medicinal Chemistry

Volume 17 , Issue 15 , 2017

DOI : 10.2174/1389557517666170216142113 (https://doi.org/10.2174/1389557517666170216142113)

Graphical Abstract:

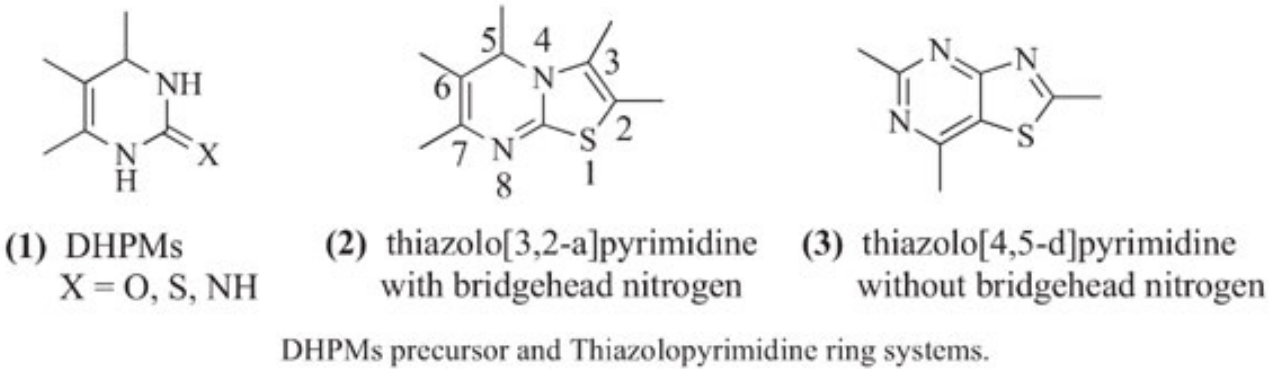

DHPMs precursor and Thiazolopyrimidine ring systems.

Abstract:

Background: Thiazolopyrimidine derivatives containing bridgehead nitrogen atom are nowa- days attracting the attention of many medicinal chemists throughout the world to explore this framework for its potential. This biologically important scaffold is formed by the fusion of two aromatic rings, thiazole and pyrimidine, in such a way that one carbon atom at the ring junction is replaced by a nitrogen atom and is, therefore, being common for both the heterocyclic rings. One of the most common example of this type of fusion is thiazolo[3,2-a]pyrimidine which is being used perpetually with tremendous success in various fields of therapeutic applications.

Method: Despite the outstanding researches on thiazolo[3,2-a]pyrimidines in the literature, hardly there is a comprehensive review on the chemistry and medicinal values of present scaffold. This review is, therefore, to endow with highlights on assorted progress made over the recent past on the basis of the development of new synthetic strategies, structure of various synthesized molecules and their promising medicinal attributes.

Conclusion: In addition, we have undertaken various scientific reports in depth, to explain spectral characterization (UV, IR, Mass, NMR and X-ray crystallography) and stereochemistry, particularly of thiazolo[3,2-a]pyrimidines.

Keywords: Biological activities, bridgehead nitrogen thiazolo[3, 2-a]pyrimidine, recent synthetic strategies, spectral characterization and X-ray crystallography, stereochemistry, thiazolopyrimidine.

Article Details

VOLUME: 17
ISSUE: 15
Year: 2017
Page: [1488 - 1499]
Pages: 12
DOI: 10.2174/1389557517666170216142113 (https://doi.org/10.2174/1389557517666170216142113)
Price: $58

URKUND

Urkund Analysis Result

Analysed Document: Amit K Keshari merged chapters 1-5.pdf (D33570185)
Submitted: 12/10/2017 1:25:00 PM
Submitted By: shodhganga.bbau@gmail.com
Significance: 0 %

Sources included in the report:

Instances where selected sources appear:

0

RESUME

AMIT KUMAR KESHARI

M. Pharm., PhD (Pharmaceutical Chemistry)

Department of Pharmaceutical Sciences,

Babasaheb Bhimrao Ambedkar University (A Central University),

Lucknow –226025, U.P., India. Mob: +91-7054090169; 9984431973

amitkeshari.pharma@gmail.com

https://www.researchgate.net/profile/Amit_Keshari

CAREER OBJECTIVES:

To enhance my research, writing, and communication skills, integrating them with a challenging work environment and associating me with an institution, where world-class science technology meets innovation.

Research Interests: Synthetic Medicinal Chemistry; Molecular Modelling; Anticancer Drug Developments; Isolation of Natural Products; NMR-based Metabolomics

Research Gate Statistics:	**RG Score**	21.41	**Publications**	32	**Filed Patent**	03
Reads	3,061	**Citations**	49	**Book Chapters**	03		

ACADEMIC QUALIFICATIONS:

- **Ph.D (Pharmaceutical Chemistry)** from **Department of Pharmaceutical Sciences, Babasaheb Bhimrao Ambedkar University (A Central University), Lucknow** in Oct, 2013 - Dec, 2017.

- **M.Pharm (Pharmaceutical Chemistry)** From **Babu Banarasi Das Northern India Institute of Technology, Lucknow** (Affiliated to Gautam Buddh Technical University, Lucknow) in Apr, 2013.

PATENT FILED:

- **AK Keshari**, S Saha, AK Singh, V Raj, A Rai. 5H-benzo[h]thiazolo[2,3-b]quinazolines containing nitrogen bridgehead as an anti-hepatocellular carcinogenic agent. **Indian Patent Application (2016), Number 201611032810.**

- AK Singh, S Saha, **AK Keshari**, SA Saraf, D Kumar, A Prakash, "Indolo Fused Pyrido-oxazepine and its derivatives for the Treatment of Hepatocellular Carcinoma" **Indian Patent Application (2016), Number: 201611016493.**

- AK Singh, S Saha, V Raj, **AK Keshari**, A Rai, P Kumar. 5H-benzo[2,3][1,4] thiazepino[5,6-b]indoles for the treatment of liver cancer. **Indian Patent Application (2017), Number: 201711026168.**

BOOK CHAPTERS:

- Sudipta Saha, Ashok K Singh, **Amit K Keshari**, Vinit Raj, Amit Rai, Siddhartha Maity. Chapter: Modern Extraction Techniques for Drugs and Medicinal Agents. **Handbook of Food Bioengineering series, Elsevier; Volume 4,** 07/2017. ISBN: 9780128115213.

- Sudipta Saha, **Amit K Keshari**, Ashok K. Singh, Priya Singh Kushwaha, Siddhartha Maity. Chapter: Emerging therapeutic targets for diabetes. **Boca Raton: Taylor & Francis,** 2017. ISBN: 9781498729994.

- Dinesh Kumar, Atul Rawat, Durgesh Dubey, Umesh Kumar, **Amit K Keshari**, Sudipta Saha, Anupam Guleria. NMR Based Metabolomics: An Emerging Tool for Therapeutic Evaluation of Traditional Herbal Medicines. **Nuclear Magnetic Resonance Spectroscopy. SM Group. 2016; 06; 1-18.**

PUBLICATIONS:

- **Amit K Keshari,** AK Singh, V Raj, A Rai, P Trivedi, B Ghosh, U Kumar, A Rawat, D Kumar, S Saha. *p*-TSA-promoted syntheses of 5H-benzo[h]thiazolo[2,3-b]quinazoline and indeno[1,2-d]thiazolo[3,2-a]pyrimidine analogs: molecular modeling and in vitro antitumor activity against hepatocellular carcinoma. **Drug Design, Development and Therapy (Impact Factor 2.88).** 2017; 11: 1623–1642.

- **Amit K Keshari,** AK Singh, S Saha. Bridgehead Nitrogen Thiazolo[3,2-a]pyrimidine: A privileged Structural Framework in Drug Discovery. **Mini Reviews in Medicinal Chemistry (Impact Factor 2.82).** 2017. DOI: 10.2174/1389557517666170216142113.

- **Amit K Keshari,** AK Singh, U Kumar, V Raj, A Rai, P Kumar, D Kumar, B Maity, S Nath, A Prakash, S Saha. 5H-benzo[h]thiazolo[2,3-b]quinazolines ameliorate NDEA-induced hepatocellular carcinogenesis in rats through IL-6 down-regulation along with oxidative and metabolic stress reduction. **Drug Design, Development and Therapy (Impact Factor 2.88).** 2017: 11; 2981–2995.

- **Amit K Keshari,** G Kumar, PS Kushwaha, M Bhardwaj, P Kumar, A Rawat, D Kumar, A Prakash, B Ghosh, S Saha. Isolated flavonoids from Ficus racemosa stem bark possess antidiabetic, hypolipidemic and protective effects in albino Wistar rats. **Journal of Ethnopharmacology (Impact Factor 3.03), Elsevier**. 2016; 181: 252-262.

- **Amit K Keshari,** Aseem Tewari, Shweta Singh Verma, Shailendra K Saraf. Novel Mannich-bases as Potential Anticonvulsants: Syntheses, Characterization and Biological Evaluation. Central Nervous System Agents in Medicinal Chemistry 07/2017;

- Amit Rai, Umesh Kumar, vinit raj, Ashok Singh, Pranesh Kumar, **Amit K Keshari**, Dinesh Kumar, Biswanath Maity, Arnab De, Amalesh Samanta, Sneha Nath, anand prakash, Sunil Gosipatala, Gyan Chand. Sudipta Saha. Novel 1,4-benzothazines obliterate COX-2 mediated JAK-2/STAT-3 signals with potential regulation of oxidative and metabolic stress during colorectal cancer. **Pharmacological Research (IF = 4.48) (Accepted), Elsevier.**

- Ashok Singh, vinit raj vinit raj, **Amit K Keshari**, Amit Rai, Pranesh Kumar, Atul Rawat, Biswanath Maity, Dinesh Kumar, anand prakash, Arnab De, Amalesh Samanta, Bolay Bhattacharya, Sudipta Saha. Isolated mangiferin and naringenin exert antidiabetic effect via PPARγ/GLUT4 dual agonistic action with strong metabolic regulation. **Chemico-Biological Interactions (IF = 3.14) (Accepted)**, **Elsevier**.

- Vinit Raj, Mohamed H. Aboumanei, Amit Rai, Suraj P.Verma, Ashok K Singh, **Amit K Keshari,** Sudipta Saha. Pharmacophore and 3D-QSAR Modeling of Novel 1,3,4-Thiadiazole Derivatives: Specificity Towards Colorectal Cancer. **Pharmaceutical Chemistry Journal (Impact Factor 0.5).** 07/2017.

- Amit Rai, Vinit Raj, Mohamed Hodhod Aboumanei, Ashok K. Singh, **Amit K. Keshari**, Suraj P. Verma, Sudipta Saha. Pharmacophore, 3D-QSAR models and Dynamic Simulation of 1,4-Benzothiazines for Colorectal Cancer Treatment. **Combinatorial chemistry & high throughput screening (Impact Factor 0.95).** 07/2017; 20(999); DOI: 10.2174/138620732066 6170509153137.

- Vinit Raj, Amit Rai, Ashok K Singh, **Amit K Keshari**, Prakruti Trivedi, Balaram Ghosh, Umesh Kumar, Dinesh Kumar, Sudipta Saha. Discovery of Novel 2-Amino-5-(Substituted)-1,3,4-Thiadiazole Derivatives: New Utilities for Colon Cancer Treatment. **Anti-cancer agents in medicinal chemistry (Impact Factor 2.8).** 2017; 06.

- Anil K Sahdev, Vinit Raj, Ashok K Singh, Amit Rai, **Amit K Keshari**, Arnab De, Amalesh Samanta, Umesh Kumar, Atul Rawat, Dinesh Kumar, Sneha Nath, Anand Prakash, Sudipta Saha. Ameliorative effects of pyrazinoic acid against oxidative and metabolic stress manifested in rats with dimethylhydrazine induced colonic carcinoma. **Cancer biology & therapy (Impact Factor 2.92).** 2017; 05.

- Atul Rawat, Swati Chaturvedi, Ashok K Singh, Anupam Guleria, Durgesh Dubey, **Amit K Keshari,** Vinit Raj, Amit Rai, Anand Prakash, Umesh Kumar, Dinesh Kumar, Sudipta Saha. Metabolomics approach discriminates toxicity index of Pyrazinamide and its metabolic products; Pyrazinoic acid and 5-Hydroxy Pyrazinoic acid. **Human & Experimental Toxicology (Impact Factor 1.7).** 2017; 04.

- Priya Singh Kushwaha, Vinit Raj, Ashok K. Singh, **Amit K. Keshari**, Shubhini A. Saraf, Subhash C. Mandal, Rajnish Kumar Yadav, Sudipta Saha. Antidiabetic effects of isolated sterols from Ficus racemosa leaves. **RSC Advances (Impact Factor 3.28).** 2015; 5; 35230-35237.

DECLARATION:

I do hereby declare that the information given above is to the best of my knowledge.

Date: 13-12-2017

PLACE: LUCKNOW **AMIT KUMAR KESHARI**